An Investigation of the Effects of Topography on Colorado Front Range Winter Storms

by
Douglas A. Wesley

Department of Atmospheric Science
Colorado State University
Fort Collins, Colorado

Roger A. Pielke, P.I.
NSF Grant # ATM-9017849
ARO DAAL03-86-K-0175

Colorado State University

Department of Atmospheric Science

Paper No. 489

AN INVESTIGATION OF THE EFFECTS OF TOPOGRAPHY ON COLORADO FRONT RANGE WINTER STORMS

Douglas A. Wesley

Department of Atmospheric Science
Colorado State University
Fort Collins, Colorado
Fall, 1991

Atmospheric Science Paper No. 489

ABSTRACT

AN INVESTIGATION OF THE EFFECTS OF TOPOGRAPHY ON COLORADO FRONT RANGE WINTER STORMS

This study utilizes both an extensive set of observations and mesoscale model simulations to isolate and describe the important influences of complex terrain on Colorado Front Range winter storms, with an emphasis on snowfall distributions. Specifically, the interaction of various types of cold, low-level air masses with topography and the larger-scale flow is described. Frequently, the heaviest snowfall does *not* coincide with the steepest terrain gradients, as might be expected, due to this interaction. Field measurements of several snowstorms during the 1987-89 time period include special CLASS (Cross-chain Loran Atmospheric Sounding System) vertical profiles, standard National Weather Service (NWS) and National Meteorological Center (NMC) surface and rawinsonde data, surface observations collected by a trained snow-spotter network, profiler data, Doppler reflectivity and velocity scans, and Geostationary Operational Environmental Satellite (GOES) images. The numerical predictions are produced by the Regional Atmospheric Modeling System (RAMS) developed at Colorado State University, using two- and three-dimensional non-hydrostatic simulations. The versions of the model employed in this study utilized both horizontally homogeneous initializations and initial fields made up of NMC upper-air grids and rawinsondes. Most simulations employed full microphysics. A comparison between model-predicted dynamic and microphysical fields and observational data is described for the 30-31 March 1988 snowstorm along the Colorado Front Range.

Of particular interest in this study is the role of trapped cold air masses over the foothills and adjacent plains during the evolution of snow-producing synoptic scale disturbances. Specifically, these include two types of precipitating easterly ("upslope") flows

along the Colorado Front Range: cold-air damming situations and arctic outbreaks. By no means are the dynamical features of these two types of storms mutually exclusive. The investigation includes detailed case studies of each storm type. The cold air damming process concentrates snowfall, typically in the foothills and adjacent areas to the east. A blocked low-level stable layer causes overrunning in a north-south band over and near the foothills. A quite different scenario, the cold outbreak, requires the establishment of an arctic air mass in the low levels. In this case, overrunning occurs as moist westerly winds aloft flow over the arctic air mass, producing snowfall in the foothills and plains.

The problems with forecasting precipitation amounts during these situations are well-known. This project isolates two of the primary mechanisms which have caused many of these problems. Both of these dynamical processes must be considered by the wintertime forecaster as major contributors to heavy snowfall in this region.

Douglas A. Wesley
Department of Atmospheric Science
Colorado State University
Fort Collins, Colorado 80523
Fall 1991

ACKNOWLEDGEMENTS

Special thanks are extended to my parents, Lewis and Shirley, for their constant support and encouragement throughout my graduate study at CSU, and my fiancee, Sandy, who exhibited unending patience and generated motivation at the critical times. My adviser, Roger A. Pielke, provided many helpful suggestions. I also thank my other committee members, Bill Cotton, Wayne Schubert, and Jack Cermak for their support.

The work was primarily supported by the Army Research Office (ARO) Center for Geosciences, contract number DAAL03-86-K-0175. Some support was provided by the National Science Foundation Grant number ATM-8915265. I would like to acknowledge Nolan Doesken of the Colorado Climate Center for providing some key snowfall and temperature observations at several sites. John Lee, Jerry Schmidt, and Mike Moran from the CSU Department of Atmospheric Science are thanked for providing consultation and assistance for this study. Ray McAnelly helped analyze the radar data. Some useful computer graphics routines were produced by Piotr Flatau. The snow spotter network was available largely because of the work of Jim Wirshborn of Mountain States Weather Services. Jim also supplied useful supplemental surface data. Paul Schultz and John Smart provided the snow crystal observations in the Boulder area, and Lew Grant assisted with observations and equipment. John Weaver helped analyze the extensive satellite data set. Cindy Olsson of the National Acid Deposition Program, National Trends Network, is thanked for providing precipitation measurements at several locations. Dallas McDonald, Bryan Critchfield, and Tony Smith provided much assistance in the preparation of the final draft of the manuscript, and Judy Sorbie-Dunn drafted several of the figures.

The interactive workstation of the Cooperative Institute for Research in the Atmosphere SERS (Storm Education and Research System) was a useful tool in perusing and

analyzing the data. The RAMS model calculations were completed at the National Center for Atmospheric Research (NCAR). NCAR is partially sponsored by the National Science Foundation. Special CLASS facilities were provided by the Office of Naval Research under contract N0014-87-K-02281/P00001.

TABLE OF CONTENTS

LIST OF FIGURES

LIST OF TABLES

Chapter 1

INTRODUCTION

The problems associated with forecasting snowfall distributions in heavy snowstorms, and their detrimental effects on transportation, are well known. The heavily-populated Front Range region of Colorado faces these storms on an annual basis, and is no stranger to the serious economic and human loss caused by such weather events (Schlatter *et al.*, 1983). Wintertime aircraft icing in these storms can pose a serious problem; the Continental crash during heavy snowfall at Stapleton Airport in November, 1987 and a commercial airline incident at Rabbit Ears Pass are recent examples, and smaller airplanes experience this problem much more frequently. This geographical region annually experiences various winter storm types, including those producing freezing drizzle, blizzard conditions, and heavy, wet snow. Since eastern Colorado experiences this variety each year, it is an excellent laboratory for winter storm studies, and has proven so for the Winter Icing and Storms Project (WISP) during the 1989-90 and 1990-91 winters (see Rasmussen *et al.*, 1991a and Rasmussen and Politovich, 1990).

1.1 General Background

Although a large number of papers in the literature address the observations and modeling of winter storms, a relatively small subset emphasizes terrain effects. In regions away from the eastern slopes of the Rocky Mountains, these studies concentrate on the Sierra Nevada, Alps, and Appalachian Mountains. All of these studies address the formation of either "blocked" or "dammed" flow. The phenomenon of topographic blocking is the deceleration and diversion of low-level air flow by terrain which can lead to cold-air damming. Specifically, in the present investigation, *blocking* refers to the deceleration of upslope flow due to rising elevation. As air parcels rise, adiabatic cooling generates a

mesoscale high pressure region over the slope. The resulting pressure gradient reduces the flow up the slope. *Damming* is the forced uplift of warm, moist air over a relatively cold, stable air mass. The two phenomena are closely related, in that the presence of a low-level cold air mass associated with damming may owe its existence to blocking. However, blocking can, and often does, occur without damming.

Based on the strong sensitivity of the atmosphere to vertical motion via its typically strong stable stratification and its richness in water vapor in the low levels, blocking produces broad excursions of the wind as it tries to flow around rather than over the mountain, as shown by Smith (1979). An enhancement in windward-slope precipitation is also produced. Orographic and blocking-induced lifting can also trigger convection. Under certain conditions, any mountain greater than 0.5 to 1.0 km in height can induce low-level stagnation upstream. Generally, these conditions require $Fr \leq 0.7$ (approximately), where $Fr = \frac{U}{Nh}$, or the ratio of wind velocity to the product of the Brunt-Väisälä frequency and the mountain height.

Pierrehumbert and Wyman (1985) pointed out the existence of blocking by the Alps during the Alpine experiment. In their analytical and numerical studies, they investigated the atmospheric response to blocking in terms of Fr and the Rossby number $Ro = U/fl$, where f is the Coriolis parameter and l is the mountain width. They noted the existence of upstream blocking when Fr fell below about 1.3 and upstream stagnation below 0.7 for an infinitely long ridge. In California, blocking was an important process in some of the SCPP (Sierra Cooperative Pilot Program) storms; the resulting barrier jet (Parish, 1982) can exert an important dynamical (and thus microphysical) effect on Sierra orographic precipitation distributions.

For the Appalachians, a number of observational studies have documented cold-air damming, a terrain-induced phenomenon that often exerts a strong influence on snowfall distributions. Bell and Bosart (1988) describe a climatology of Appalachian damming, assessing the roles of evaporative and adiabatic cooling in forming and maintaining the U-shaped low-level cold dome east of the mountains. Flow within the cold air is generally mountain-parallel due to geostrophic adjustment. Figure 1.1 shows a conceptual model of

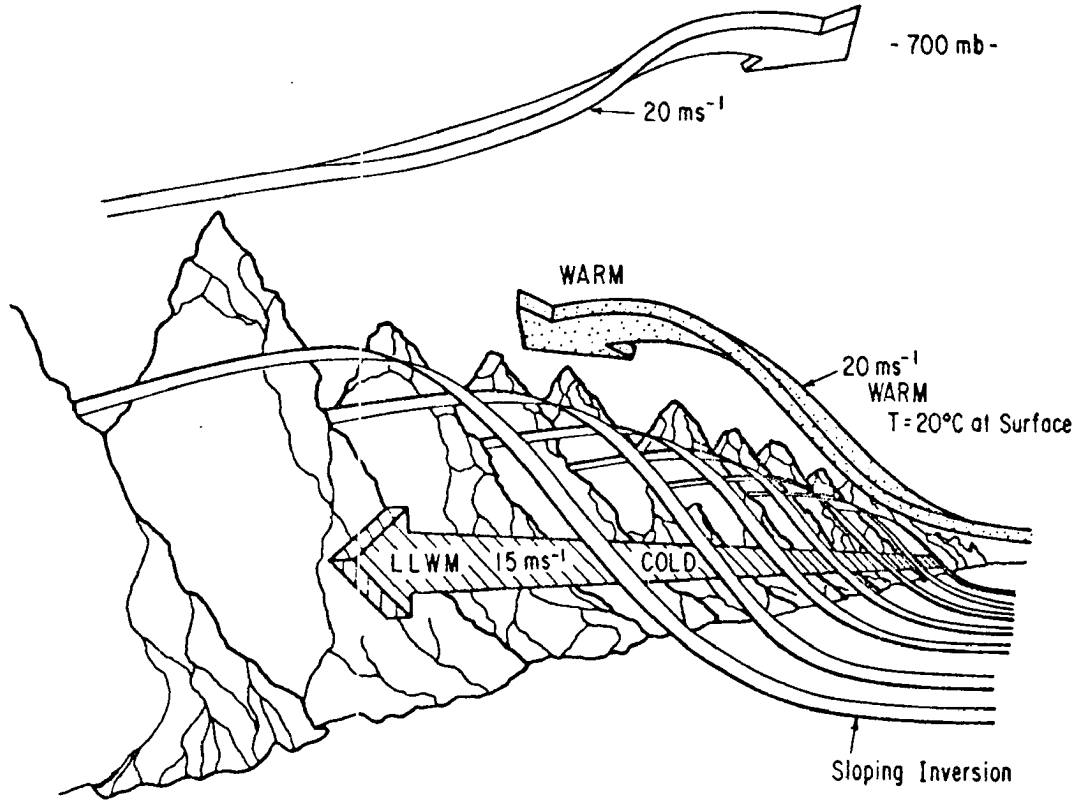

Figure 1.1: Conceptual model of cold-air damming as it existed at 1200 UTC 22 March 1985. Note the strong low-level wind maximum (LLWM) within the cold dome, the easterly (or southeasterly) flow just above the cold dome associated with strong warm advection into the warm air above the dome, the sloping inversion of the cold dome top, and the southerly and southwesterly winds above 700 mb associated with the advancing short-wave trough west of the Appalachians. Adapted from Bell and Bosart (1988).

the analysis including the low-level jet and overrunning induced by damming. In Virginia, for example, the entrenchment of a cold air mass east of the Blue Ridge leads to serious degradation of winter storm precipitation forecasts as snow and freezing precipitation typically persist for hours beyond the NMC guidance predictions (Michaels, 1991). Also, as Michaels points out, the large elevation gain between the eastern plains of Colorado and Wyoming and the Continental Divide traps a much deeper cold air mass, producing snow as opposed to the sleet and freezing rain in the mid-Atlantic states. Among many others, Forbes *et al.* (1987) present a case study of a typical cold-air damming scenario east of the Appalachians. Nielsen (1989), in a detailed study of New England coastal fronts, documented a special type of coastal front (his Type C) which formed near the base of the mountains and did not depend on the land-sea temperature difference. It is this type of front which has a direct analogy to the damming-induced meso-front in northeastern Colorado described in Chapter 2.

The existence of a barrier jet (Parish, 1982; Marwitz and Day, 1991; and Bell and Bosart, 1988) is essentially an extreme case of blocking. The presence of prolonged large-scale upslope flow, and subsequent deceleration due to blocking, leads to a barrier-parallel ageostrophic acceleration in the low-levels toward lower pressure. Such acceleration, if long-lived, can lead to a low-level wind maximum on the upwind side of the barrier. Typically this process requires 6 or more hours of development. In Colorado, the northerly barrier jet may be enhanced by cyclogenesis to the south and east.

Snowbands have been documented in many studies in the eastern United States. For example, O'handley and Bosart (1989) and Sanders and Bosart (1985) discuss snowbands whose widths (i.e. 70 to 100 km) were much larger than those discussed in this study, and were produced primarily by synoptic-scale frontogenetic forcing. Dunn (1988) documented a long-lived snowband in northeastern Colorado, of dimensions approximately 500 km in width and 200 km in length, which occurred in September 1985. Through a detailed analysis, he determined that synoptic-scale ageostrophic circulations associated with an upper-level jet streak and frontogenesis were responsible for the band. These circulations occurred in a region favorable for conditional symmetric instability (Bennetts and Hoskins, 1979; Emanual, 1983).

Hjelmfelt and Braham (1983) discussed a narrow shore-parallel snowband associated with a lake-effect storm over Lake Michigan in December 1977. With an approximate width of 20 km and length of 75 to 100 km, the snowband was produced by the land breeze circulation. Radar reflectivities within the band ranged from 20 to 35 dBz.

Carlson (1980) described air motions through a typical midlatitude cyclone using relative isentropic analysis in conjunction with satellite images. He documented a frequent westward extension of the synoptic-scale comma cloud system; this extension was the product of ascent within the so-called cold-conveyor belt. This belt was an organized flow of air, originating within the exiting low-level anticyclone to the east, which undercut the ascending southerly moist jet (the warm conveyor belt) and overran the low-level cold air to the rear of the surface low. The cold-conveyor belt may influence the evolution of Front Range storms, and one such case is examined in Chapter 2.

1.2 Observations in the Rocky Mountains

Generally, two types of snow-producing circulations occur in the eastern Colorado region: (i) well-developed, deep cyclonic circulations; and (ii) shallow anticyclonic systems (Reinking and Boatman, 1986). Many storms, of course, have both cyclonic and anticyclonic features at various levels in the atmosphere (see, for example, Cotton and Anthes, 1989). One classic example is the 30-31 March 1988 event, which is described in detail in Chapter 2. Precipitation events are generally post-frontal, in contrast to the classic Norwegian model of the synoptic-scale cyclone. All of the storms in this region exhibit characteristically complex low-level (i.e., lowest 150 mb of the atmosphere) dynamic and thermodynamic structure, the details of which determine the resulting snowfall distributions. The topography of the Front Range region is frequently responsible for the rapid variation with height of lapse rates and winds in the low levels and highly variable snowfall distributions. Figures 1.2 through 1.5 present the topography and precipitation distributions for four recent storms (14-16 January 1987, 30-31 March 1988, 10-11 February 1988, and 1-5 February 1989, respectively). The degree of variability is large. Another example is the blizzard of 5-7 March 1990, which exhibited extremely high east-west *and* north-south gradients in snowfall just east of the foothills (Marwitz and Day, 1991).

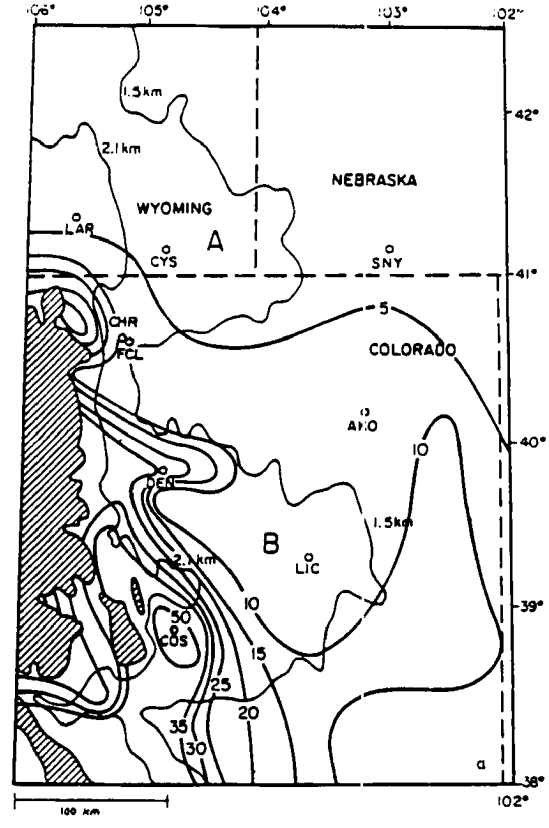

Figure 1.2: Snowfall distribution (cm) along the northern Colorado Front Range for 14-16 January 1987. Elevation contours (km) are the thin lines. Elevations above 2.7 km are shaded. NWS station identifiers are as follows: Laramie (LAR), Cheyenne (CYS), Sidney (SNY), Akron (AKO), Fort Collins (FCL), Limon (LIC), Denver (DEN), Colorado Springs (COS), and Christman Field (CHR). State borders are the dotted lines. The capital letters A and B refer to the Cheyenne Ridge and Palmer Divide, respectively. Secondary locations mentioned in the text are Akron (AKO) Boulder (B), Limon (LIC), Vail (V), Estes Park (E), Glenwood Springs (G), Rifle (1V1), Leadville (LXV), and Winter Park (W).

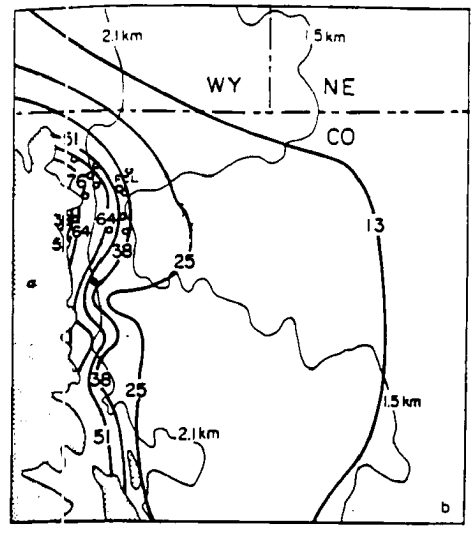

Figure 1.3: Snowfall distribution (cm) along the northern Colorado Front Range for 30-31 March 1988. Elevation contours and station identifiers are as in Figure 1.2.

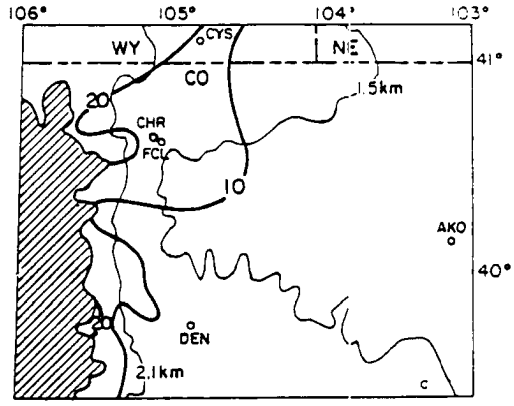

Figure 1.4: Snowfall distribution (cm) along the northern Colorado Front Range for 9-10 February 1988. Elevation contours and station identifiers are as in Figure 1.2.

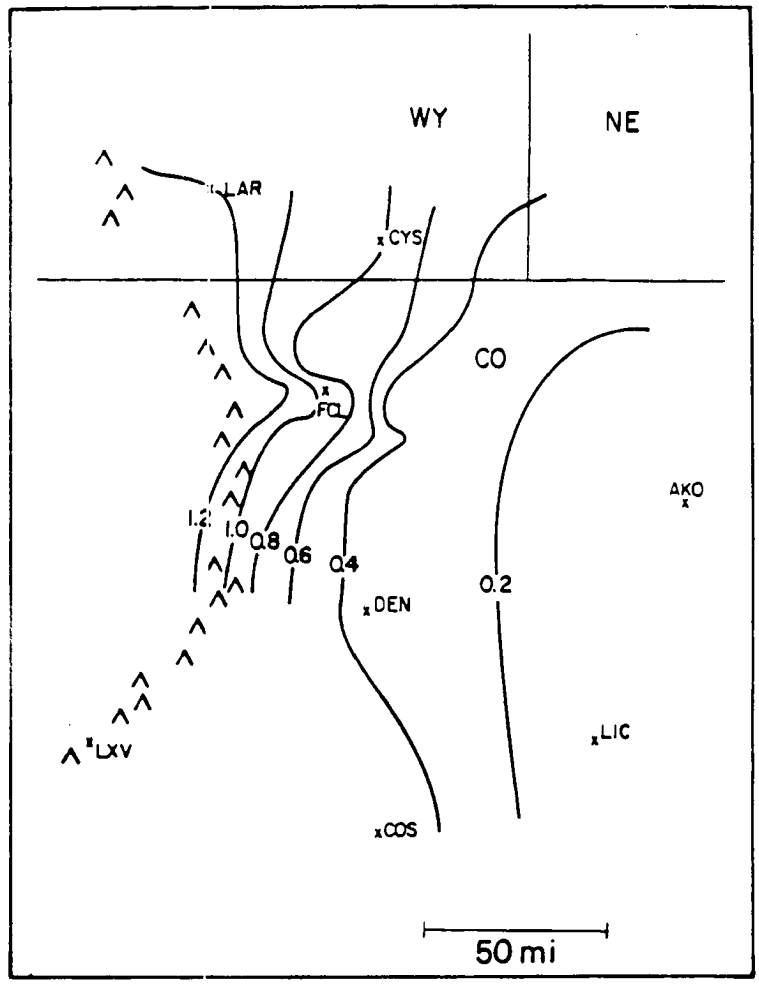

Figure 1.5: Liquid equivalent (inches) along the northern Colorado Front Range for 1-5 February 1989. Elevation contours and station identifiers are as in Figure 1.2.

Over the winter seasons of 1984 through 1991, the author has documented a persistent pattern in a vast majority of winter storm events in the Fort Collins region. This is a tendency toward a strong snowfall gradient oriented east-west within a 20 km-wide north-south swath *east* of the first foothill of the Front Range. Figure 1.6 shows an east-west vertical cross-section of terrain height, extending from the Continental Divide to the Kansas border at a latitude of 40.7°. Immediately apparent is the lack of slope from FCL to about 100 km east of FCL. In fact, the averaged eastern slope of the state east of FCL only produces about 1 cm s^{-1} of upward motion during 10 knots of easterly surface wind. Thus, the direct orographic lift associated with low-level "upslope" flow is weak and cannot account for the snowfall gradient. However, the steep terrain gradient from FCL to the west is of critical importance. It is responsible for blocking of upslope flow and subsequent upstream convergence and/or overrunning which often does explain the snowfall contours. The author's qualitative observation of a majority of winter precipitation in Fort Collins occurring during surface winds oriented westerly to northerly is further evidence of this phenomenon. These features will be documented in later chapters of this dissertation.

Other meteorological conditions associated with severe winter storms in eastern Colorado, such as temperature, wind and moisture, also exhibit large variation. Surface temperature ranges from 0°C to −25°C. Mid-level (i.e., 700 to 500 mb) winds may exhibit strong westerly components (Wesley *et al.*, 1990) or strong easterly components (Wesley and Pielke, 1990), as well as varying meridional components and speeds. The storms frequently exhibit blocking of low-level easterly flow (Dunn, 1987; Wesley and Pielke, 1990), but some events do not. Along the Front Range, the correlation of precipitation rate and surface pressure increases is high, in accordance with the post-frontal nature of most events; this phenomenon is addressed in detail in Chapters 2 and 3.

The importance of riming in the formation of precipitating ice crystals is often critical. Many storms contain persistent layers of supercooled water having liquid water content values greater than 0.1 g m^{-3}, resulting in occasionally severe aircraft icing (Rasmussen *et al.*, 1991b and Politovich, 1989). Supercooled water regions are often located in proximity to frontal or blocking-induced inversions. For many of the colder systems, strong inversions

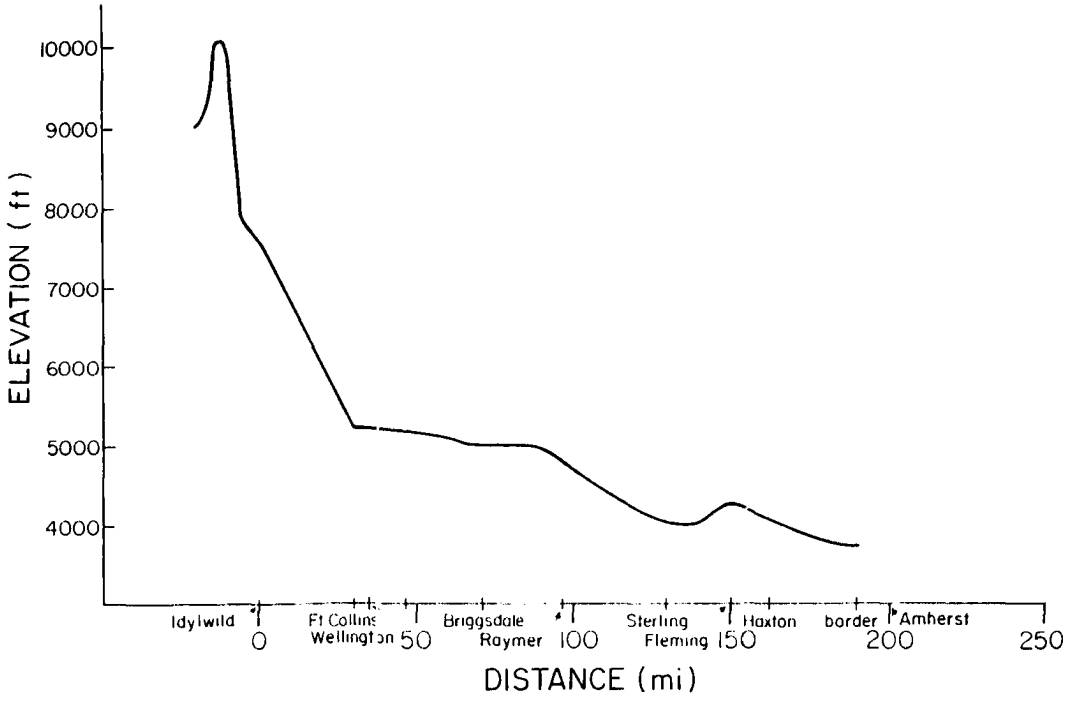

Figure 1.6: East-west profile of topography over northeastern Colorado at 40.7° latitude.

form at the top of a low-level cold pool and persist throughout the heavy snowfall (Wesley *et al.*, 1990). A local observational study of snow crystal types at the surface, utilizing a snow spotter network of approximately 50 spotters, found a predominance of heavily-rimed, aggregated dendrites during moderate to heavy snow for all storms occurring during the 1987-88 winter (Wesley and Pielke, 1990). The frequency of heavily-rimed crystals for storms occurring during the 1989-90 winter was also very high. Auer and White (1982) noted that heavy accumulations of snowfall are most frequently associated with large dendritic aggregates; climatologically, in the U.S., these episodes exhibit maximum vertical velocities within the temperature range of dendrite growth (i.e. $-12°C$ to $-17°C$).

However, the current understanding of mesoscale processes leading to localized regions of heavy snowfall is limited, especially in complex terrain. This deficiency applies to eastern Colorado. The reasons for this shortcoming are twofold: (i) measurements of wind and thermodynamic data at the surface and aloft have been too coarse to resolve mesoscale processes, and (ii) traditionally, mesoscale numerical models have been characterized by coarse horizontal and vertical resolutions, or too small a domain, to correctly simulate the details or scale interaction present in storm development. There are several other complicating factors. Typically, regions of heavy snowfall are not correlated with the coldest cloud tops in satellite data (e.g. Dunn, 1987). Simple topographical lifting concepts often do not correspond with regions of strongest ascent (Dunn, 1988; Wesley and Pielke, 1990). Favorable atmospheric snow-producing conditions are typically manifested in very narrow convective snowbands (approximately 5 to 25 km wide). The question faced by the forecaster of a heavy snow event occurring *somewhere* along the Colorado Front Range is often not a difficult one to answer 12 to 24 hours in advance. A more precise location of the event, however, generally cannot be predicted with any confidence more than a few hours in advance, given the present state of measuring and modeling systems. The forecasting problems encountered during the first year of the WISP are excellent examples. Such a situation is indicative of the current need for improvement in understanding the mesoscale circulations in these storms. This objective forms a substantial portion of the goals of WISP.

The mesoscale variability in snowfall amounts in recent Front Range storms (Figures 1.2-1.5) is accounted for by the presence of mesoscale snowbands, producing locally intense snowfall rates. Doppler radar observations of these storms frequently exhibit banding in the reflectivity structure for the low- and mid-levels (Lilly, 1981; Dunn, 1988; Wesley and Pielke, 1990). Both quasi-stationary and propagating bands occur, with various orientations, apparently depending on the wind direction aloft or on the occurrence of terrain blocking. Wesley and Pielke (1990) showed examples of both quasi-stationary and transient snowbands for two storms in 1988. Analyses of surface observations indicated a high correlation of reflectivity with snowfall intensity. Typical band dimensions were 50 to 100 km in length and 5 to 20 km wide. Wolfsberg *et al.* (1986) proposed that mesoscale symmetric instability (Bennetts and Hoskins, 1979) was responsible for similar banding in a New England winter storm. Middle atmospheric lapse rates in Colorado storms are frequently similar to those observed by Wolfsberg *et al.* (1986). Dunn (1988) demonstrated that this type of instability played a key role in the location of heaviest snowfall in the Colorado storm of 28-29 September 1985. Whether this instability is important in generating a significant portion of Colorado snowbands is not known at this time.

Boatman and Reinking (1984) studied the dynamics and microphysics of two arctic anticyclonic "upslope" events over the high plains, occurring 15-16 January 1982 and 3-4 February 1982. In each case, the depth of the cold air mass was approximately 100 mb. The cold layer contained upslope (low-level) clouds in a water-saturated, weakly-turbulent environment. These clouds were seeded by ice crystals from separate mid-level clouds, and the upslope cloud lifetimes were about 18 hours in both cases. The slope of the cold air mass was very small. According to thermodynamic cross-sections taken between Denver (DEN or Stapleton Airport) and Dodge City, Kansas, and DEN and North Platte, Nebraska, terrain-induced ascent rates of 1-2 cm s^{-1} occurred in the arctic air mass. Some liquid water in the mid-level cloud layer (400 to 500 mb) was observed for the 15-16 January, 1982 storm with an FSSP (Forward Scattering Spectrometer Probe), but only large (400 to 500 μm largest dimension) crystals were found in the low cloud layer

(730 to 800 mb). The crystal types and sizes observed implied that significant aggregation did not take place within the low cloud layer. For the 3-4 February 1982 case, aircraft measured significant liquid water concentrations (up to about 0.1 g m^{-3}) in the lower cloud layer (about 760 to 820 mb), but reported only small icing amounts. The seeder-feeder mechanism apparently was operating despite a dry layer between 700 and 750 mb, where relative humidity with respect to ice was about 40%. Aggregation was again minimal in the low cloud.

The cold-air damming scenario has been documented in two case studies (Dunn, 1987 and Wesley and Pielke, 1990) in eastern Colorado, but these studies were not meant to be comprehensive or applicable to a more generalized dynamical structure. The phenomenon is briefly summarized here. Figure 1.7 is a series of representative soundings near Fort Collins (FCL) during the early stages of heavy snowfall during the 30-31 March 1988 event. Note the shallow stable layer near the ground (layer 1), characterized by weak northwesterly flow. This layer was created as moist low-level easterly flow decelerated as it was blocked by the terrain-induced local pressure gradient directed west-to-east. The blocked layer apparently formed in-place, as in the case studied by Dunn (1987), with some enhancement by low-level cold advection. Analysis of these soundings, along with detailed analysis of meso-network data and low-level Doppler radar reflectivity and velocity scans, indicated that the stable layer caused enhanced overrunning (of layer 1 by layer 2) in a north-south band near the foothills. A surface convergence zone (a meso-front) formed at the eastern edge of layer 1 (see Figure 1.8). The front formed 20 to 50 km east of the foothills. The convergence was quasi-steady for many hours, and enhanced low-level vertical motion led to bands of heavy snowfall to the west of and nearly parallel to the convergence zone. Resulting snowfall measurements revealed a corresponding band of heavier accumulation in the same area (see Figure 1.3). The present study documents the evolution of the layered vertical structure, and examines the low-level upslope with mesoscale model simulations.

Barrier jet formation, an extreme case of cold-air damming associated with a prolonged period of low-level easterly flow over the plains and possibly cyclogenesis to the

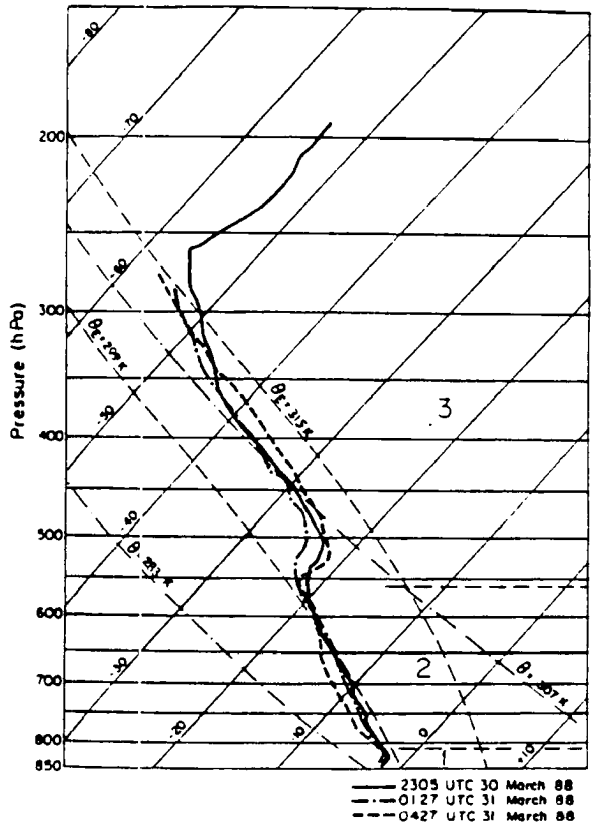

Figure 1.7: (a) CLASS temperature profiles for the first three balloon releases at CHR, for the 30-31 March 1988 storm. Horizontal solid lines are pressure (mb or hPa). Temperature (°C) values are the solid diagonal lines. Two labeled adiabats (dashed lines) are shown, as well as two moist adiabats (dashed-dotted lines). Horizontal dashed lines divide the atmosphere into three layers, denoted 1, 2, and 3 (see text for discussion of the layered structure).

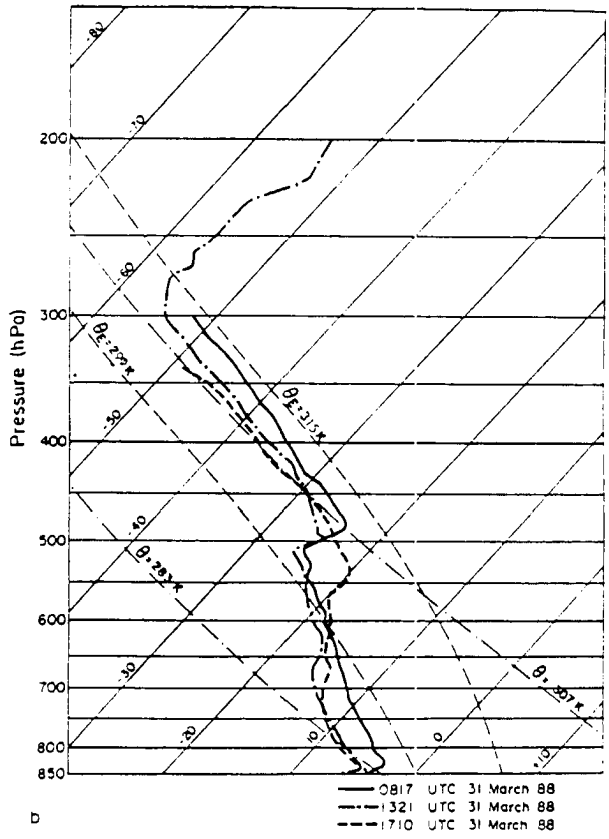

Figure 1.7: (b) CLASS temperature profiles for the final three balloon releases at CHR, for the 30-31 March 1988 storm.

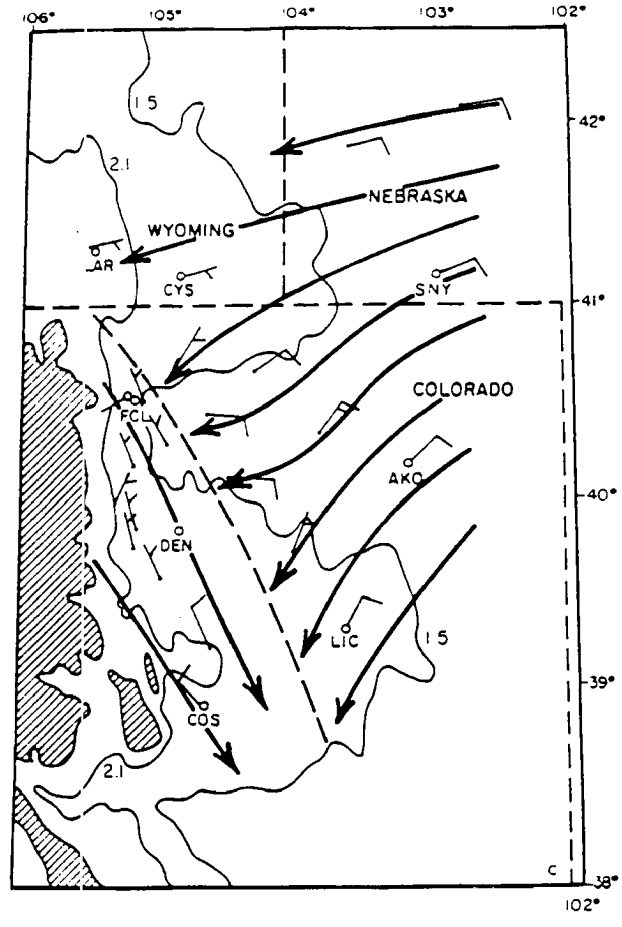

Figure 1.8: Streamline analysis for 0100 UTC 31 March 1988. Convergence line denoted by heavy dashed line.

south, *may* occur during these events; when present, northerly to northwesterly flow may reach speeds of 10 to 20 m s^{-1} to the west of the convergence line (the 5-7 March event during WISP year 1 is an excellent example; see Marwitz and Day, 1991). The barrier jet may occasionally serve as the primary forcing of precipitation, as easterly flow rides over the jet. In some warm cases, melting processes significantly enhance low-level convergence. As Wesley and Pielke (1990) report, however, for many situations the blocking is of shorter duration and much less pronounced, but can still cause strong localized convergence.

Lilly (1981) presented Doppler radar and meso-network observations of an upslope snowstorm over the Front Range on 9-10 February 1981. This storm, similar to the 10-11 February 1988 case study in this paper (Chapter 3), involved the invasion of a low-level arctic air mass as heavy snow fell over portions of the Front Range, with blocking-induced convergence and precipitation upstream over the adjacent plains. Significant entrainment through the inversion at the top of the arctic air characterized the dynamics of the storm. The Doppler radar radial velocity field revealed small (on the scale of a few km) elongated regions of enhanced velocity both near the surface and aloft. The zone of westerlies aloft apparently served as an important source of precipitation particles.

The second major storm type in eastern Colorado is the prolonged arctic outbreak, which was clearly pronounced during the 1-5 February 1989 event in eastern Colorado. Frequently, frigid low-level air masses become trapped east of the Rocky Mountain barrier (Cotton and Anthes, 1989). Wesley *et al.* (1990) describe in detail a case study of such an event; it is briefly summarized here and addressed in detail in Chapter 3. Heavy snow fell along the Front Range in this case despite surface temperatures averaging -20 to $-30°C$ and strong west-southwesterly winds at and above 700 mb. This unique situation contradicted traditional theories concerning snow systems in this region; specifically, the requirement of moisture advection aloft from the south for the rain-shadow effect of the Rocky Mountain barrier to be negated (Reinking and Boatman, 1986) so that significant precipitation can occur to the east. Figure 1.9 is a sounding released at DEN during the developing stages of the arctic outbreak. Note the intense low-level inversion and southwesterly flow aloft. The arctic air mass was firmly entrenched along the eastern slope

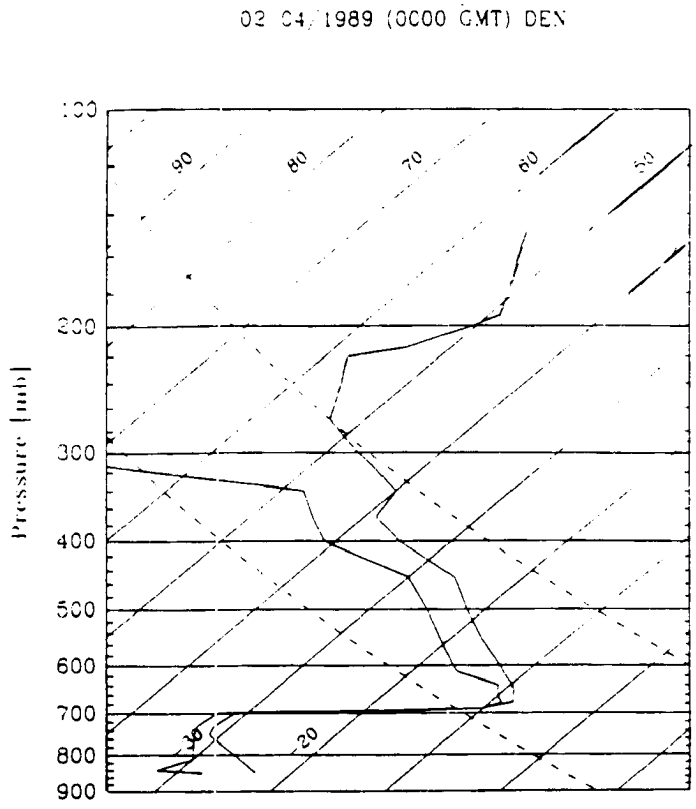

Figure 1.9: (a) Skew-T diagram for Denver's Stapleton Airport (DEN) radiosonde data at 00 UTC on 4 February 1989. Isotherms (°C) are the diagonal solid lines running upward from left to right. Dotted lines are selected dry adiabats.

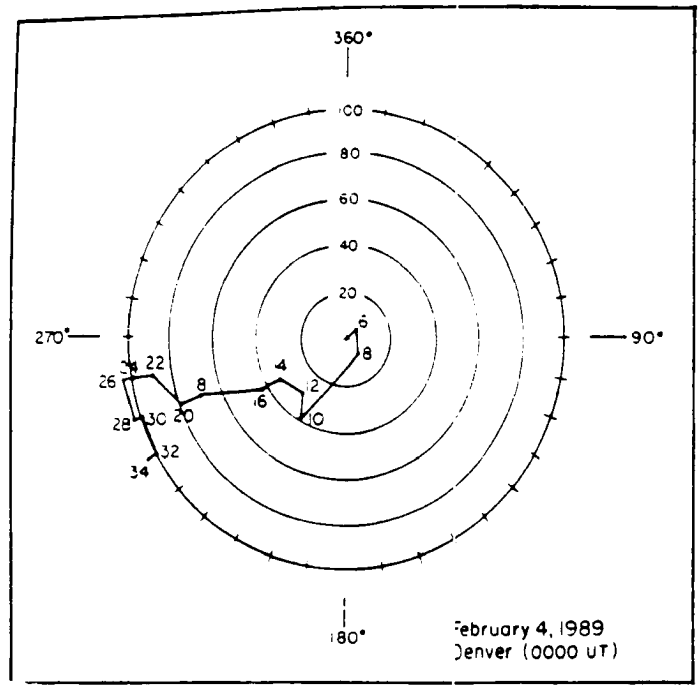

Figure 1.9: (b) DEN hodograph at 00 UTC on 4 February 1989. Wind speeds are labeled on the endpoints in knots. Heights along the profile are in thousands of feet, MSL.

of Colorado, but was occasionally significantly deeper close to the foothills, apparently due to blocking of accelerating upslope flow. Heaviest snowfall occurred beneath the western edge of the cold air mass. The well-defined stable layer was of sufficient depth to prevent downslope winds from developing in the lower atmosphere to the lee of the barrier. Downslope winds did not reach the surface east of the mountains for several days, and the intense upsloping arctic cold pool over the Front Range was the major preventative factor. A significant correlation occurred between snowfall intensity and both an increasing cold pool depth and moisture advection aloft. Model simulations indicate that the interaction between the western edge of the cold pool and the overrunning westerly flow induced deep tropospheric ascent in a narrow vertical zone. This is discussed further in Chapter 4.

1.3 Modeling Experiments

Mesoscale modeling studies of these storms have been limited in number due to the complexity and scale interaction typically present in Colorado snowstorms. NMC-based models such as the Nested Grid Model (NGM) are well known to have serious problems with those wintertime systems including low-level inversions. The modeling studies of Wesley and Pielke (1988) and Wesley *et al.* (1988) successfully simulated blocking and subsequent upstream microphysical enhancement for a horizontally homogeneous initialization, using an actual pre-storm sounding. Similar results were obtained in the two-dimensional simulations of Peterson *et al.* (1991), although the inherent three-dimensional nature of topographical effects was not addressed. They investigated the upstream effects of the Park Range in the Rocky Mountains on precipitating *westerly* flow. In the case of strongly blocked or decoupled low-level flow, significant upward motion and condensation occurred well upstream of the initial terrain ascent.

The lack of larger-scale effects on the simulations in all of these studies prevented a realistic assessment of the interaction between the upslope flow and the terrain. The recent advances in computing capabilities at NCAR and research efforts at CSU have enabled RAMS to include interactive nesting and non-homogeneous initialization, thereby permitting sufficient model resolution of these mesoscale features while at the same time

retaining larger-scale influences. The modeling portion of this investigation consisted of a series of mesoscale model simulations employed to test the sensitivity of snowfall distributions to various topographical effects. Table 1.1 lists the various physical processes considered in this study, along with the most relevant model-predicted fields.

Table 1.1: RAMS Winter Storms Studies.

Process	Key model field
cold-air damming	low-level stability, low-level wind profile, topography
seeder/feeder	moisture profile
evolution of inversion at the top of cold pool	wind profile, turbulence parameterization
precipitation	stability, wind profile, topography, moisture
evaporation	low-level moisture profile
mountain waves	wind profile, topography, low level stability
aggregation	temperature aloft, moisture profile, crystal habit parameterization
riming	ice nuclei concentration, temperature profile
frontal lifting	stability, wind profiles
large-scale storm evolution	model initialization and boundary conditions

Wesley *et al.* (1988) presented mesoscale model simulations of terrain blocking of low-level easterly flow along the Colorado Front Range using the pre-storm DEN sounding of 30 March 1988. Though limited by the horizontally homogeneous initialization in those simulations, low-level cooling and deceleration of easterly surface winds occurred with initially slightly stable conditions near the ground. A mesoscale high pressure zone developed over and immediately adjacent to the foothills (see Figure 1.10). Convergence, upward motion and microphysical enhancement in ice crystal and aggregate concentrations were noted **east** of the foothills near the Denver region at an approximate height of 1.5 km (see Figure 1.11), which agreed qualitatively with the observed storm development. The experiment demonstrated the potential of the RAMS to investigate cold-air damming in this region. However, the model was not able to capture the evolution of the topographical effects. Thus, it could not produce a successful simulation of actual local measurements

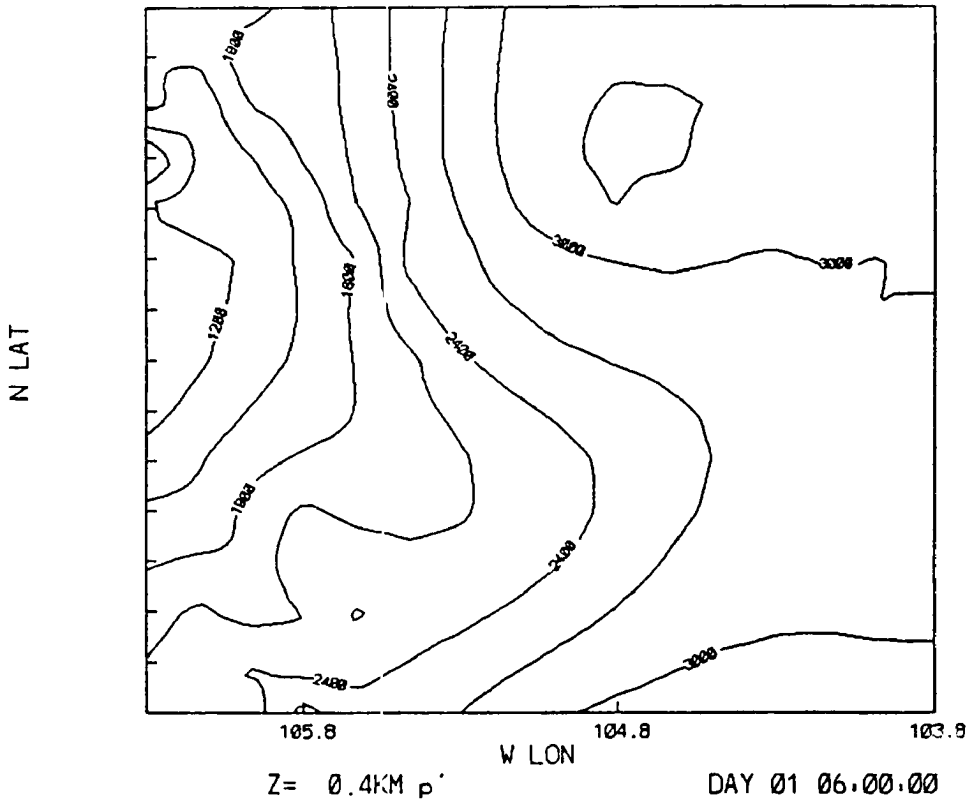

Figure 1.10: Model-predicted pressure perturbation (microbars) at 0.4 km for an $x - y$ cross section. Latitude range along the ordinate is 38.5° to 40.7°.

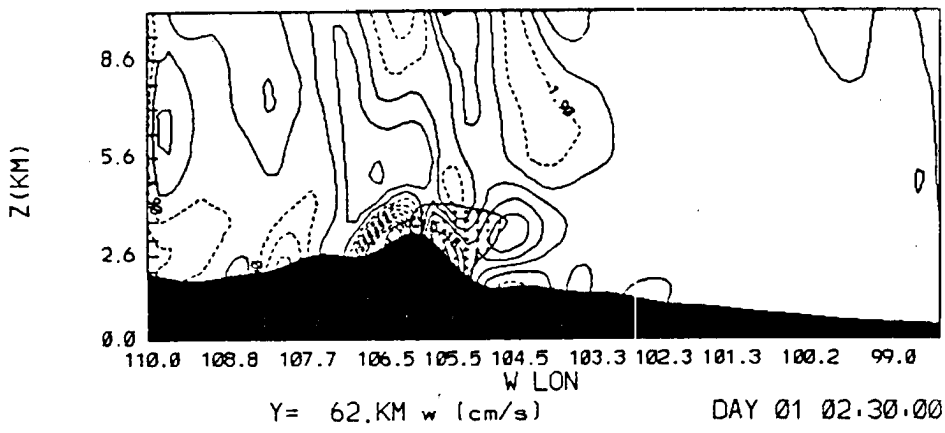

Figure 1.11: Model-predicted w field (cm s^{-1}) for an $x - z$ cross section. Hatched region is cloudy.

of surface wind and thermodynamic data, and vertical CLASS profiles. A major problem with these simulations was the initialization, which was horizontally homogeneous. An initialization utilizing the standard wind and thermodynamic fields in the NMC data set covering a much larger domain is required in order to reproduce observations in this region. Synoptic-scale influences are frequently critical in setting the stage for the mesoscale circulations to develop. In order to capture the effects of terrain on the large-scale flow, the model must simulate the full temporal and spatial evolution of this flow. These effects are manifested on the meso-γ scale.

Other relevant modeling studies have been undertaken during the past decade. The Abbs and Pielke (1987) investigation utilized the three-dimensional mesoscale model developed in Pielke (1974), and Mahrer and Pielke (1977) to isolate the importance of terrain forcing in selected upslope snowstorms in Colorado. The capabilities of this model were incorporated into the RAMS structure. The simulations included two major snowstorms (23-25 December 1982 and 8-9 December 1985) where terrain-induced ascent under different prevailing surface wind directions led to distinctly different snowfall distributions (Figures 1.12 and 1.13). Specifically, the former case, where strong northeasterly winds prevailed at 850 mb, exhibited observed maximum snowfall on the north side of the Palmer Divide. The latter case, in which southeasterly 850 mb flow dominated, led to heavy snowfall on the south side of the Cheyenne Ridge.

Mesoscale model simulations for both cases produced enhanced low-level vertical motions due to terrain which corresponded well with the areas of maximum snowfall. For the December 1985 case, model input moisture contents in the lowest 3 km apparently were critical to the actual snowfall distribution. A trough moving southward through the Front Range region was successfully simulated and produced strongly enhanced regions of ascent in agreement with the snowfall distribution (Figure 1.14); the presence of the trough was necessary to qualitatively reproduce the observations. The southward progression of the trough was blocked by the Palmer Divide, thereby concentrating maximum ascent rates on the southern slopes of the Cheyenne Ridge. The blocking effect of the Palmer Divide was not quantitatively evaluated, however. This finding again emphasized the need to include large-scale effects in simulations of these storms.

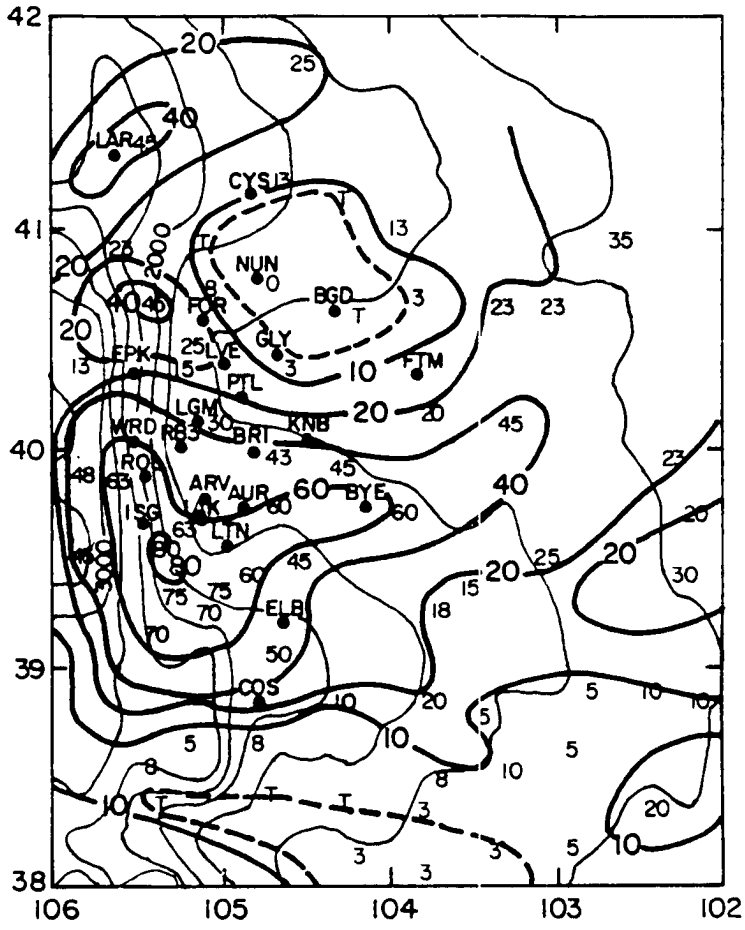

Figure 1.12: Snowfall distribution (cm) for the Colorado Front Range, 23-25 December 1982.

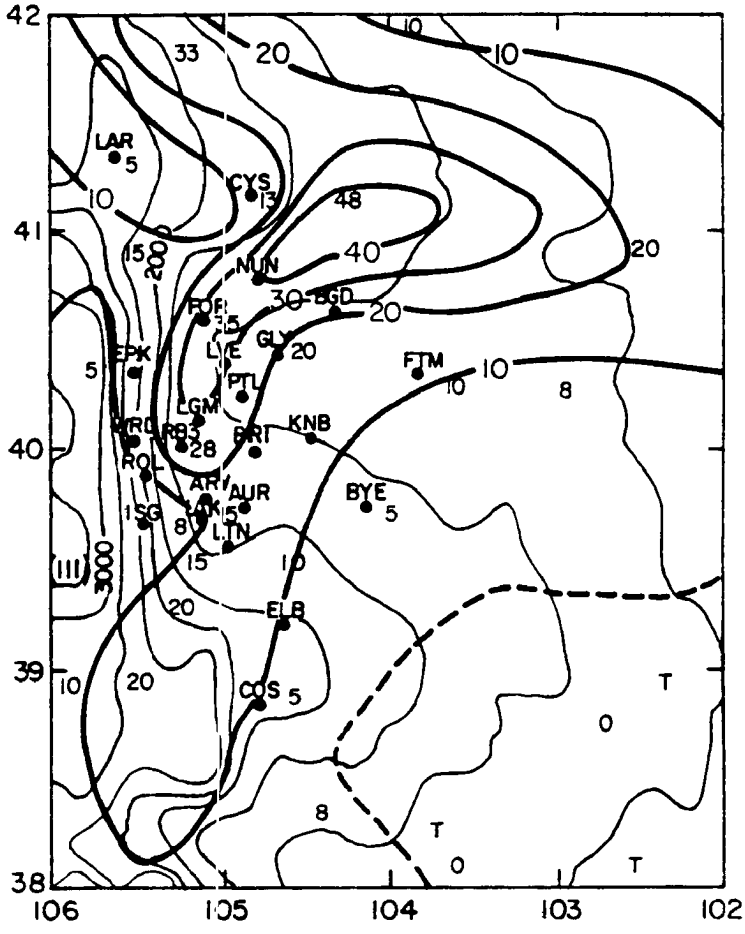

Figure 1.13: Snowfall distribution (cm) for the Colorado Front Range, 8-9 December 1985.

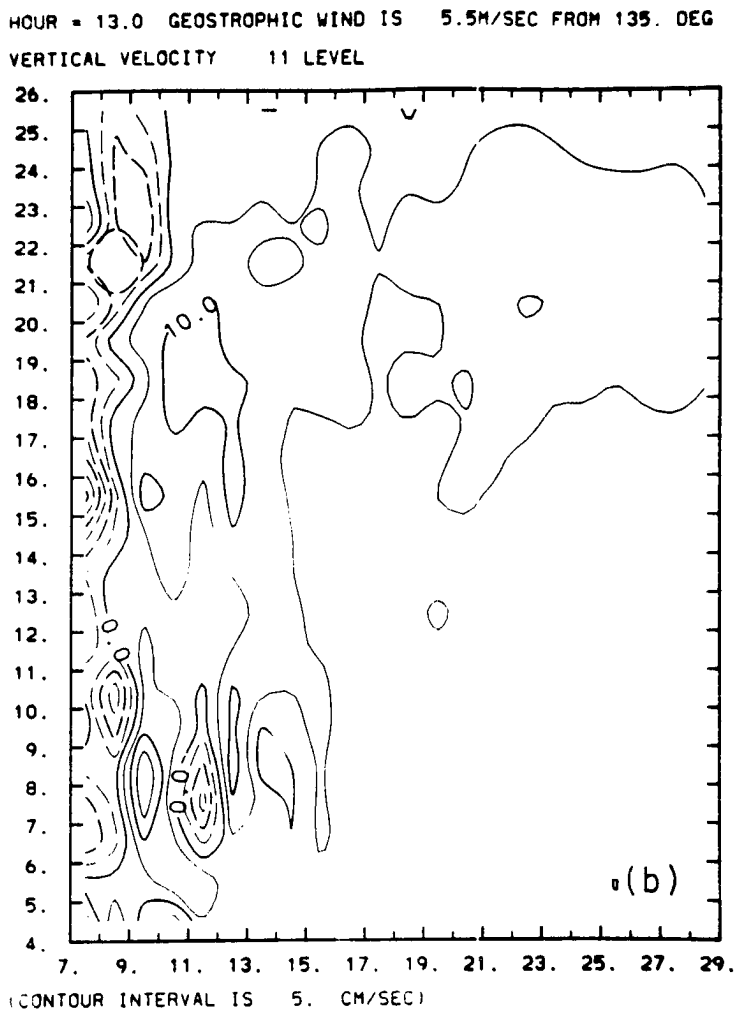

Figure 1.14: Model-predicted w field (cm s^{-1}) at 1.35 km. Adapted from Abbs and Pielke (1986).

The Lee *et al.* (1989) study focused on the interaction of mesoscale cold air masses and the ambient synoptic flow to the lee of the Rocky Mountains. It included the simulation of a coupling mechanism between a pool of cold air east of the Colorado Rockies and the synoptic flow aloft. In these dry simulations, the cold air remained trapped until surface low pressure to the east of the mountains caused flushing. Furthermore, the cold and stable pool of air modified the mountain waves in the overlying flow very significantly, not only near the surface but also aloft. Essentially, and very importantly, the top of the cold pool acted very much like terrain with a similar shape. Such a finding has direct implications toward anticyclonic upslope circulations associated with arctic air masses entrenched against the Front Range of the Rockies during winter, and the resulting snowfall distribution. This phenomenon played a key role in the development of the 1-5 February 1989 storm, which is discussed in detail in Chapters 3 and 4.

Arritt *et al.* (1987) simulated the well-documented mesoscale Denver cyclonic circulation, or convergence zone, which develops in a stably stratified environment with southeasterly surface winds (see also Wilczak and Christian, 1990). They examined the temporal evolution and vertical structure of the convergence zone, including the role of the ambient wind. The model sensitivity experiments discovered a diurnal dependence of the circulation, as well as the requirement of a southerly component in the surface large-scale wind field. In Abbs and Pielke (1986), mesoscale model simulations of the development during the summer of the Denver convergence-vorticity zone due to the presence of elevated terrain were presented (see Figure 1.15). However, this study did not attempt to address the role of blocking. The convergence zone has been associated with wintertime systems (Dunn, 1987 and Szoke, 1991), and exhibits some similarity to the meso-front induced by cold-air damming, which typically extends northward to the Wyoming border. A similar phenomenon, albeit anticyclonic, occurs to the lee of the Cheyenne ridge (but with northerly component synoptic flow), and can also create areas of low-level convergence during winter storm circulations.

In the present investigation, portions of the extensive observational data set collected for two major storms along the Front Range serve as model initialization. As preliminary

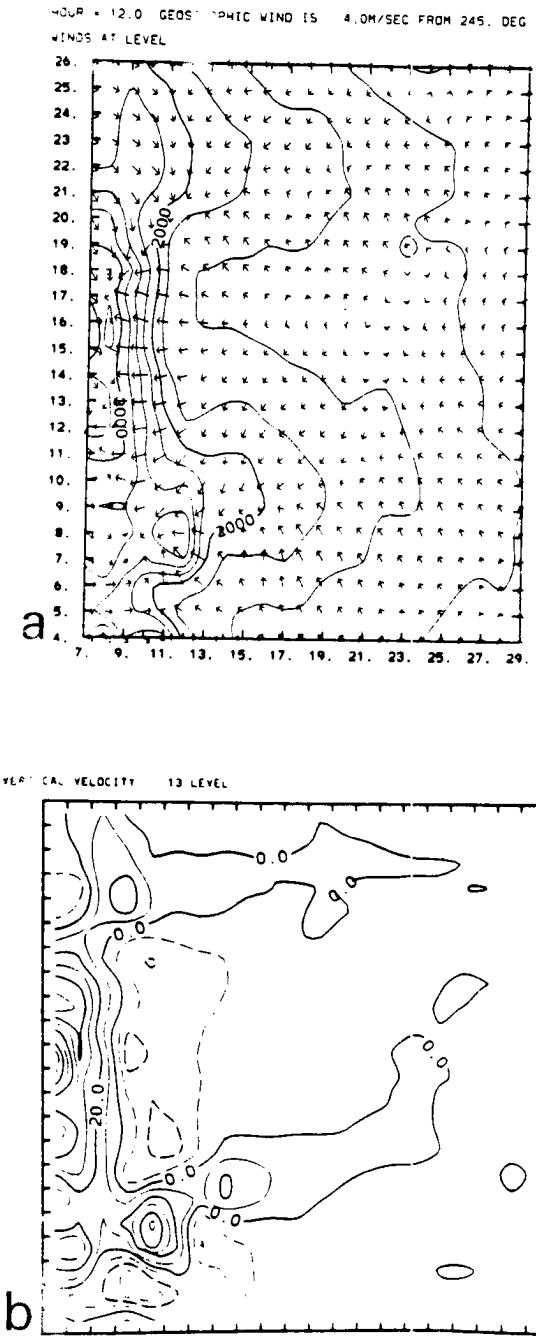

Figure 1.15: Model-predicted (a) surface wind vectors, and (b) w field (cm s^{-1}) at 1.35 km. Adapted from Abbs and Pielke (1986).

simulations, two-dimensional, initially horizontally homogeneous runs are performed. Subsequent RAMS simulations utilize three-dimensional computations, with full microphysics and nonhomogeneous initial fields. Through comparison of model results with observations, a preliminary assessment is made of the ability of RAMS in the latter mode to simulate a winter storm in complex terrain.

1.4 Snow Spotter Network

An important component of the data collection for this study was an extensive snow spotter network, centered on the Fort Collins/Boulder area, measuring snow accumulation and snow crystal types observed at the ground. This data source was particularly important in the analysis of the microphysical processes within and between snowbands. Approximately 50 spotters comprised the program for the 1987-89 winters. At time intervals of one to six hours, spotters measured snow intensity, accumulation, liquid equivalent and standard surface meteorological data (temperature, wind, etc.), as well as snow crystal type (e.g. dendritic, platelike, graupel, etc.), size, and degree of riming and aggregation. These measurements were made primarily only during significant snowfall at the spotter's particular location. Coupled with CLASS profiles and Doppler radar measurements, these data were critical for the evaluation of the thermodynamic structure in the precipitation regions in these cloud systems, as crystal habit was closely related to temperature and moisture characteristics in the cloud (Pruppacher and Klett, 1980). The snow measurements were also critical to RAMS model validation of precipitation type and intensity. This was an important test of the microphysical parameterizations in the model.

Horizontal spacing between the 50 or so spotters in the region was highly variable due to the volunteer nature of the program. This spacing ranged from a few km in the immediate Fort Collins vicinity to 50-75 km well east of the I-25 corridor (e.g. the Akron area).

Chapter 2

COLD-AIR DAMMING: A CASE STUDY

The topography in Figure 1.2 shows several important features along the Front Range, such as the formidable Rocky Mountain barrier located approximately 50 km to the west. The Cheyenne Ridge and Palmer Divide (labeled A and B, respectively, in Figure 1.2) are east-west ridges on the plains which create 0.6 km north-south variations in elevation. The orientation of the foothills is approximately north-south from just west of FCL to southwest of DEN. All of these topographical features have direct influences on low-level upslope, easterly flow (Toth, 1987) which develops during the approach and passage of a synoptic-scale disturbance from the west or southwest. For example, blocking-induced convergent motion and precipitation can occur on sloping plains well east of the foothills (Lilly, 1981, and Schultz *et al.*, 1985).

2.1 Evidence of Blocking

The storm of 30-31 March 1988 along the Front Range, which deposited approximately 60 cm (two feet) of snow in the northern portion (Figure 1.3) was characterized by a similar dynamic structure to the 8-9 December 1985 situation reported by Dunn (1987). Note the extension of heavy snowfall onto the plains just east of the foothills near the FCL area. On the synoptic scale, at 1200 UTC 30 March, an amplifying shortwave was evident on the 500 hPa Nested Grid Model (NGM) analysis centered over east-central Nevada. By 0000 UTC 31 March, snowfall was increasing in intensity in the northern portion of the Front Range. At this time, the 700 hPa analysis revealed a cutoff low just north of the Four Corners region; the surface low pressure, centered in central New Mexico, was pumping warm, moist air into Colorado from the southeast. Winds were easterly at the

surface in northeastern Colorado (and approximately parallel to the isobars east of the Front Range). At 1200 UTC 31 March (see Figure 2.1), when snowfall intensity at FCL was very heavy, the 500 hPa analysis indicated a strong, negatively tilted cutoff low over north-central Arizona, with weak positive vorticity advection in northeastern Colorado. The corresponding 700 hPa low center was located just to the east (Figure 2.1b), with east-southeasterly, moist flow over the area of interest. The 850 hPa analysis (Figure 2.1c) indicated a strong low just south of the Four Corners, with very strong easterly flow over northeastern Colorado. A weak wedge or nose of low-level high pressure existed over the Front Range at this time (dotted line in Figure 2.1d) according to the mean sea level pressure NMC analysis. This ridging was the result of the development of a cold pool of air against the foothills as both adiabatic cooling and cold advection characterized the low-level flow in this region. The cooling created slightly higher surface pressures along the Front Range than in regions to the east. Such an anticyclonic feature in the isobars occurred also in Dunn's December 1985 storm.

Figure 2.2a-d presents the surface streamline analyses for the PROFS meso-network during the early stages of the storm (on the evening of 30 March). Figure 2.3a-d presents the corresponding temperature and dew point analyses. The analyses indicate the initiation of a quasi-stationary convergence line due to the establishment of a stably stratified, low-level cold pool over and just east of the foothills. This line developed as the cold pool induced uplift of the upstream easterly flow. The meso-front is similar to the one analyzed in Dunn (1987; his Figures 13 through 18), and exhibits characteristics similar to coastal fronts on the U.S. east coast, which mark the eastern edge of overrunning (see, for example, Bosart, 1975).

At 0100 UTC 31 March (Figure 2.2c), the northeasterly flow (speeds approximately 2.5 to 7.5 m s^{-1}) on the plains converged with north-northwesterly flow (2.5 to 5.0 m s^{-1}) along a northwest-southeast line indicated by the heavy dashes. This orientation was in some contrast to Dunn's north-south line, and determined to some degree the location of heaviest snowfall. Maximum convergence occurred along the northernmost portion of the meso-front (near FCL). The presence of colder air to the west of this line was readily

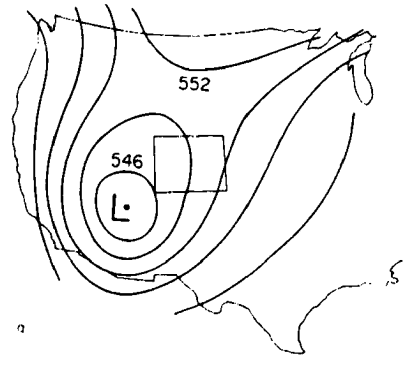

Figure 2.1: (a) National Meteorological Center (NMC) height analysis for the 500 hPa surface at 1200 UTC 31 March 1988. Heights are in dm. The state border of Colorado is outlined.

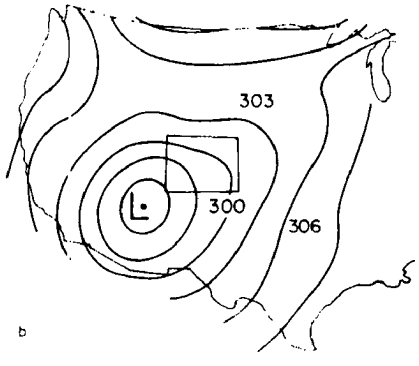

Figure 2.1: (b) Same as (a) except for the 700 hPa surface.

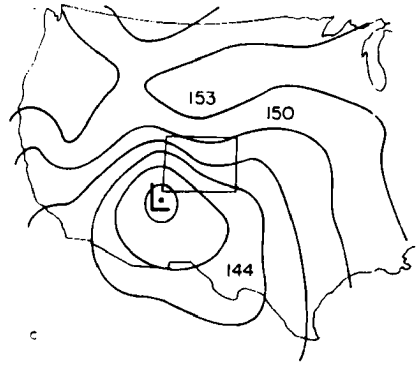

Figure 2.1: (c) Same as (a) except for the 850 hPa surface.

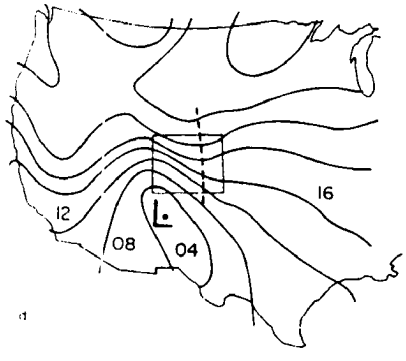

Figure 2.1: (d) NMC mean-sea level pressure (hPa) analysis for 1200 UTC 31 March 1988. Heavy dashed line is a convergence line (see text).

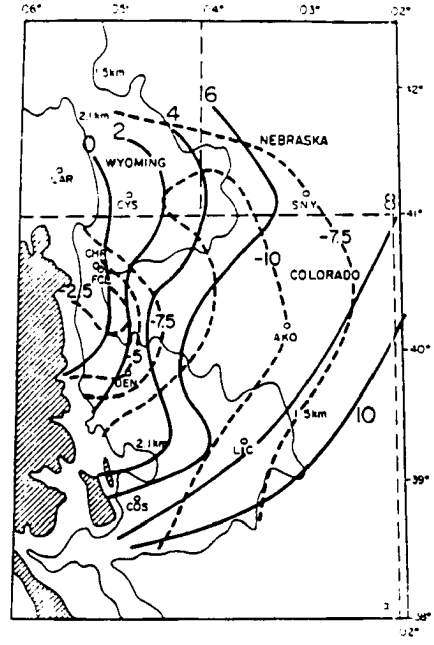

Figure 2.3: (a) Surface meso-analysis of temperature (°C; solid lines) and dew point (°C; dashed lines) over the PROFS meso-network (see text) at 1900 UTC 30 March. Extreme northern and southern portions of the figure are not analyzed due to lack of data. Elevations, station identifiers, etc. are as in Figure 1.2.

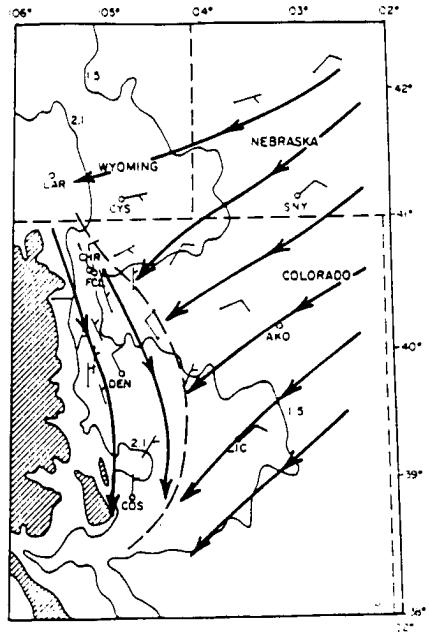

Figure 2.2: (b) As in Figure 2.2a except for 2200 UTC 30 March 1988. Convergence line (see text) is shown as a heavy dashed line.

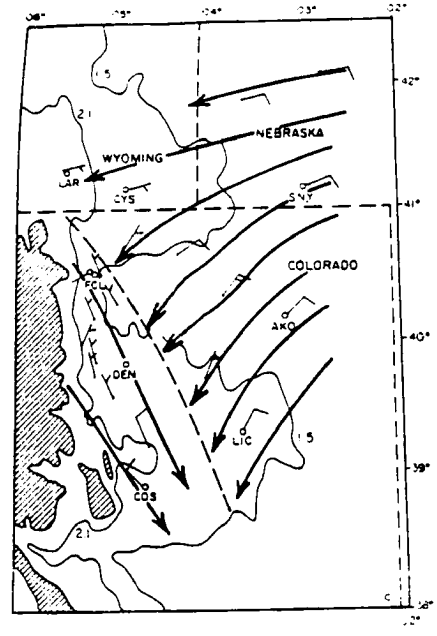

Figure 2.2: (c) As in Figure 2.2a except for 0100 UTC 31 March 1988. Convergence line (see text) is shown as a heavy dashed line.

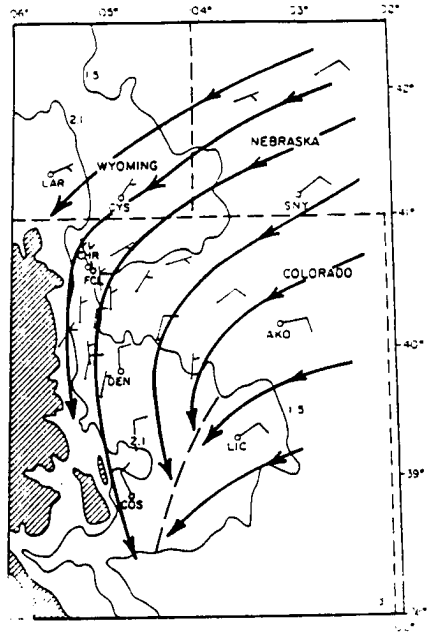

Figure 2.2: (d) As in Figure 2.2a except for 1800 UTC 31 March 1988. Convergence line (see text) is shown as a heavy dashed line.

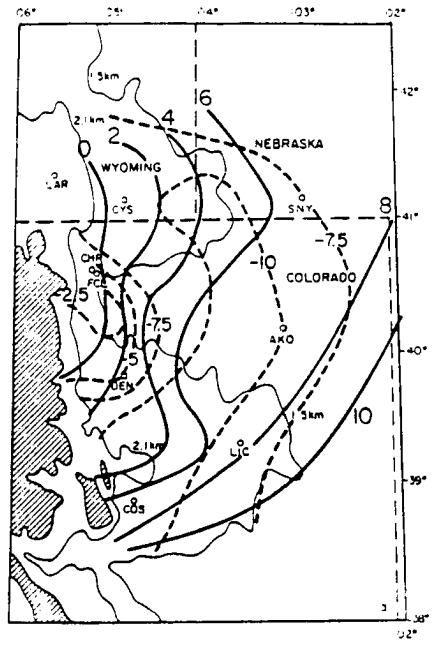

Figure 2.3: (a) Surface meso-analysis of temperature (°C; solid lines) and dew point (°C; dashed lines) over the PROFS meso-network (see text) at 1900 UTC 30 March. Extreme northern and southern portions of the figure are not analyzed due to lack of data. Elevations, station identifiers, etc. are as in Figure 1.2.

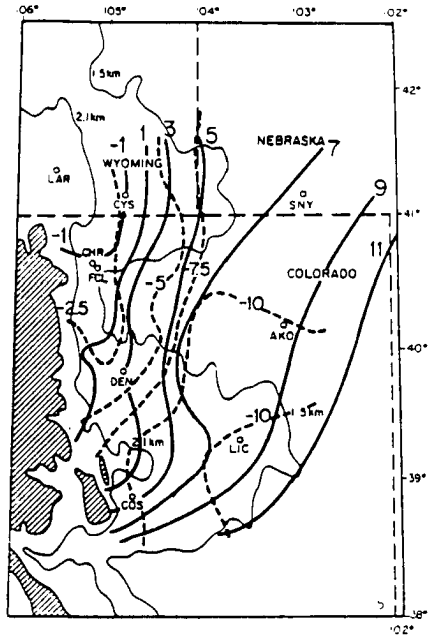

Figure 2.3: (b) Same as (a) except for 2200 UTC 30 March 1988.

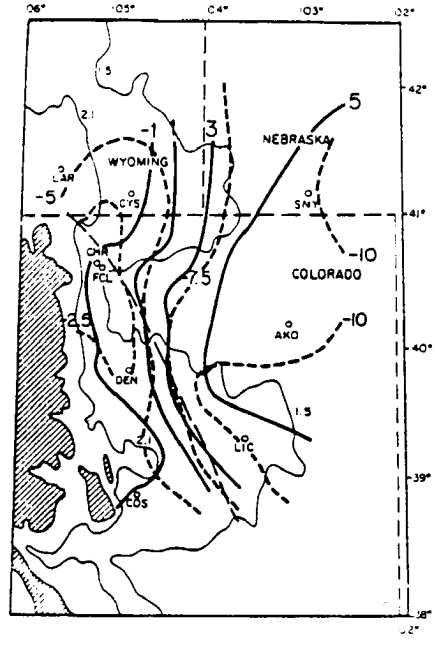

Figure 2.3: (c) Same as (a) except for 0100 UTC 31 March, 1988.

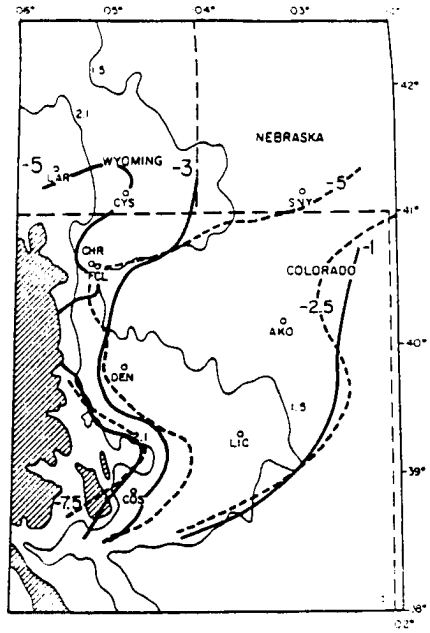

Figure 2.3: (d) Same as (a) except for 1800 UTC 31 March, 1988.

apparent (e.g. Figure 2.3b), as was a tendency for the line to move southeastward (Figure 2.2d) during the latter portion of the storm; both of these characteristics were noted by Dunn. The wind speeds were generally weaker by 2.5 to 5.0 m s^{-1} in the present case. The snow intensity measurements are shown in Table 2.1.

Table 2.1: Snowfall intensity and wind observations at Christman Field for the 30-31 March 1988 storm.

Time, UTC	snowfall intensity†	wind direction	wind speed (m s^{-1})
1715	M	E	1.5
2300	L	NNW	2.5
0130	M	ENE	5.0
0200	H	N	2.5
0230	M	N	5.0
0430	M	NW	5.0
0530	H	NW	6.5
0600	H	NE	5.0
0700	H	WNW	5.0
0830	H	NW	6.5
0900	H	NE	5.0
1330	H	NW	6.5
1400	H	NW	6.5
1730	L	NW	5.0

†Snowfall intensities are based on horizontal visibility V.
H = heavy: V less than 0.6 km
M = moderate: V greater than 0.6 km but less than 1.2 km
L = light: V greater than 1.2 km

The low-level wind pattern during the height of this storm (see Figure 2.2c) bears strong resemblance to the numerical model results reported in Crook *et al.* (1990). In their Figure 14b, low-level flow with an easterly component over the eastern Colorado plains, turns abruptly toward the south over and near the foothills due to blocking-induced deceleration and geostrophic adjustment. Low $Fr(\approx 0.2)$ characterized the upstream flow as it approached the Continental Divide.

In Figure 2.4, surface potential temperature values are contoured for the PROFS mesonet. The cold pool to the west of the convergence line is readily apparent. Incoming

low-level easterly flow (Figure 2.3b) encountered a strong θ gradient directed east-west in the northern portion of the mesonet, inducing low-level ascent in this region.

During the early portions of the storm on the evening of 30 March, surface observations taken at CHR indicated oscillations of wind direction from easterly to northwesterly; these seemed to have an approximate period of a few hours (see Table 2.1). The convergence line may have been crossing the area during this time, producing changing wind directions. Examination of the surface analyses in Figure 2.2 revealed some movement of the convergence line with time. Snow intensity observations taken at the same times also indicated some oscillation from moderate to heavy, although not clearly in phase with the wind direction. Generally, heavy snow was observed at CHR during the brief periods of northwest winds. This observation is not surprising, considering the vertical storm structure described previously, where lifting along the upper portion of the cold pool was suggested to create the heavy snowfall.

A more detailed look at the vertical structure in this storm is shown in the CLASS soundings in Figures 1.7, 2.5 and 2.6. Special CLASS balloon releases just northwest of Fort Collins, Colorado at Christman Field (CHR) provided vertical profiles of wind, temperature and moisture at two- to three-hour intervals during the storms. These soundings contained data at 50 m intervals in the vertical. Measured vertical profiles associated with the blocked surface patterns revealed a distinctly layered temperature and wind structure. The temperature profiles are in Figure 1.7a-b, with Figures 2.5 and 2.6 presenting the observed wind and relative humidity profiles for the storm. The vertical profile at 0427 UTC in Figure 1.7a was measured during the first few hours of moderate to heavy snowfall in FCL. As shown, three distinct layers of the atmosphere are apparent:

1. a shallow low-level layer of cool air (west of the convergence line shown in Figure 2.2c) exhibiting weak northwesterly surface winds and stable conditions (approximately 840 to 810 hPa),

2. a moist mid-level easterly upslope flow (810 to 570 hPa) which includes a potentially unstable layer from 810 to 770 hPa, and

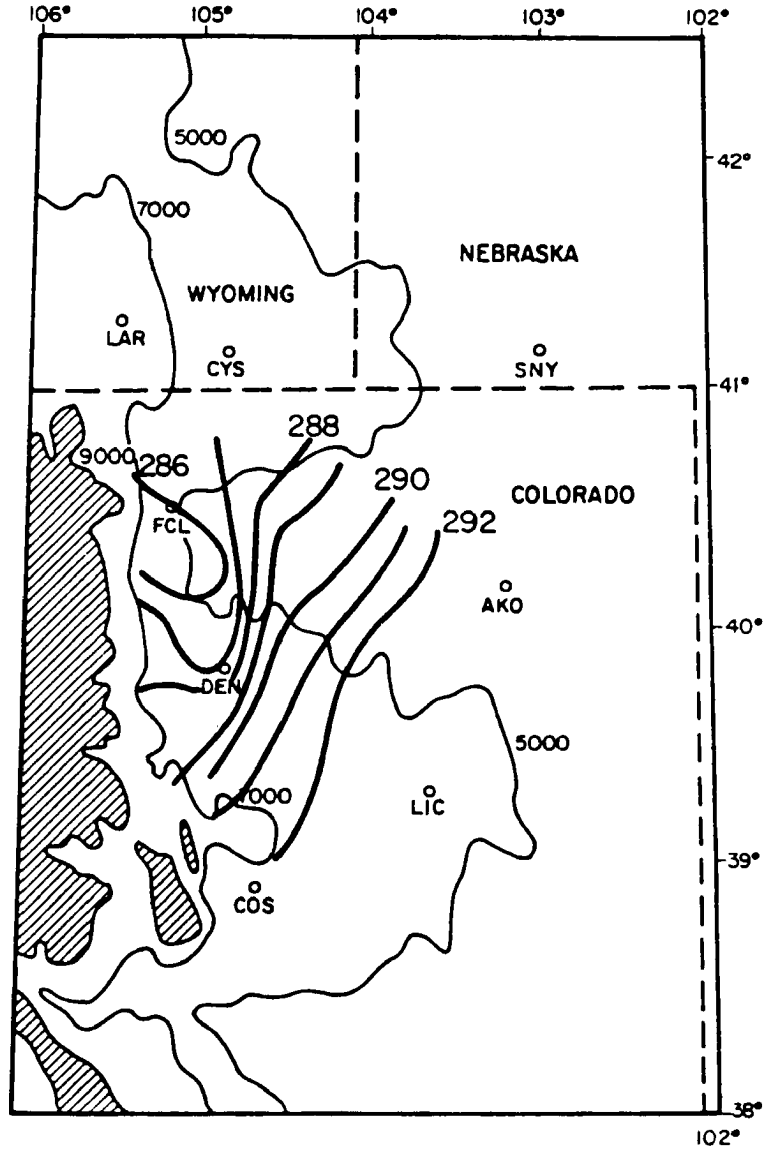

Figure 2.4: Surface θ (K) analysis at 0100 GMT on 31 March 1988.

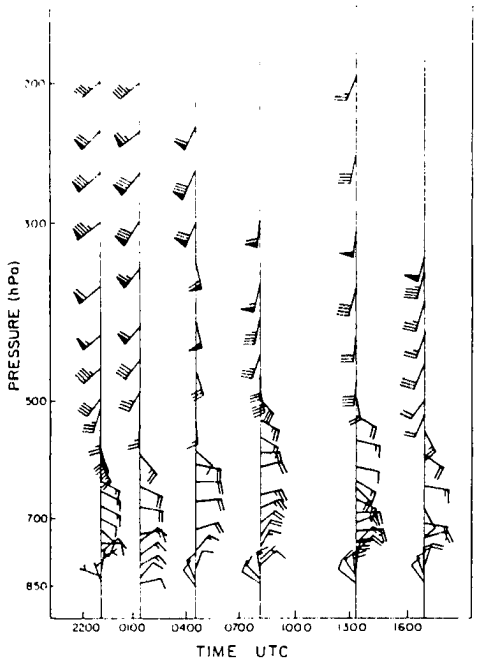

Figure 2.5: CLASS wind profiles for the 30-31 March 1988 storm. One full wind barb equals 5 m s^{-1}; one flag equals 25 m s^{-1}.

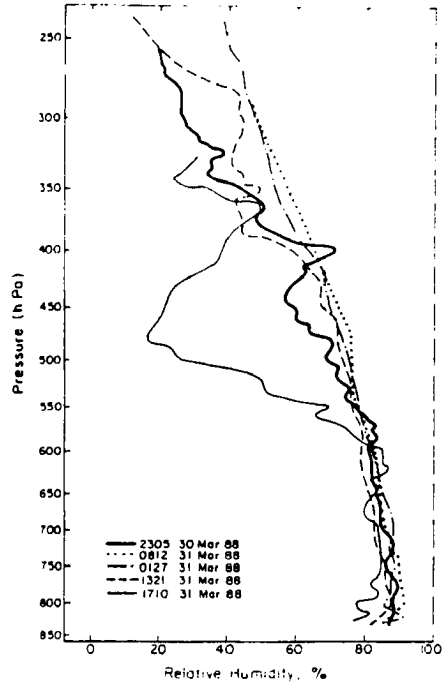

Figure 2.6: CLASS relative humidity profiles for the 30-31 March 1988 storm.

3. a moist upper layer consisting of strong southerly winds (above 570 hPa); this layer represents the synoptic flow around the cutoff low pressure system to the southwest.

The first four soundings in this storm, shown in Figure 1.7a-b and spanning nine hours, are characterized by this layered structure.

Thus layer 2, dammed by the cold pool, overrides layer 1, creating enhanced vertical motions in a moisture-rich region. The mid-level easterly flow was persistently moist and strong, reaching approximately 12.5 m s^{-1} near the end of the period of moderate to heavy snow intensity at CHR. This flow may be equivalent to the "cold conveyor belt" which frequently develops in deepening extratropical cyclones (see Carlson, 1980, Cotton and Anthes, 1989, and Iskenderian, 1988). In the Colorado case, this low- to mid-level moist easterly flow was lifted over the dammed layer prior to meeting the steep topography. In addition, very heavy snowfall was also observed over the steep topography (Figure 1.3). Visual observations of cloud base height at 2305 UTC 30 March indicated an approximate value of 1.1 km, or 740 hPa, which corresponds with the lower portion of layer 2 at this time, as shown in Figure 1.7a.

Similarly, layer 3 overrides layer 2. The strong frontal inversion (550 to 500 hPa) developed, strengthened and rose slightly during the storm progression. The moist conditions observed in layer 3 indicated a potential seeder mechanism by this region for the lower layers (Jiusto, 1967, and Reinking and Boatman, 1986). Importantly, crystals nucleated in layer 3 probably did not evaporate while descending into lower layers, and were able to grow to large (2 to 4mm diameter according to surface observations) sizes due to the presence of moist easterly flow from 700 to 650 hPa. Temperatures in layer 2 were conducive to dendritic crystal growth; these temperatures, ranging from $-12°C$ to $-16°C$, occurred in relatively strong (10 to 15 m s^{-1}), moist easterly flow. As noted previously, Auer and White (1982) found that in a vast majority of major U.S. snowstorms, strongest ascent occurred in the dendritic temperature zone.

The snowfall distribution for the storm (Figure 1.3) indicated that intense production and growth of precipitation particles occurred as the layer 2 ascended over layer 1, before

the easterly flow reached the barrier. As shown in Figure 2.2b-d, the surface convergence line separated layer 1 from layer 2, and the demarcation between the layers apparently sloped upward to the west, yielding a cold pool approximately 30 hPa deep over CHR.

In Figure 2.7 the measured θ_E profile is shown for 0427 GMT (see also Figure 1.7a). The layer between 820 and 725 mb is slightly convectively unstable and coincides well with the blocking-induced region of lifting. It is entirely possible that convection induced by this lifting was responsible for a portion of the observed precipitation amounts shown in Figure 1.3, as well as the varying snow intensity observed in Fort Collins (see Table 2.1).

2.2 Doppler Radar Scans

Radial velocity and reflectivity for this storm, via PPI (plan-position indicator) scans at two angles, 0.2° and 0.7°, were supplied by operation of the CP-2 single Doppler radar just southeast of Boulder, Colorado. Figure 2.8 presents a composite of reflectivity scans in an $x - y$ plane at a height of 1 km above the radar for the three hour period between 0640 and 0940 UTC 31 March. This time period, as shown in Table 2.1, coincided with the heaviest snowfall at CHR, a period marked by strong blocking. As shown, an area of markedly enhanced averaged reflectivity, generally located west of the convergence line, corresponded with the overrunning scenario discussed previously and with heaviest snowfall (see also Smart and McGinley, 1989). Cold pool depth at CHR was approximately 200 to 300 m during this time. Averaged reflectivity values exceeded 20 dBz in this region, and this three-hour average showed the quasi-stationary nature of the feature. This enhancement was not a coherent, distinct band, but a band with non-distinct edges over and just east of the foothills. The region was oriented approximately north-south, and extended from DEN to just north of FCL. Other bands of enhancement occurred far to the southeast of DEN and may have been the result of blocking on the north side of the Palmer Divide, but this is inconclusive due to the lack of detailed surface observations in this region.

During most of the precipitation event, narrower, more distinct bands were observed on the reflectivity scans. These bands generally moved rather rapidly east-to-west, and

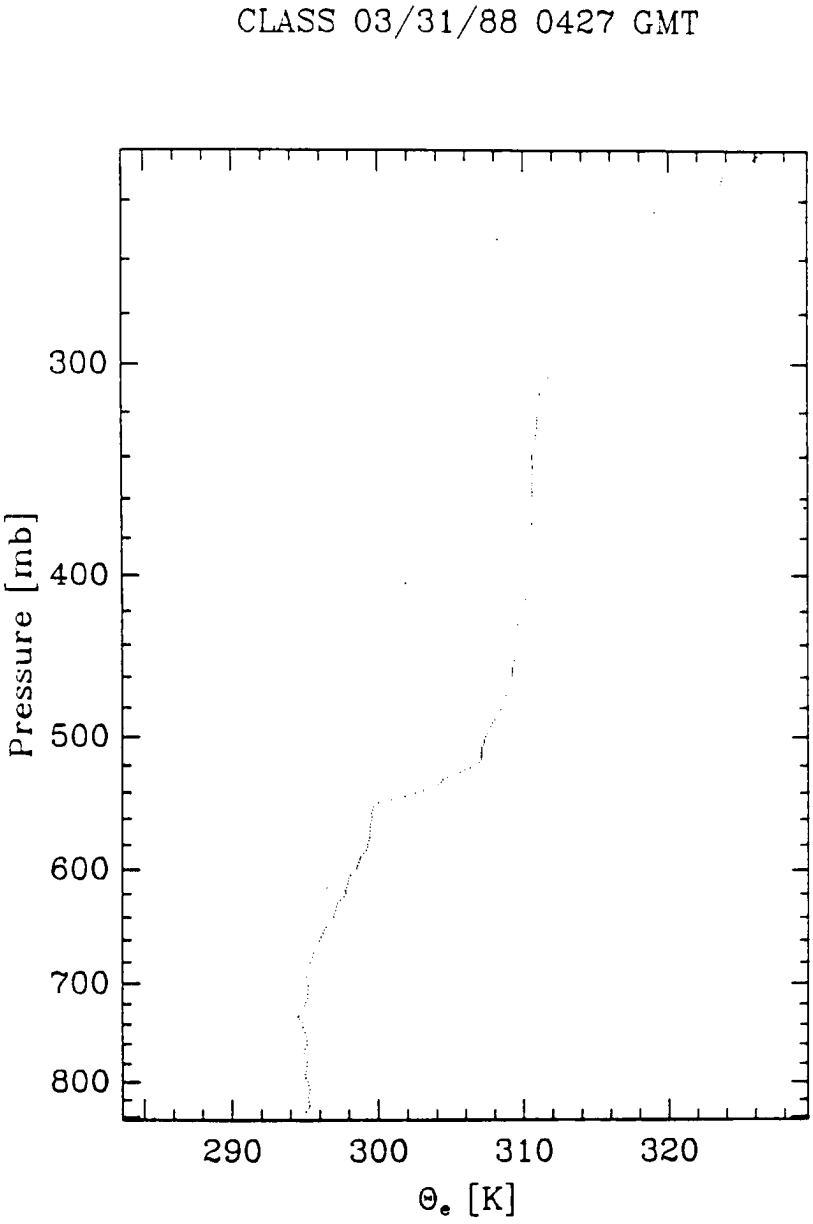

Figure 2.7: θ_E (K) CLASS sounding profile at 0427 GMT on 31 March 1988.

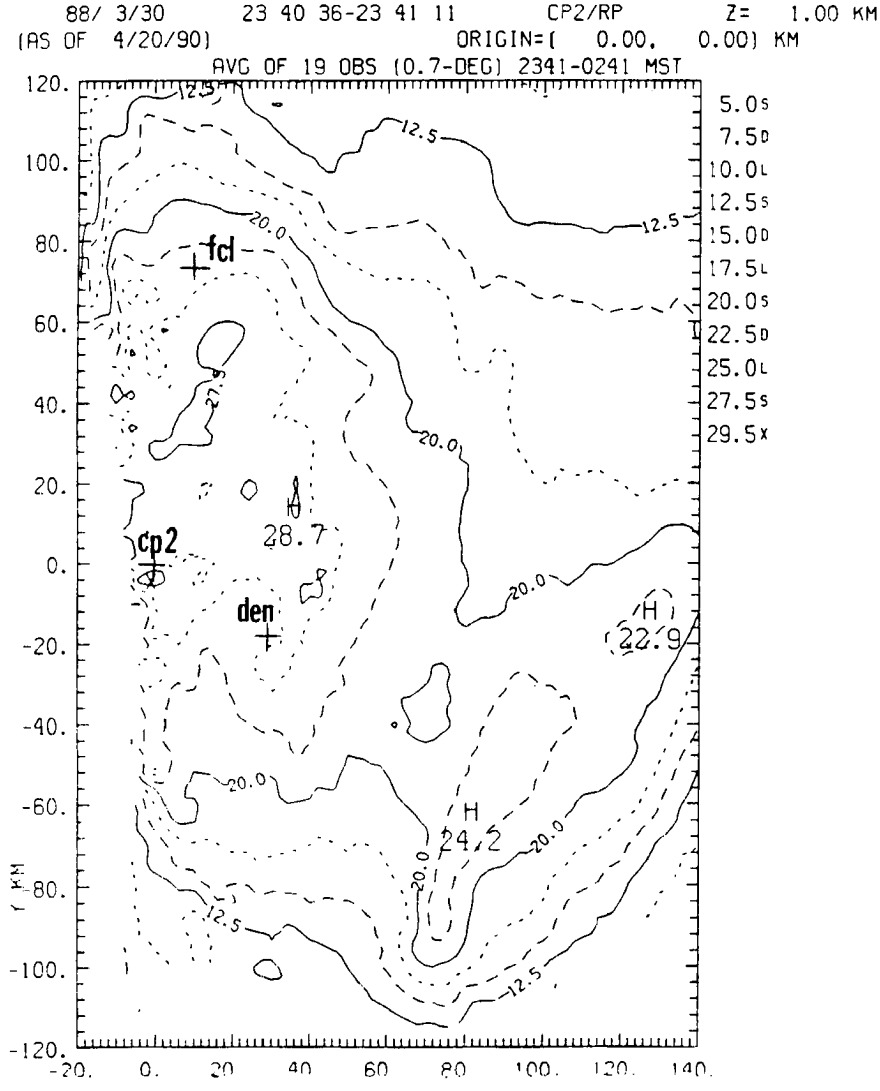

Figure 2.8: Doppler radar reflectivity, 3-hr average 0100 to 0400 UTC 31 March 1988.

were not found to be prolonged heavy snow producers. Figure 2.9 shows an example of a PPI scan at 0920 UTC 31 March 1988. The band east of DEN oriented north-northeast to south-southwest was moving rapidly westward into the wide region of damming-induced enhancement. The mean 700-500 hPa shear vector at CHR (this layer encompasses the upper frontal zone for most of the storm; see Figure 1.7) was oriented approximately north-south at 0800 UTC 31 March. It is entirely possible that larger-scale processes were responsible for the smaller, more transient bands. Generally, the transient bands appeared to be approximately 10 km wide, 25 to 75 km long and traceable for the entire horizontal range of the radar. PPI radar scans at 0.2° showed generally stronger reflectivity maxima than those at 0.7°; thus these precipitation cores may indeed have been generated in the lower regions of layer 2 in Figure 1.7a, as discussed previously. Of course, further snow crystal growth between the two scan levels could have accounted for the difference in reflectivity. The 0.2° scan crosses a vertical column about 250 m above the ground at CHR, and the 0.7° scan at 900m. Stronger reflectivities are thus observed near the upper portion of the cold pool at CHR, and may be related to the enhanced upward motion created as the upslope layer rises over the dammed cold pool.

2.3 The Role of Moisture Content in the Upslope Layer

A critical difference exists in the moisture content of the incoming surface easterly flow (inflow) in the 30-31 March 1988 storm when compared to the 8-9 December 1985 storm presented in Dunn (1987). This difference exerts a major influence on the corresponding snowfall distribution. As shown in Figure 2.3b and c, typical inflow surface temperatures and dew points upstream of CHR were approximately 1 to 2°C and −6 to −4°C, respectively, whereas the corresponding values for the 1985 case were around −2 to 0°C and −4 to −2°C (see Figures 14-16 of Dunn, 1987). The snowfall distribution shown in Figure 1.3 for the Front Range exhibited a snowfall maximum roughly 50 to 80 km west of the average position of the surface convergence line, depending on latitudinal position along the Front Range. In Dunn's case, the maximum occurred just 15 to 30 km west of

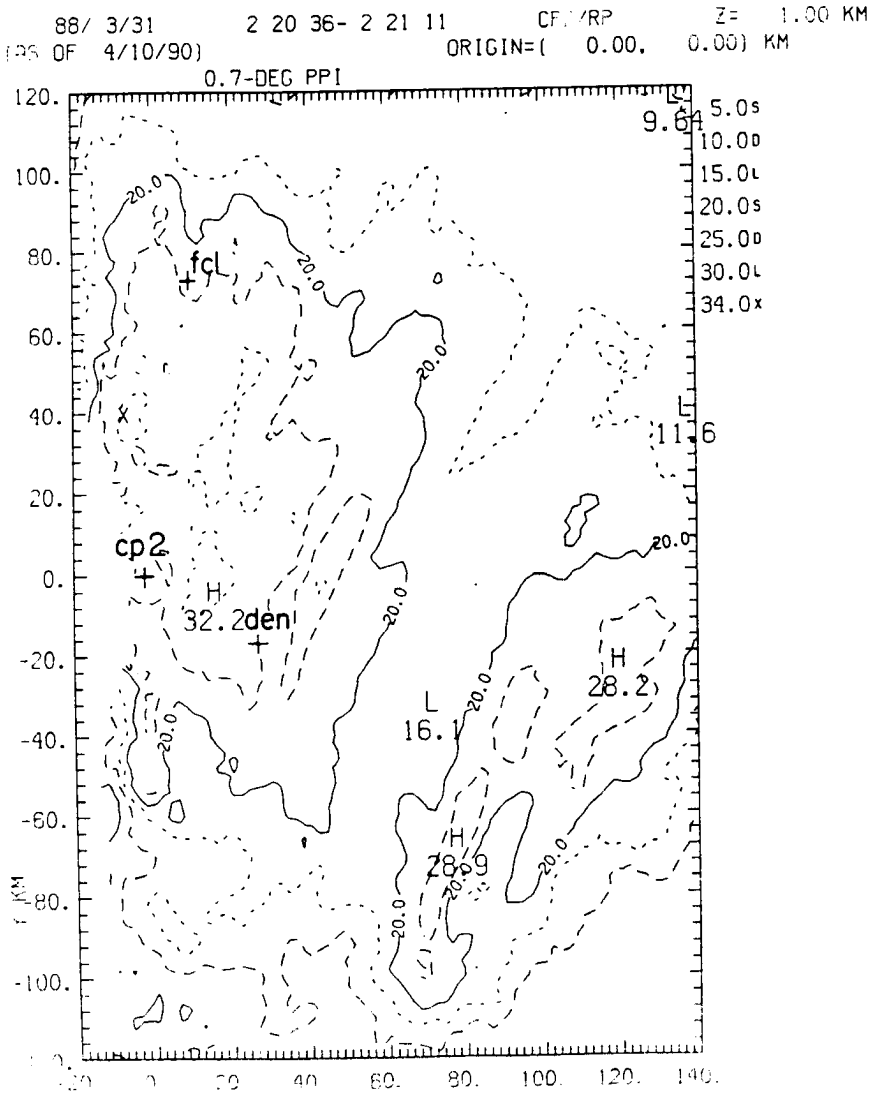

Figure 2.9: Reflectivity for Doppler radar PPI scan, 0920 UTC 31 March 1988.

the convergence line. The moisture content of the inflow may therefore be critical to the evolution of the snowfall event.

Cold-air damming persisted at about the same strength for more than 12 hours (note the similarity in low-level winds at 0427, 0812 and 1321 UTC 31 March, Figure 1.7a-b). The slope of the eastern edge of the dammed cold pool (layer 1 in Figure 1.7a) can be estimated for the case of 30-31 March. This sounding indicated the depth of the cold pool to be approximately 250 m over CHR during much of the heavy snowfall; the snow accumulation maximum was about 30 to 40 km from FCL. The convergence line was typically only 25 to 35 km away, although it was not clear, due to relatively coarse surface data, whether the line remained quasi-stationary between available observations. A parcel rising dry adiabatically with the aforementioned initial conditions would reach saturation at a height of approximately 700 m. Extrapolating the sloped lifting surface linearly to the west implies saturation (at 700 m above the convergence line) approximately 70 km west of the line; this location is in approximate agreement with the location of the snowfall maximum. Thus, it is probable that the upslope layer is lifted to condensation, creating a liquid water generation region directly above the heaviest snowfall. For this lifted parcel, adiabatic cooling leads to ice saturation at a height of about 600 m above CHR, or, hypothetically, 60 km west of the convergence line. These crystals fall into a layer (marked 1 in Figure 1.7a), which is near water saturation and has temperatures -2 to -5°C, and thus can grow by deposition, riming, and aggregation until they reach the ground. Of course, the winds experienced by the falling snow crystals would have a significant influence on the location of ground target; however, the soundings in Figure 2.5 indicate that they would first advect to the west, but then to the southeast in the lowest levels as they fell. Such a trajectory could result in landfall close to an area directly below the crystal generation region.

Some simple thermodynamic calculations of lifting a layer, rather than a parcel, lend support to this hypothesis. Figure 2.5 indicates that the layer of easterly winds spans about 300 hPa (or 3.2 km) vertically. Uplift (with constant equivalent potential temperature)

of this *entire* layer, which initially exhibits an approximate temperature range of 1.5°C to −21°C, would produce a total of approximately 0.25 cm of liquid condensate. The easterly flow, at about 10 m s^{-1}, would require about two hours to reach from the convergence line to the region of maximum condensation, or about 40 to 50 km west of CHR. The resulting hypothetical rate of liquid condensate in this layer is 0.12 cm hr^{-1}, which would account for a significant portion of the snowfall in this storm, even though topographical lifting, large-scale ascent, and additional crystal growth by deposition, riming, and aggregation have been ignored for this analysis. Observations showed that the layered structure in Figure 1.7 persisted for more than 12 hours.

Hypothetically, using the lifted parcel calculation for the 8-9 December 1985 storm, and a similar cold pool slope for CHR (Dunn, 1987 does not present a thermodynamic sounding) yields saturation at the upper boundary of the cold pool approximately 25 km west of the convergence line, which is in close agreement with snowfall maxima observations (see Figures 3 and 16 in Dunn, 1987; the snowfall maximum occurred 15 to 30 km west of the convergence line). Using Dunn's BAO data (his Figure 19), the slope of the upper boundary of the cold pool may be steeper than that estimated (about 0.6°) for the March 1988 storm. As mentioned previously, the convergent regions shown in Figure 2.2 are strongest along the northern Front Range, as are the snowfall depths. The vertical motions over the eastern portion of the cold pool probably cause considerable condensate production. The location, depth and orientation of the cold pool have a direct effect on the height and location of maximum condensate production, and thus on the precipitation distribution.

2.4 Interpretation of Snow Crystal Types

Observations of snow crystal types provide additional insight into the precipitation mechanisms discussed previously. Spotters were instructed to record the predominant crystal types at hourly intervals during moderate or heavy snowfall. During the 30-31 March storm, the spotter network reported predominantly aggregated, heavily-rimed spatial dendrites, as well as several 15- to 30-minute graupel episodes. Table 2.2 presents the

tabulated results of these reports. Many of the dendrites making up the large aggregated snowflakes contained heavily-rimed single crystals in their cores. This tendency for riming to be concentrated near the centers of the individual dendrites rather than the branches implies that liquid water was present in layer 3 (see Figure 1.7a), with subsequent dendritic crystal growth occurring in layer 2. As shown by Byers (1965), temperatures (−12°C to −16°C) in layer 2 were favorable for rapid dendritic growth. The observation of rimed cores may be the result of liquid water accumulation near cloud top, as in the northern Colorado mountain cloud systems reported in Rauber *et al.* (1986). Unrimed and unaggregated crystals comprise only about 9 percent of the observations in the March 1988 case. These results indicate that liquid water layers played a significant role in precipitation production, although the exact nature of this role (e.g. the location of these layers) is not readily determinable from these data.

Table 2.2: Snow crystal observations for the spotter network shown in Figure 1.3 for the 30-31 March 1988 storm.

Crystal Type	Total No. Occurrences
heavily-rimed, aggregated spatial dendrites	41
heavily-rimed irregulars	29
graupel	18
rimed, aggregated plates	11
rimed sector plates	9
heavily-rimed stellars	7
unrimed stellars	4
lightly-rimed dendrites	4
unrimed plates	3

The predominance of significant dendritic growth implies once again that layer 2 probably contained areas of strong upward motion (needed to obtain saturated conditions with respect to liquid water, and thus favored dendritic growth), as discussed previously. The moist layer 3 was a crystal generator region, reaching ice saturation as uplift occurs. The soundings in Figures 1.7 and 2.6 indicate slight supersaturation with respect to ice at −30°C. Layer 3, too cold for dendritic growth, probably produced platelike or columnar

crystals which may have been masked by riming. These crystals served as cores for further riming and dendritic growth below.

2.5 Observations of Storm Termination

Dunn (1987) noted that decreasing snowfall was related to the termination of upslope flow at 700 mb (i.e. veering from southeasterly to southwesterly) for the 8-9 December 1985 storm. Associated with this veering was a weakening and southeastward propagation of the surface convergence line. Both tendencies were indeed observed in the 30-31 March 1988 storm. The last CLASS sounding, released at 1710 UTC 31 March as the snowfall at CHR was decreasing indicated some significant trends which could explain the conclusion of heavy snowfall (Figures 1.7, 2.5, and 2.6). Although cold-air damming persisted as shown by the low-level northwesterly flow, the mid-level upslope weakened and became discontinuous in the vertical. The easterly component of upslope flow had decreased by 25 to 50% in magnitude, and the layer also cooled by several °C and moisture content decreased rapidly in a relative *and* absolute sense. The upper portion of this layer (700 to 550 hPa) stabilized significantly, as shown in Figure 1.7b. A decrease in wind speed by 5 to 10 m s^{-1} occurred above the frontal inversion (Figure 2.5), which lost most of its identity by 1700 UTC. Layer 3 also became much drier than in the previous sounding (Figure 2.6) indicating that the seeder-feeder process probably had ceased by this time. FCL and CHR received only light snow afterwards. The 0000 UTC 1 April sounding for DEN also indicated that as the snowfall subsided, the southerlies weakened significantly. It is not clear if the snowfall subsided when this warm, moist flow lost its large-scale upward motion, or when uplift over layer 2 weakened.

Chapter 3

ARCTIC OUTBREAKS: CASE STUDIES

3.1 1-5 February 1989

During the period 1-5 February 1989, a record-breaking arctic air mass invaded the western United States, abruptly ending a period of unusually warm weather that had characterized the region during most of January. The post-frontal upslope flow along the eastern slope of Colorado and Wyoming, along with relatively warm, moist westerly flow aloft, produced periods of heavy snow despite surface temperatures averaging −21 to −29°C (−5 to −20°F).

Auer and White (1982) found that for the vast majority of heavy snowfall events in the United States, the region of most favorable dendritic ice crystal growth (−12 to −16°C) is found between the heights of 3.4 and 5.2 km MSL (or, for the present case, approximately 620 to 550 mb) in the atmosphere, a situation not generally associated with 850 mb temperatures colder than −10°C (assuming typical low-level lapse rates). Table 3.1 presents a chronology of daily surface observations at FCL during this episode. Note the occurrence of heaviest snowfall on the coldest days. One important precipitation enhancement mechanism, terrain blocking, is examined here by analyzing the roles of the moisture source above the cold air, the depth of the cold air and the snow intensity.

The schematic in Figure 3.1 depicts the blocking-induced circulation observed over the region for several days during the arctic outbreak. In such cases, the moist flow aloft rises over the Rocky Mountains, generating precipitation particles. With the arctic air entrenched over the eastern foothills, downslope flow and drying are significantly reduced. In fact, the western edge of the cold pool is occasionally deeper due to blocking of the upslope flow. Precipitation can thus be heavier on the western edge of the cold pool. The

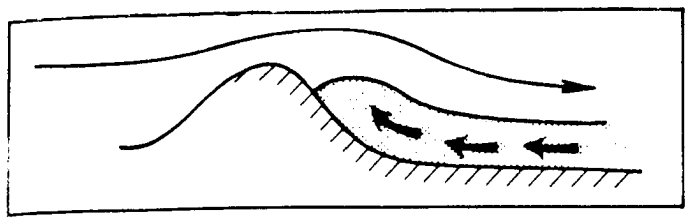

Figure 3.1: Schematic of the dynamical circulations present over and east of the Rocky Mountains during an arctic outbreak. Shaded area is the cold pool, characterized by weak to moderate easterly flow. Overrunning westerly flow is strong and extends from just above the cold pool into the stratosphere.

Table 3.1: Daily surface weather observations for Fort Collins, Colorado, during the arctic outbreak of February 1989.

Date (1989)	maximum temperature (°F)	minimum temperature (°F)	snowfall (inches)
Feb. 1	30	4	0.4
Feb. 2	4	−14	2.6
Feb. 3	−11	−18	6.5
Feb. 4	−10	−18	4.9
Feb. 5	5	−19	0.5
Feb. 6	17	−17	T
Feb. 7	24	−13	0

precipitation enhancement over the foothills and immediate areas to the east is especially important as synoptic-scale disturbances embedded in the westerly flow aloft propagate over the cold pool, generating solid and liquid hydrometeors as the mountain barrier is met. The resulting precipitation distribution for the entire February 1-5 event, shown in Figure 1.5, demonstrates the extension of significant precipitation amounts 15 to 30 km east of the foothills along Colorado's northern Front Range. Effectively, the cold pool acts as a terrain feature to the overlaying air mass. Meanwhile, further to the east over the Wyoming and Colorado plains, stronger downslope flow reduces precipitation.

The precipitation intensities mentioned in the next several sections are based on two surface measurements: visibility and liquid precipitation rate. In order to assess the role of fog in reducing visibility during this storm, the two measurements at FCL were plotted against each other for the five-day period. The result was a very high correlation between low visibility and precipitation rate. Generally, all of the 6-hour heaviest snow periods exhibited visibilities much less than one mile, while those periods producing only a trace to 0.25 mm of melted snow per 6 hours (usually with fog present) corresponded to visibilities greater than 5 km. Furthermore, surface wind speeds were too low (2.5 to 7.5 m s^{-1}) to produce any significant amounts of blowing snow.

3.1.1 Synoptic overview and the moisture source

During the latter half of January 1989, temperatures in northeastern Colorado were remarkably warm. At the same time, a record-breaking anticyclone was strengthening over Alaska and western Canada and was responsible for new all-time minimum temperature records in that region (see Tanaka and Milkovich, 1990). This air mass began to move rapidly southward during the last few days of January. The leading edge of the arctic air mass reached the Front Range on the evening of 31 January. Shallow upslope cloudiness followed the frontal passage, as strong easterly winds encountered the eastern Colorado sloping plains and foothills. Low clouds and light snow showers are the typical weather scenario in this region if a southward-propagating surface high pressure system is present in the central Great Plains (see Boatman and Reinking, 1984), and light snowfall did accompany the upslope clouds on 1 February in northeastern Colorado (see Table 3.1). Figure 3.2 shows the NMC analysis at 1200 UTC 1 February.

Over the next several days the arctic air mass deepened significantly over the Front Range area as the upslope flow persisted. Figure 3.3 presents a series of the DEN National Weather Service (NWS) soundings for 0000 UTC 3 February through 1200 UTC 4 February. While the inversion depth was only about 450 m (about 50 mb) several hours after frontal passage, the cold air deepened to about 1500 m (150 mb) by 1200 UTC 4 February (also see Figure 3.4 for the wind profile at that time). However, mixing ratios within the cold air mass were consistently 0.4 to 0.5 g kg^{-1} during the period, which could not account for the moderate to heavy precipitation observed in FCL on 2-4 February, even if strong surface convergence had been present.

To demonstrate this fact, representative precipitable water values were calculated for the cold air mass during the storm evolution, using the DEN soundings (refer to Figure 3.3). The approximate precipitable water value is 0.5 mm within the cold air mass for the three-day period shown. Consider an upslope flow velocity of 5 m s^{-1} in the cold air (this value is probably overestimated for the present case, considering the surface and sounding wind observations, but is used here for demonstration purposes). Thus a parcel

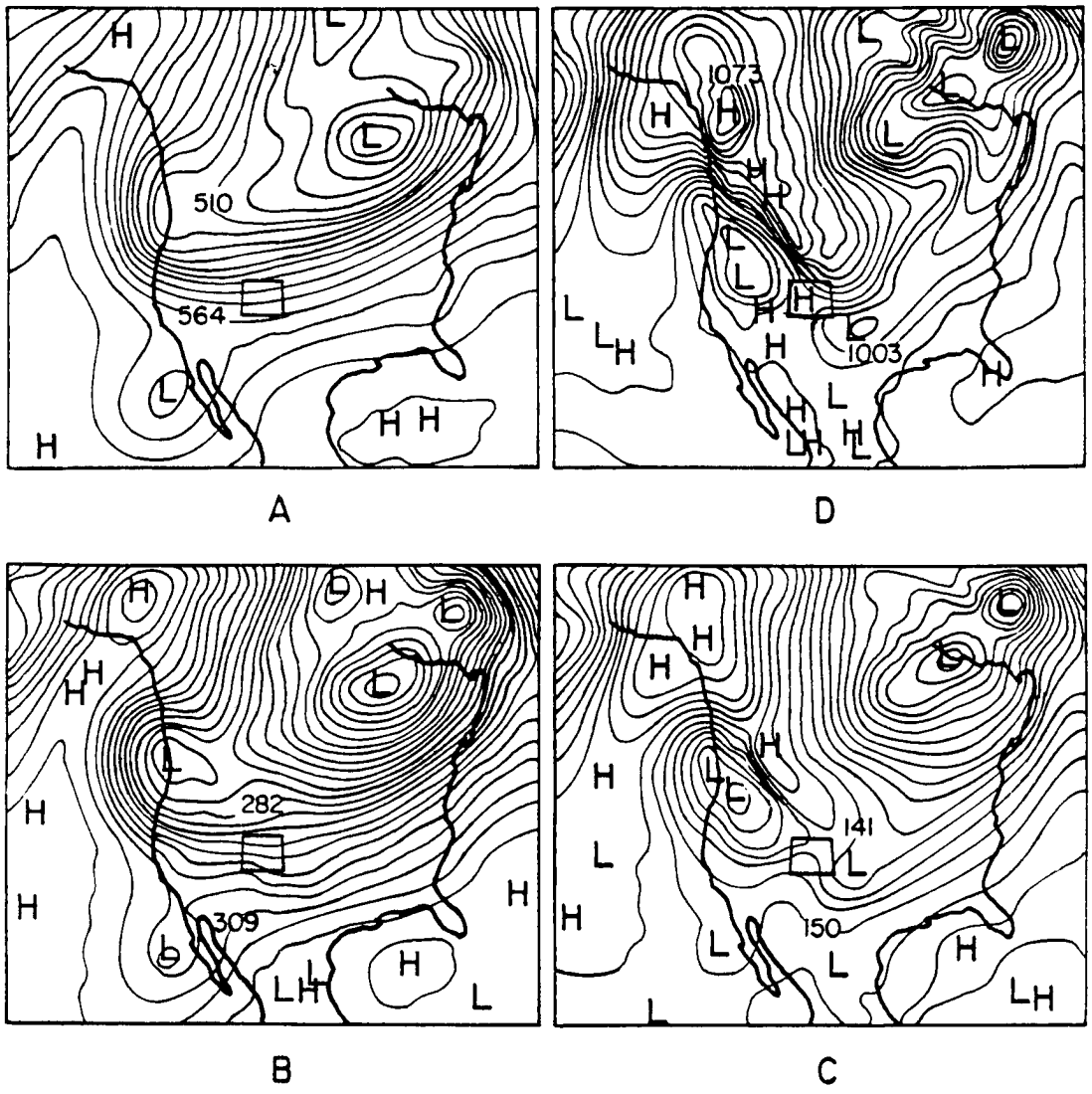

Figure 3.2: National Meteorological Center Nested Grid Model height analyses at 1200 UTC on 1 February 1989. (a) 500 mb (b) 700 mb (c) 850 mb (d) Sea-level pressure. Heights are labeled in dm. The state border of Colorado is heavily outlined.

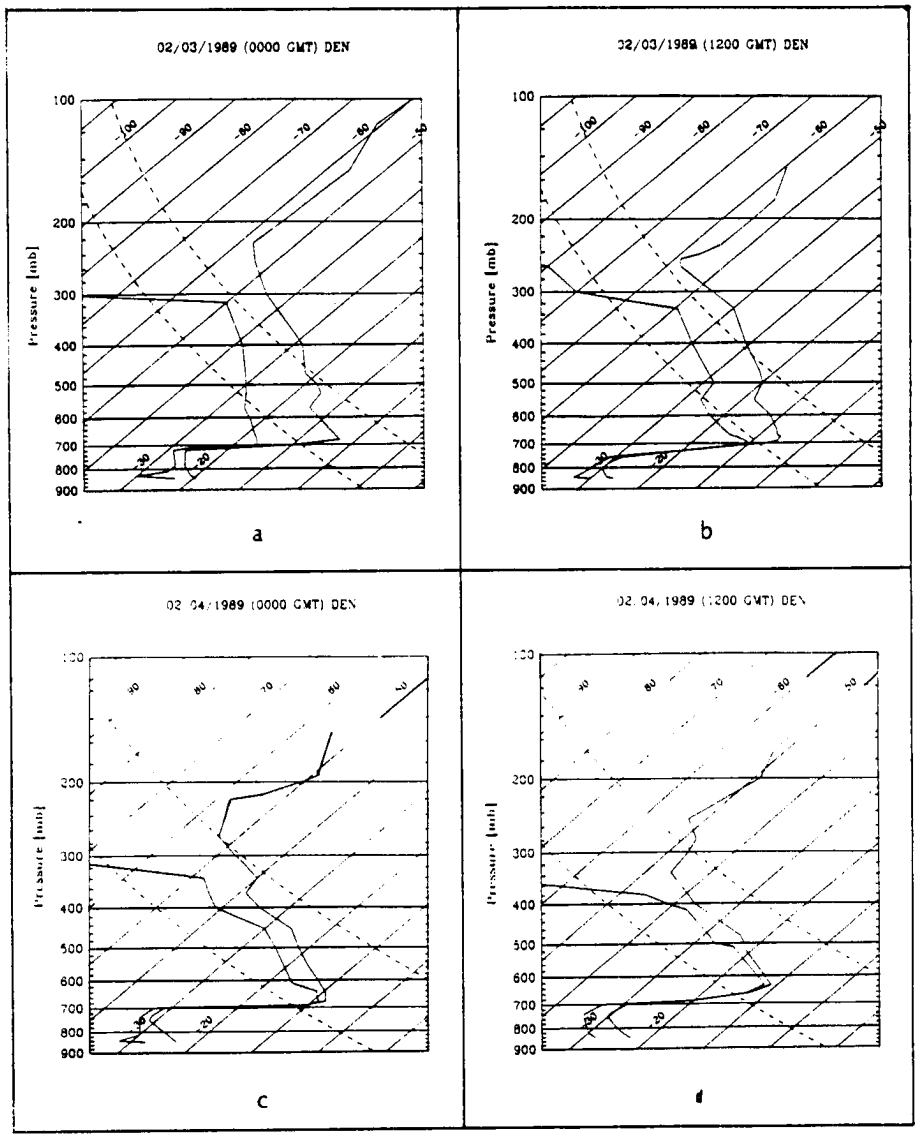

Figure 3.3: Skew-T diagram for DEN radiosonde data. Isotherms (°C) are the diagonal solid lines running upward from left to right. Dotted lines are selected dry adiabats. (a) 0000 UTC 3 February 1989, (b) 1200 UTC 3 February 1989, (c) 0000 UTC 4 February 1989, and (d) 1200 UTC 4 February 1989.

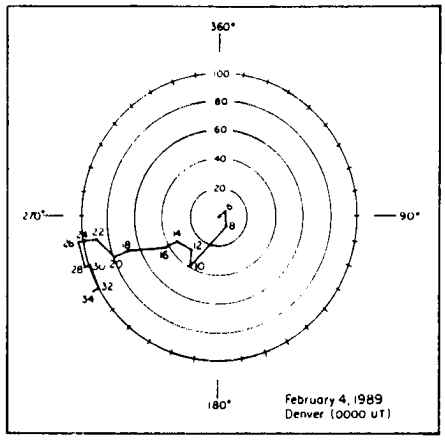

Figure 3.4: DEN hodograph at 0000 UTC on 4 February 1989. Wind speeds, labeled on the radii, are in knots. Heights along the profile are in thousands of feet, MSL.

in the cold air moves approximately 100 km in 6 hours. Assuming that during a six-hour period, all of the water vapor in a 100 km wide swath condenses and precipitates over a 30 km width (see the precipitation distribution in Figure 1.5), approximately 1.5 mm accumulates. This value underestimates observed precipitation rates during several portions of the storm along the northern Front Range by more than a factor of five, assuming a precipitation efficiency of unity. Of course, this approach also assumes that only two-dimensional convergence is occurring, and it ignores the contribution of pre-existing cloud liquid or ice particles. Nevertheless, it underscores the inability of strictly low-level moisture to account for most of the precipitation received.

Most of the average terrain height along the Continental Divide in northern Colorado and southern Wyoming ranges from 2 to 3 km (7000 to 10000 ft) MSL. In the case of the February 1989 storm, the deepening of the cold air to and above 3 km (10000 ft) was followed by propagation of the cold air westward, over the Divide and down the western slope of Colorado. In fact, this 'spillover' induced extremely heavy snowfall in those regions. Westward propagation in this type of storm in inevitable if the cold air deepens to a height greater than the average barrier height, given the dense, coherent, and persistent nature of this air mass.

During the initial analyses, the author examined the radiosonde data from Grand Junction, Colorado (GJT) along with many other relevant surface and sounding data discussed in the next section. In obtaining a representative sample of the low-level over-running air mass, the profiles measured at GJT were probably more appropriate than local surface observations at Craig, Eagle, and Rifle, for example. Also, the persistent wind direction of 240° in the mid-levels at GJT conveniently places FCL directly downstream of GJT. The important aspects of those profiles are repeated here.

Relatively warm, moist conditions developed at GJT during the 4-day period as westerly flow strengthened. At 0000 UTC on 3 February 1989, surface temperature and dew point at GJT were $+10°C$ and $-5°C$, respectively. A nearly dry adiabatic lapse rate characterized the layer from the surface to about 600 mb, with increasing relative

humidities to nearly 70% at 600 mb, and southwesterly winds increasing from 20 to 50 kts through the layer. By 0000 on 4 February 1989 (see Figure 3.5), the atmosphere above GJT was nearly saturated up to 400 mb, with surface temperatures just above freezing. Winds in the 800-600 mb layer had veered slightly to approximately 250° and strengthened. Twelve hours later, after a strong shortwave had passed to the east, surface temperature remained at freezing, with a strongly stable lapse rate to 800 mb, and a nearly dry adiabatic profile to 700 mb. The lapse rate above this level was slightly more stable. The dew point profile revealed nearly saturated conditions at the surface and in the 700-550 mb layer. At 800 mb, the relative humidity was 67% within a shallow drier region. Winds remained west-southwesterly and strong through the 800-400 mb layer.

This time period (0000 UTC 3 February to 1200 4 February) covers most of the periods of heavy snow observed at FCL. Upon comparison with the Denver soundings in Figure 3.3, the GJT profiles are in good agreement with those measured at DEN *above 700 mb*. A representative wet-bulb θ_E value is approximately +10°C for the 800-600 mb layer (downstream overrunning of the arctic air mass would probably induce significant upward motion in this layer). A buoyant parcel would thus yield strongest dendritic growth in the 650-600 mb layer; this layer of about 2000 ft depth is centered at about 3000 ft above the top of the cold air at DEN.

From these radiosonde data, the author noted that westerly flow aloft became more moist with time both in a relative and absolute sense (see Figure 3.3), a situation conducive to deeper cloud development in and above the cold air (Boatman and Reinking, 1984). Larger-scale disturbances moving through this moistening westerly flow produced significant amounts of precipitation-sized ice crystals which fell through the cold air to the ground. The hourly visibility and temperature observations in FCL are shown in Figure 3.6. As mentioned previously, heaviest snowfall occurred during the periods of very low visibility.

During some of the periods of heavy precipitation along the Front Range, rapidly rising surface pressures, deepening of the cold pool, and the advection of deep cloudiness

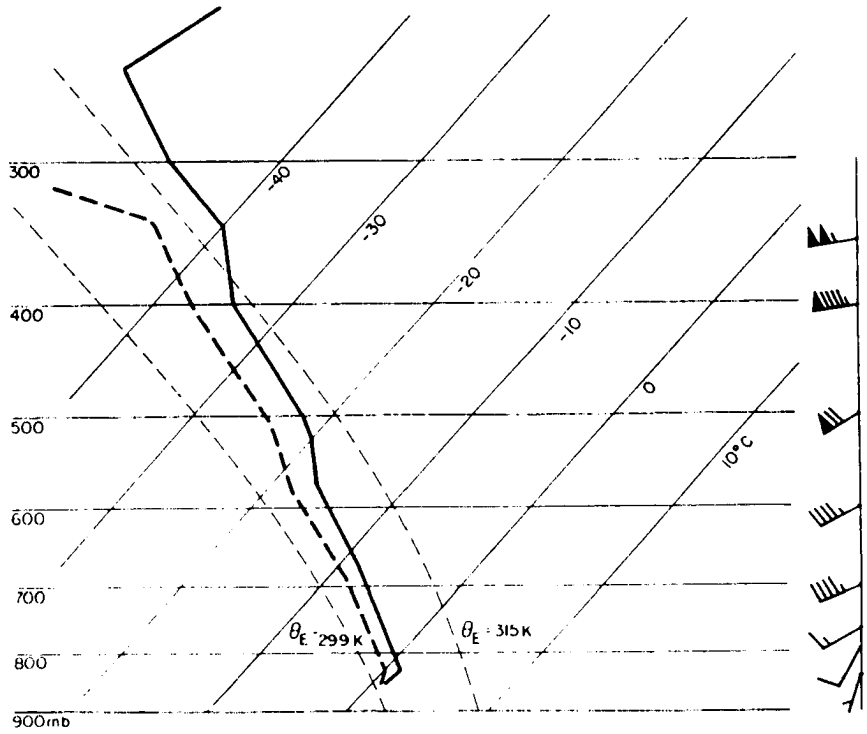

Figure 3.5: Skew-T diagram for GJT radiosonde data at 0000 UTC on 4 February 1989. Isotherms (°C) are the diagonal solid lines. Dashed lines are selected moist adiabats.

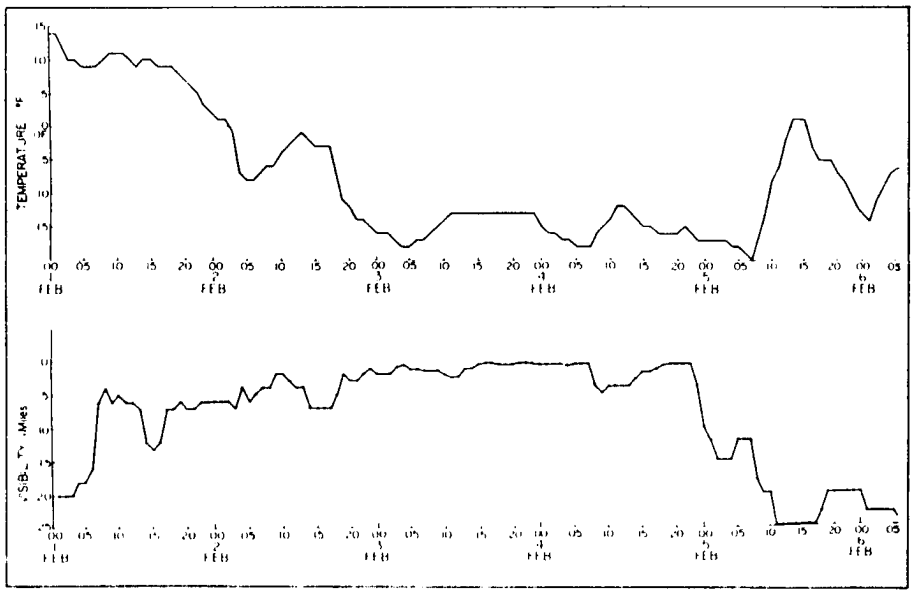

Figure 3.6: Selected surface observations for Fort Collins. These data were obtained by averaging those observed at the FCL campus weather station and at MSWS (Mountain States Weather Services) (a) temperature (°F), and (b) visibility (mi).

over the region all occurred nearly simultaneously. Surface pressure rises were the result of the accumulation of cold air over and near the foothills as low-level easterly flow over the plains strengthened. These observations indicate that the damming-induced bulge along the western edge of the cold pool played a critical role in the precipitation dynamics in this storm. More evidence for this feature is described in the next three sections. The precipitation gradient near the foothills (Figure 1.5) is similar to that of the March 30-31 1988 storm (see Chapter 2), in which cold-air damming was a major contributor to the snow production. Overrunning in this case, however, occurred in predominantly *westerly* flow.

Some regional snowfall totals for the 1-5 February 1989 storm included FCL at nearly 40 cm (2.0 cm liquid), 50 to 75 cm in Estes Park and 33 cm (2.3), 28 cm (2.0) and 38 cm (2.3) at Cheyenne (CYS), Boulder, and Colorado Springs (COS), respectively. The following sections describe a sequence of events which characterize the evolution of the storm, and explain most of the observations.

3.1.2 Storm chronology

Geostationary Operational Environmental Satellite (GOES) visible and infrared data, along with DEN soundings, wind profiler and NMC surface and upper-air analyses, enabled a detailed assessment of the cloud systems responsible for the heavy snowfall during 1-5 February 1989 along the Colorado Front Range. Observations from the PROFS meso-network were also utilized. The data are discussed in relation to standard surface observations at FCL, CYS, and DEN.

0700-1300 UTC 1 February 1989

Frontal passage occurred several hours prior to midnight, and light snow began (trace amounts) during this period in FCL. DEN recorded frontal passage between 0700 and 0900 UTC. The 1200 UTC NGM analyses shown in Figure 3.2 suggest that the cold air mass was very shallow (confined to below approximately 750 to 800 mb). Surface observations during this period confirm that the western edge of the cold pool was located below an

elevation of about 2 km MSL (or 800 mb in the standard atmosphere). For example, just west of Denver in the foothills (at this approximate elevation) temperatures reached 7°C (45°F) during the daytime hours of 1 February (see Wesley *et al.*, 1990). The NGM analyses also revealed that a strong sea-level pressure (SLP) gradient, directed northeast-southwest, had developed over the region. This gradient was overestimated to some degree, a result of errors produced by the standard pressure reduction algorithm when a shallow arctic air mass is present over complex terrain (e.g.. Pielke and Cram, 1987). It was not clear during this period whether the light snowfall was due to the shallow upslope flow, and/or the weak shortwave seen in Figure 3.2. The presence of a cold-cloud streak over the region on satellite (not shown) also supported the possibility of synoptic forcing.

1300-2000 UTC 1 February 1989

The cirrus streak moved off early in the period (Figure 3.7). At the same time, the snow intensity *increased* somewhat, as implied by a decrease in visibility (Figure 3.6) and a slight increase in the 6-hour snowfall total reported at 1800 (0.8 cm). Northeastern Colorado, including the Front Range, was engulfed in low-level cloudiness, with GOES infrared (IR) 11.2 μm cloud-top temperatures (CTTs) ranging from -15 to -20°C. At about 1500, slightly colder (-18 to -25°C) cloud tops were evident in a narrow strip over the northeasternmost foothills of the Front Range on the western edge of the cold pool (see Figure 3.7). It was apparent from the satellite and upper-air analyses that the light precipitation during this time period was probably driven by upslope flow (see surface analyses in Figure 3.2d).

Nearby, apparently cloud-free areas (implied by surface and visible satellite data) were in the -5°C to -10°C temperature range. These values were consistent with shelter temperature measurements, and illustrated that the GOES IR data were consistent with other data sources in this case.

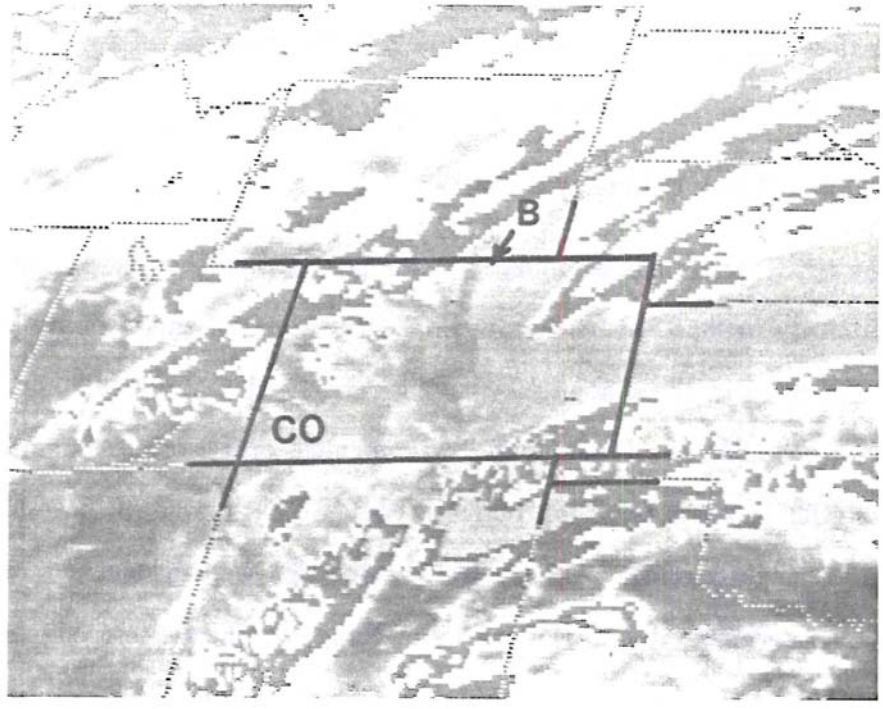

Figure 3.7: GOES-IR image (from GOES east) at 1501 UTC for 1 February 1989. Note the cold streak of upper-level clouds to the east of the Front Range. Also, notice the bright band (B) on the western edge of the upslope cloudiness along the Colorado Front Range.

2000 1 February – 0600 UTC 2 February 1989

The narrow north-south GOES IR bright band remained along the foothills (Figure 3.8). Over the FCL region, CTT was approximately −20°C while the shelter temperature was −13°C (+9°F). The bright band extended from CYS to DEN and followed the approximate shape of the 5000 foot elevation contour along the northern Front Range. As mentioned previously, this colder band was probably a bulge in the cold air resulting from damming. Strengthening easterly flow within the arctic air over the plains encountered both rising topography and a strong inversion as it moved toward the Front Range. This, in turn, led to blocking, a buildup of cold air over the foothills, and a heightened inversion on the western edge of the cold pool. Comparison of DEN and Dodge City, Kansas soundings during later periods revealed that the inversion and wind shift at the top of the arctic air mass consistently occurred at a slightly lower pressure at DEN despite the poor vertical resolution in these data. The inversion was also much more coherent (i.e. more abrupt at its base) at the DEN site. The satellite observations suggested that the eastward extent of the cold air bulge from the foothills of the Front Range was only several tens of kilometers.

Snow intensity in FCL was mostly of the "trace" variety early in the period, and shelter temperatures remained about −12.2°C (+10°F). At 0000 UTC, the surface wind shifted from southeast to east at FCL and the snowfall intensified slightly at this time. NGM analyses at 0000 UTC (not shown) indicated an increasingly intense SLP gradient over the region (again, exaggerated by the SLP reduction). Deep cloudiness, however, was confined to the north and west of the northern Front Range. All of these factors, taken together, suggest that "upslope" was still the primary precipitation mechanism at work.

0700-1200 UTC 2 February 1989

Light snow (1.3 cm $(6\ \text{hr})^{-1}$) continued at FCL through the period. A band of of higher clouds (Figure 3.9) stretched from extreme southwestern Colorado into eastern Wyoming (where heavy snow was falling). FCL was situated along the southern or southeastern edge of this band. While the primary precipitation mechanism was probably

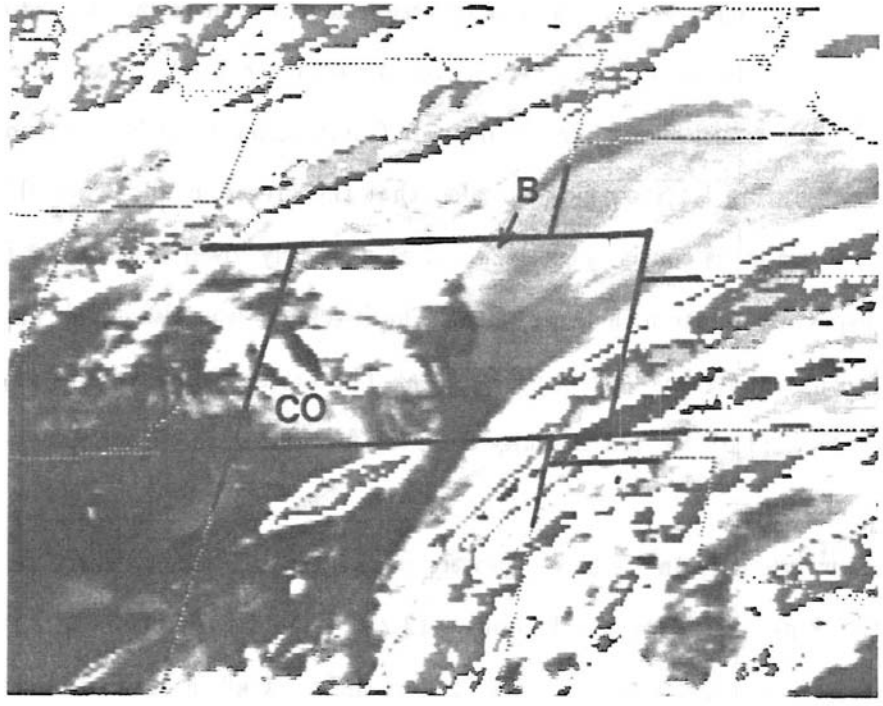

Figure 3.8: GOES-IR image (from GOES east) at 0531 UTC 2 February 1989. The band of colder tops over extreme northeastern Colorado was moving rapidly eastward. The bright band (B) remained along foothills. (Note: difference in contrast between this IR image and that of Figure 1.13 is due to the use of separate look-up tables.)

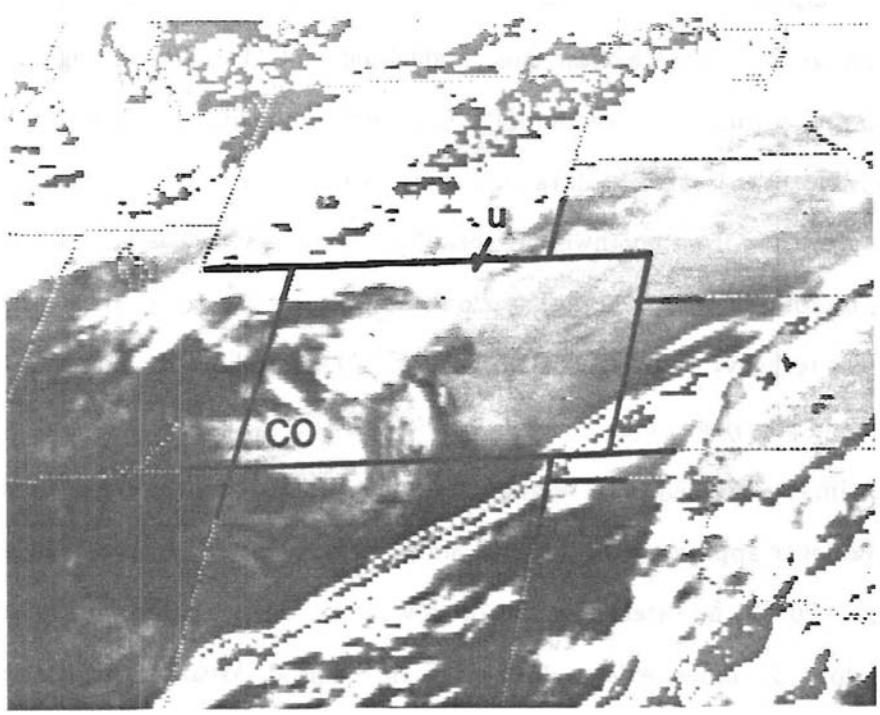

Figure 3.9: GOES-IR image (from GOES east) at 1031 UTC for 2 February 1989. Note the cold streak of upper-level clouds to the east of the Front Range and the band of higher clouds from southwestern Colorado into southeastern Wyoming (u).

upslope, the presence of higher cloudiness indicated that some of the snowfall may have originated at higher levels. Thus, a seeder-feeder process may have been contributing to the snowfall. The NGM analyses in Figure 3.10 continued to show the intense SLP gradient and strong westerly flow aloft in northeastern Colorado.

1200-1800 UTC 2 February 1989

This period was generally marked by snowfall at a rate of 1.5 cm hr^{-1} and warming shelter temperatures (from −22°C to −19°C (−8°F to −2°F) during the 6 hours). Snow intensity at FCL was heaviest from 1600-1800. NGM analyses (Figure 3.10) suggested weak positive vorticity advection (PVA) at 500 mb beginning after 1200.

Visible (VIS) satellite data (available after 1430) confirmed that a band of higher clouds stretched from northwest Colorado, across the southeastern half of Wyoming, into South Dakota (Figure 3.11). The cloud band appeared to be thick, and CYS received moderate to heavy snowfall during this time (0.43 cm liquid). The southern edge of this cloud band was over FCL.

Estimates of satellite IR temperatures just southeast of the cloud band at 1700 yielded CTT values of approximately −20°C. Since shelter temperatures at 1700 were also approximately −20°C, the satellite was probably seeing surface-based radiation and, therefore, less upslope cloudiness existed during this time period. Weather and obstruction to visibility listed "light snow showers" at several reporting times, with an occasional "BINOVC" comment. The reporting station at Mountain States Weather Services (MSWS) in eastern Fort Collins recorded thin spots in the low overcast at 1700 and 1800. The observations for this period, taken together (particularly the decreased low-level cloudiness), imply that most or all of the light snowfall was occurring due to synoptic-scale ascent in the mid- and upper-levels of the atmosphere.

1800 UTC 2 February – 0000 UTC 3 February 1989

Snowfall during this period amounted to only a trace in FCL. After 2200, the larger band of deep cloudiness began to move off slightly to the north of the FCL area, and the

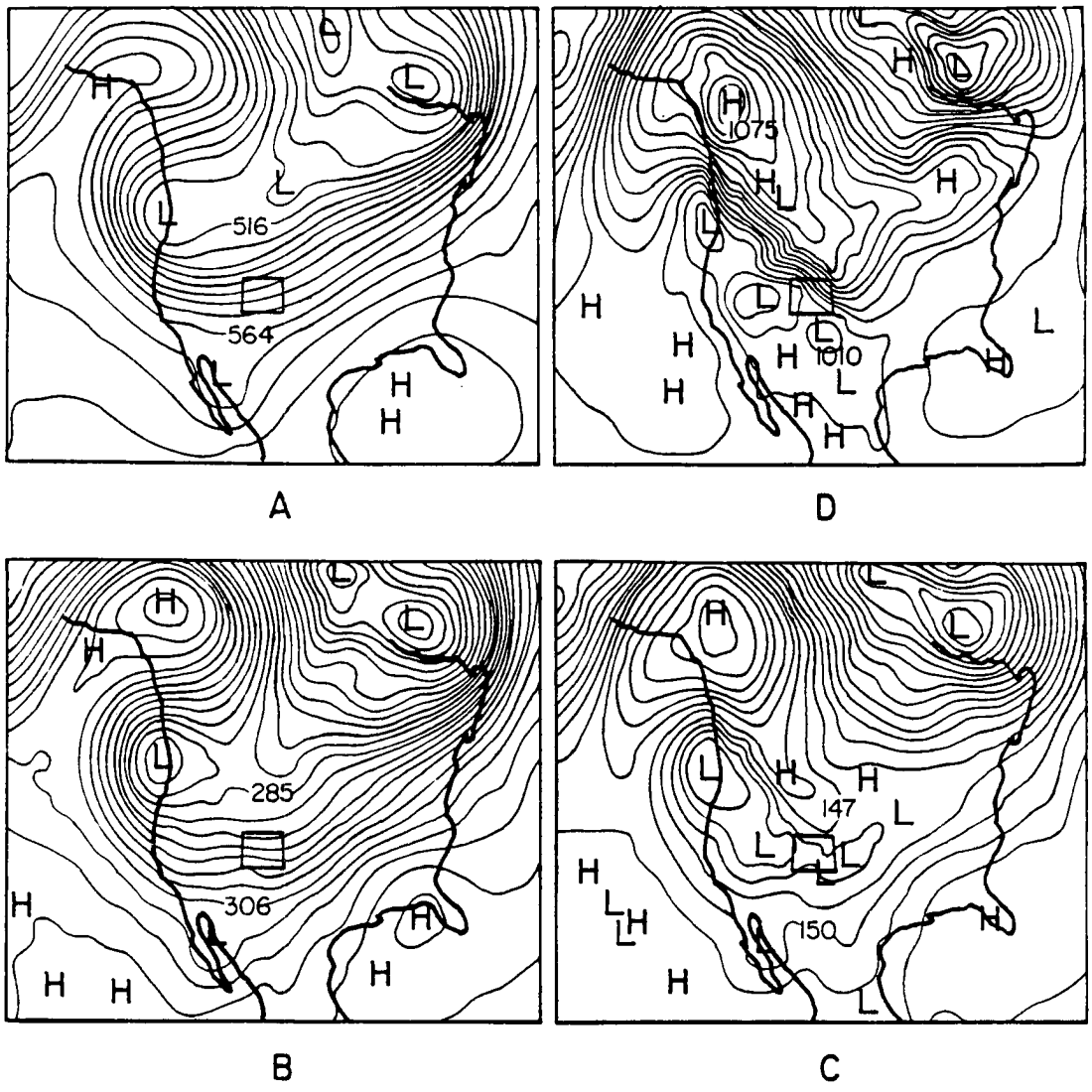

Figure 3.10: National Meteorological Center Nested Grid Model height analysis for 1200 UTC on 2 February 1989. (a) 500 mb, (b) 700 mb, (c) 850 mb, and (d) sea-level pressure. Heights are labeled in dm. The state border of Colorado is heavily outlined.

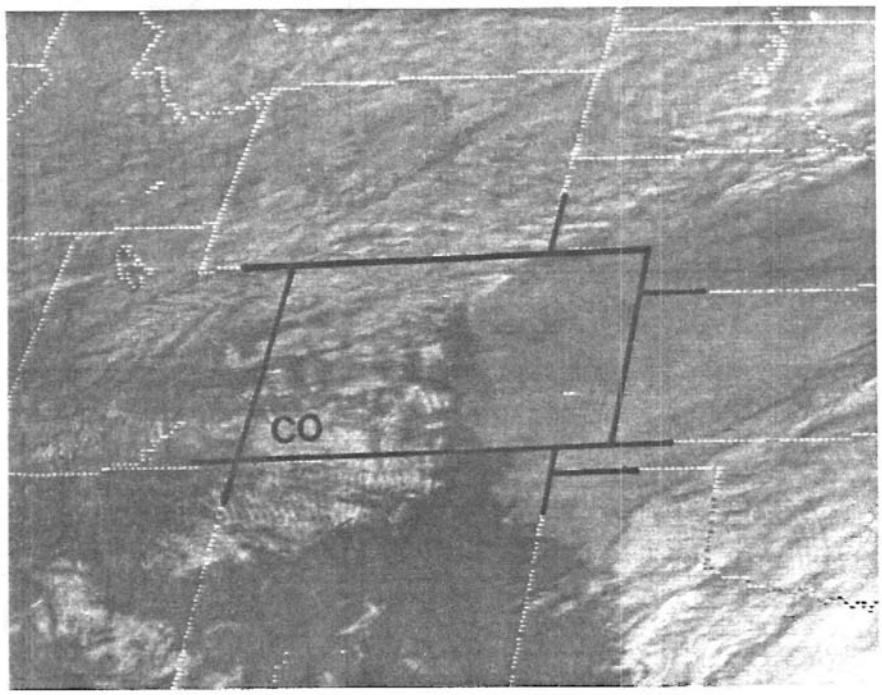

Figure 3.11: GOES-VIS for 1631 UTC on 2 February 1989. Deep cloudiness was located to the north and west of the Colorado Front Range at this time.

bright band along the western edge of the upslope cloudiness became less distinct. The visibility increased at FCL according to observations, while remarks included reports of snow showers visible to the southwest, west, and northwest. Satellite data (not shown) suggested that a few scattered upper clouds remained over most of the region, but were thinner to the south. This was confirmed by the fact that DEN, Limon and Akron reported only fog (not snow). At 2330, the northern Front Range was not entirely free of higher clouds. However, the main deep cloud was again confined to regions north and northwest of FCL.

0000-0700 UTC 3 February 1989

While the upper cloud cover increased only slightly during this period, the snow intensified substantially. The precipitation rate increased to 5.8 cm $(6\ \text{hr})^{-1}$ of dry, powdery snow, with much more snow reported along the western fringe of FCL. The liquid equivalent at FCL was reported as only 0.13 cm. However, this value may not have been representative of the actual precipitation, since several observers in and near the western portions of the city reported more than 0.5 cm during this period. Again, precipitable water values in a column between the surface and the top of the cold air were approximately 0.05 cm, based on the DEN sounding (Figure 3.3a). A faint bright band could also be seen along the Front Range in the IR images, which indicated that another bulge in the cold air had developed. This bulge was probably associated with a secondary surge of cold low-level air. The DEN wind profiler data during this period indicated an increase in the depth of the upslope flow, beginning at 2300 and lasting for about three hours (not shown). The cold surge was measured in the profiler data as a marked increase in strength of low-level upslope winds. The PROFS mesonet station (FOR) in northwestern Fort Collins measured a rapidly rising surface pressure (about 4.5 mb $(3\ \text{hr})^{-1}$) beginning at 2130, accompanied by a temperature drop of 4.4°C (8°F) in 3 hr and strengthening northeasterly surface winds (Note: FOR is approximately 6 km west-northwest of FCL, and about 30 m higher in elevation).

Deepening of the arctic air was also accompanied by westward propagation of the front to higher elevations. At a volunteer observer site (Coal Creek) in the foothills to the west of DEN (about 730 mb), frontal passage occurred at around 2200 UTC and the temperature fell more than 22°C (40°F) in a few hours.

As a result of the secondary cold surge, FCL shelter temperature fell from −19 to −27°C (−2°F to −17°F) in just a few hours. Some of these factors (cold low-level surge, little increase in upper cloudiness, increased snowfall rate) implied that the dynamics for the snow was created by upslope flow within the cold pool. However, sounding data indicated that the source of moisture must have been located above the cold air mass, and profiler and satellite measurements supported this possibility. NGM analyses at 0000 UTC did not indicate any significant synoptic forcing of upward motion (i.e. PVA or warm advection above the cold pool), but did specify relative humidities above 50% in the surface-to-500mb layer across northern Colorado and Utah. The evidence supports the role of the deepening cold air mass in enhancing snowfall along the foothills during this period.

0700-1200 UTC 3 February 1989

By 0700 UTC, a deep, moist air mass was being caught up in the trough in the westerlies and rapidly moving into western Colorado. Enhancement of snowfall along the western edge of the cold pool continued during the period, and FOR surface pressure continued to rise, although at a slower rate. By 0900, the edge of very cold cloud tops had reached the Front Range and were found over and just south of FCL. Bands of upper cloud were evident over FCL (−32°C ±2°C), which masked the upslope cloud cover. Further eastward movement was somewhat retarded due to subsidence east of the Rockies in strong westerly flow (over a shallower cold pool). A weak shortwave trough (12×10^{-5} s^{-1} absolute vorticity) began to affect the eastern Colorado region toward the end of this period, accompanied by weak thermal forcing aloft according to the NGM thickness and height analyses. Visibility remained fairly low (see Figure 3.6b). Both FCL and MSWS observations indicated that the snowfall rate exhibited a maximum from 1000 to 1200 (at

1200, FCL reported moderate snowfall). The total snowfall at FCL for this period was 5.8 cm.

To the west, a second, stronger wave was entering Utah by 1200 (Figure 3.12). A broad, cold band of higher clouds (−43°C) had developed from southeastern California through eastern Utah and into western Colorado. In northeastern Colorado, the intense SLP gradient persisted, and relative humidity in the 850-500 mb layer had begun to increase. This is also readily apparent in Figure 3.3a-c for the 700-400 mb layer.

1200-1800 UTC 3 February 1989

This segment was characterized by light snow at approximate accumulation rates of 3-4 cm $(6\ hr)^{-1}$. Overall during this period, a large mass of very cold clouds (associated with a shortwave) began to organize over southern Utah, then move into Colorado (Figure 3.12). However, as the cloud mass moved into the Colorado Rockies it appeared to begin to break up again. This was accompanied by cloud-top warming. Over FCL this breakup was quite evident in both VIS and IR satellite data (not shown). At 1200, FCL reported moderate snow and CTTs of approximately −30°C were found overhead. The snow was light at 1500 under a break in the cold cloud. At 1600, the breaks were more apparent, and the snowfall was even lighter. CYS reported about 0.05 cm hr^{-1} precipitation (liquid equivalent) from 1300 to 1700, with moderate snow and deep cloud coverage at 1630. At 1700, a marked split in upper level cloud was evident along the Wyoming/Colorado border north of FCL. The last two hours of the period found the visibility increasing. FCL reported "BINOVC E" and "PCPN VRY LGT" at 1800.

1800 UTC 3 February – 0000 UTC 4 February 1989

The upper cloud deck over western and north-central Colorado continued to appear fragmented on both VIS and IR imagery. NGM analyses indicated a correlation of the breakup in Colorado with negative vorticity advection (NVA) (Figure 3.13a). This lasted until about 2000, at which time it began to fill in and expand again toward the Front Range. The apparent intensification in northeastern Colorado may have been in response

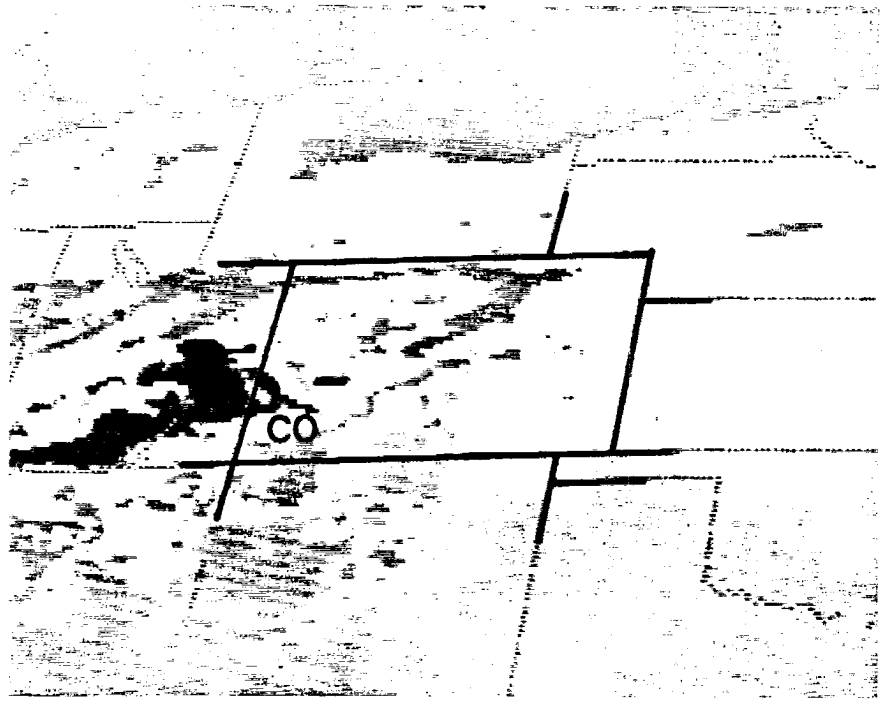

Figure 3.12: GOES-IR image (from GOES east) at 1201 UTC 3 February 1989. Very cold cloud tops were located from southern Utah into western Colorado.

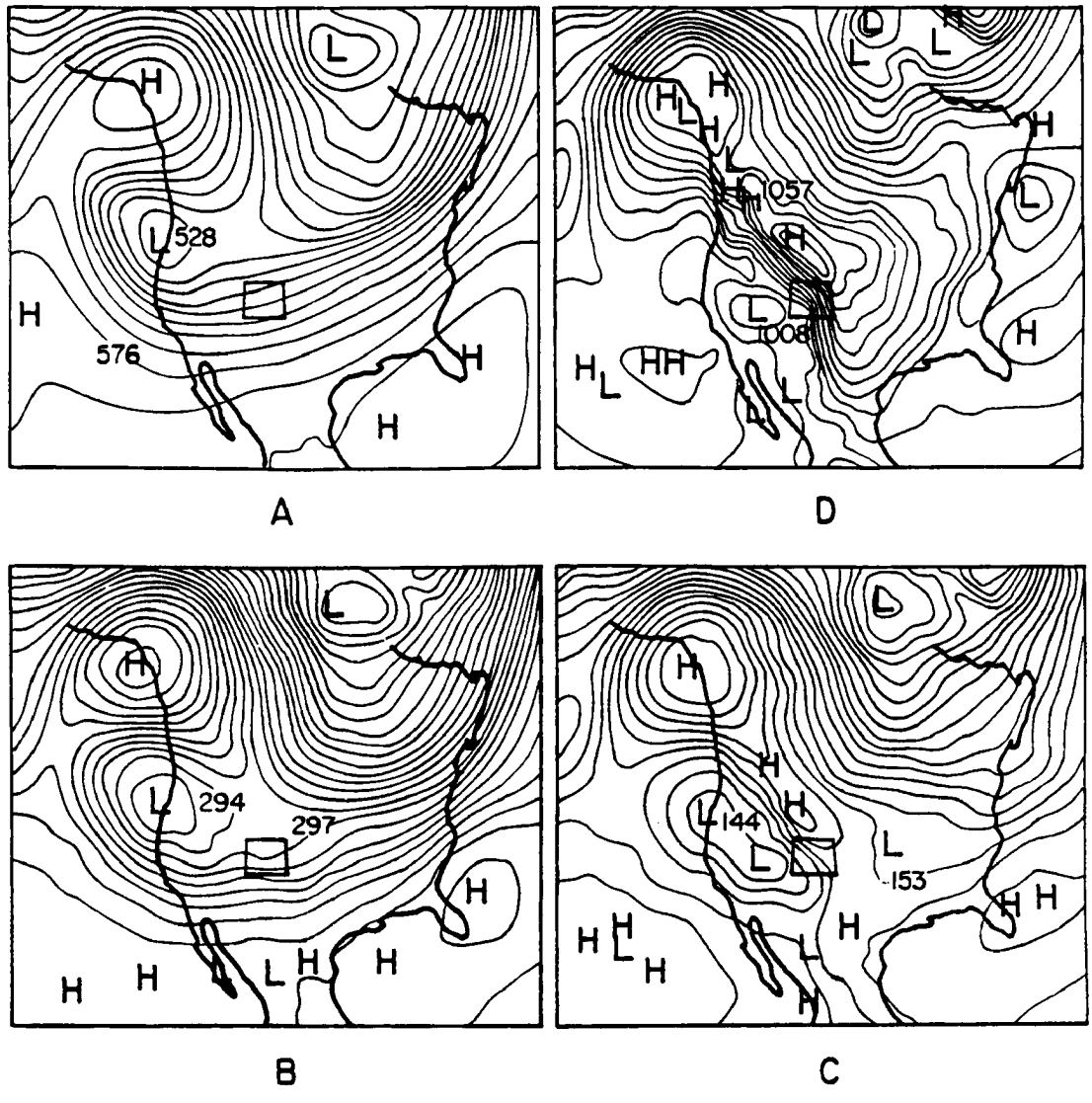

Figure 3.13: National Meteorological Center Nested Grid Model height analyses for 0000 UTC on 4 February, 1989. (a) 500 mb, (b) 700 mb, (c) 850 mb, and (d) sea-level pressure. Heights are labeled in dm. The state border of Colorado is heavily outlined.

to a weak-to-moderate shortwave ($12x10^{-5}$ s^{-1} absolute vorticity) which was entering west-central Colorado by 0000 UTC. It also coincided with the arrival of a very moist, cloudy air mass in the 700-500 mb layer, which had exhibited lower relative humidity and dew points until this time (Figure 3.3b-c). At 2100, the coldest IR tops were just barely west of FCL (Figure 3.14). Over and south of DEN, where few high clouds were evident, snow occurred in only trace amounts. At 2200, a marked boundary between deep, cold cloud to the northwest and low cloud to the southeast was apparent from approximately CYS to LXV.

The snow intensity at FCL increased dramatically during the latter part of the period (beginning at 2000), with visibility decreasing to 0.5 mi or less and weather remarks at both the 2300 and 0000 times reporting heavy snow (S+). At FOR, where precipitation rates dramatically increased at 2215 (from trace amounts to 0.25 – 0.5 cm hr^{-1}), pressure began to rise at 2100 after a rapid fall, indicating some deepening of the cold pool. The dramatic increase in snowfall intensity at FCL beginning at 2200 was accompanied by a marked increase in high cloud coverage over the Front Range at approximately the same time. The cloud increase was especially notable between FCL and LXV. Much lower precipitation amounts were measured to the east and northeast of FCL, however. DEN reported little or no increase in snowfall rate, and the deeper cloudiness did not arrive until about 0630. The strong southeasterly SLP gradient continued at 0000 UTC on the NGM analyses (Figure 3.13d).

0000 UTC – 1200 UTC 4 February 1989

During this period the area of cold cloud tops over Colorado expanded to cover most of the state. The coldest tops were in the west and southwest, and it is there where maximum snow accumulations occurred. The following 24-hour liquid precipitation totals were recorded in cm: Glenwood Springs 2.8, Rifle 1.9, Winter Park 1.7, Grand Junction 1.5, and Estes Park 1.3. Interstate 70 at Vail Pass closed periodically overnight and numerous vehicles were stranded to the west. There were 61 cm of snowfall reported at Beaver Creek ski resort (just west of Vail) for the 24 hours ending at 1200 UTC. A

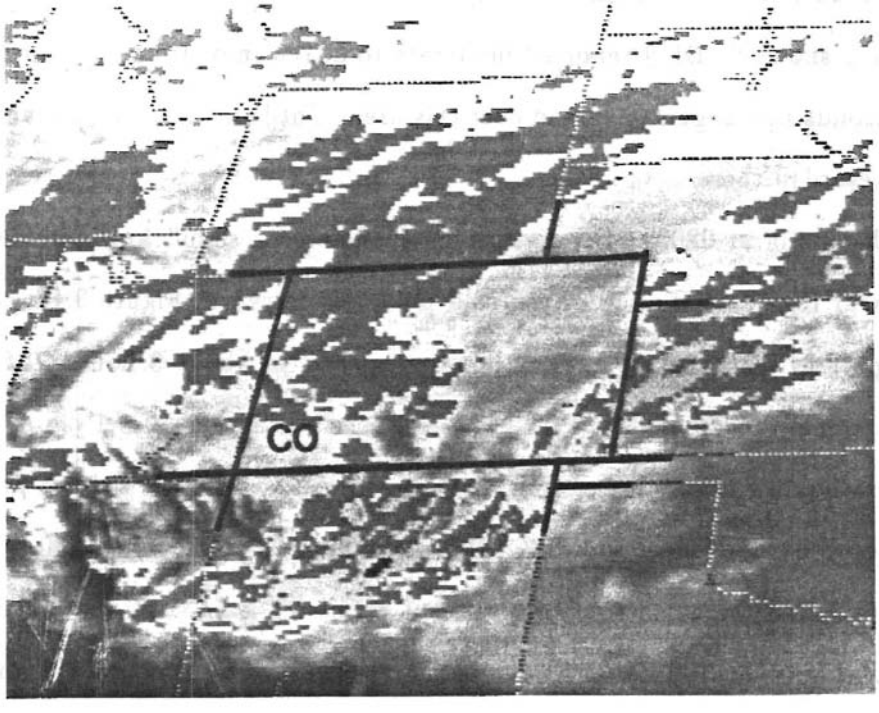

Figure 3.14: GOES-IR image (from GOES east) at 2101 UTC on 3 February 1989.

significant shortwave crossed the area during the period, with NVA beginning at about 1200 along the Front Range (see Figure 3.15).

At 0000 UTC 4 February, a southwest-northeast band of very cold tops (−35°C) through northeastern Colorado was clearly identified. By 0100, FCL was under deep cloud coverage (Figure 3.16). At this time, very low visibilities existed along the northern Front Range, caused by moderate to heavy snowfall. CYS reported heavy snow at 0400 and 0500, with liquid precipitation rates at about 0.05 cm hr^{-1}. At 0831, the band of deep cloud covered the FCL-CYS region, and was well-correlated with areas of moderate to heavy snowfall. DEN reported moderate to heavy snow from 1000 to 1200, just as the deep clouds had begun to spread over this area. Until this time, only trace snow amounts were recorded there.

Beginning at 0200, DEN profiler data indicated a significant increase in elevation of the shear region at the top of the cold pool. As shown in Figure 3.17, the depth of the upslope flow increased by several hundred meters in about 9 hours. After about 1100, snow intensity decreased at FCL. The city received a total of 9.1 cm of snow overnight (.64 cm liquid); about 1.8 cm fell at DEN. In this case, FOR surface pressure rises did not occur during heavy snowfall. DEN soundings at 0000 and 1200 UTC 4 February (Figure 3.3c-d) revealed a mixing ratio of about 0.3 g kg^{-1} in the cold pool. However, the layer between 700 mb and 500 mb (above the inversion) contained about 1.5 g kg^{-1}. This fact, combined with the observation that heavy precipitation began as colder IR CTT's developed and spread eastward, was further evidence for the moisture source being advection of Pacific air from the west, over the cold air. The satellite, precipitation, pressure and sounding data along with the NGM analyses indicated that synoptic forcing was providing widespread light snowfall east of the Continental Divide during this period, with a continued enhancement in and near the foothills along the northern Front Range.

1200-1800 UTC 4 February 1989

Coldest tops during this period were to the south and southeast of FCL (Figure 3.18). Upper clouds continued to dominate most of Colorado, but a few breaks developed

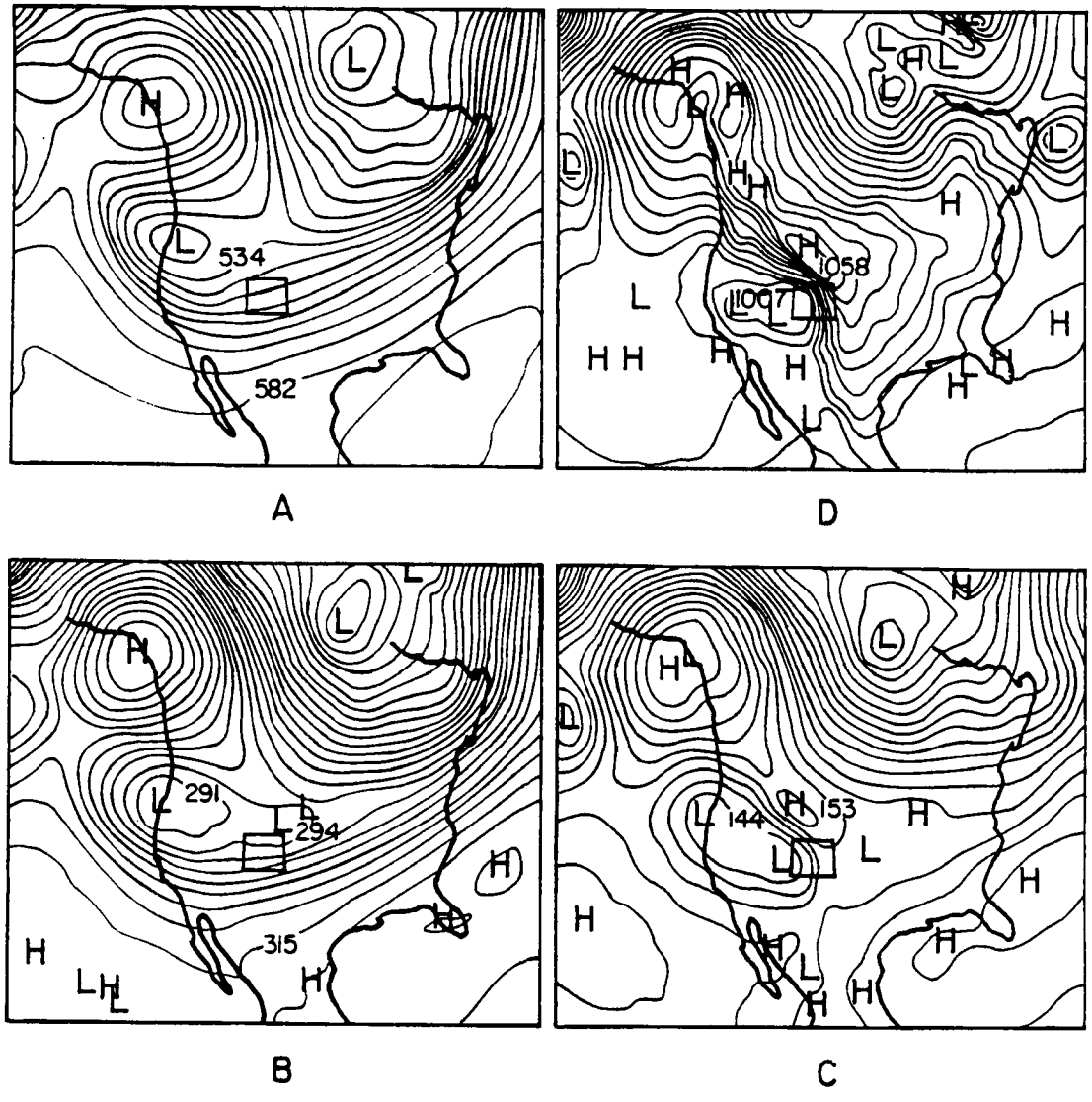

Figure 3.15: National Meteorological Center Nested Grid Model height analysis for 1200 UTC on 4 February 1989. (a) 500 mb (b) 700 mb (c) 850 mb (d) Sea-level pressure. Heights are labeled in dm. The state border of Colorado is heavily outlined.

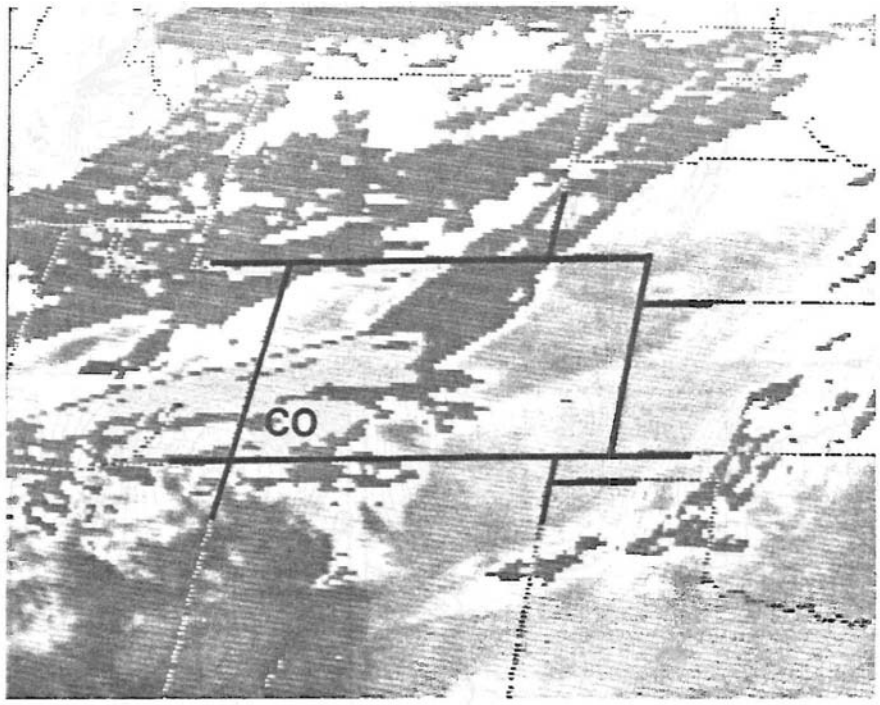

Figure 3.16: GOES-IR image (from GOES east) at 0101 UTC on 4 February 1989. The northern Front Range was under deep cloud coverage at this time.

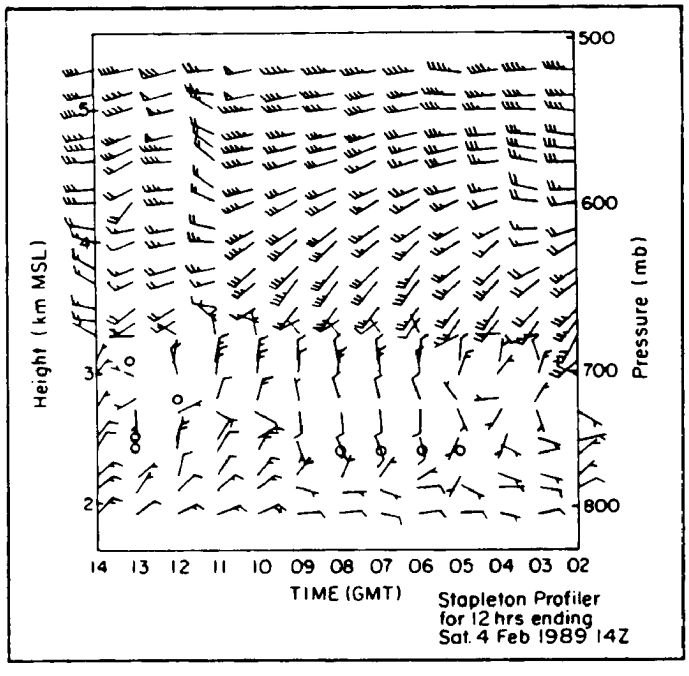

Figure 3.17: A series of profiler-derived winds at DEN for 12 hours beginning at 0200 UTC 4 February 1989 and ending at 1400 UTC 4 February 1989. Units for wind barbs are use standard notation in knots. Circles denote calm winds.

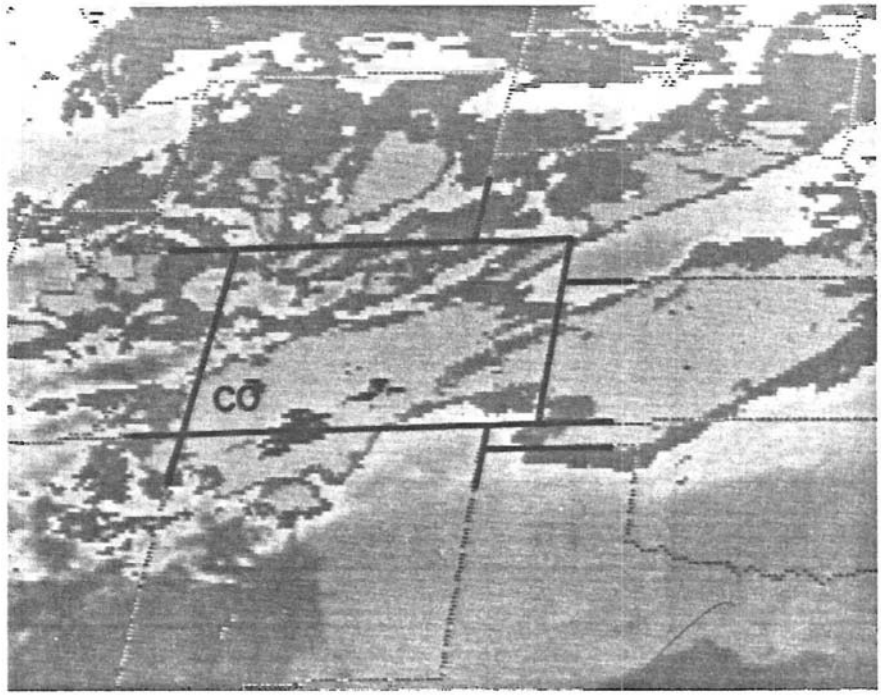

Figure 3.18: GOES-IR image (from GOES east) at 1201 UTC for 4 February 1989. Most of Colorado was covered by deep cloudiness with some breakup evident over the northern portions of the state.

in the coldest cloud top regions. At about 1500 UTC, the visibility at FCL rapidly increased from less than 1.6 km to 6.4 mi or greater. The snow total for this 6 hr period was 1.5 cm in FCL, with about 0.025 cm hr^{-1} liquid rate until around 1500 and trace amounts afterwards. CYS reported 0.75 mm between 1100 and 1200 with some broken deep cloudiness overhead. Precipitation rates thereafter decreased to only a trace hr^{-1}, as the upper cloud dissipated.

The NGM initial analysis at 1200 UTC (Figure 3.15) showed that one shortwave trough was exiting the northeast Colorado region, while another, moderately strong wave was just entering eastern Utah. At the same time, the 700 mb analysis showed lower relative humidity in the surface-to-500 mb layer behind the first wave. There were warmer cloud tops over FCL at 1500 than at any time since before 0700. This was correlated well with the decrease in snowfall. From 1500 to 1800, the high cloud coverage remained about the same (i.e. broken).

1800 UTC 4 February – 0000 UTC 5 February 1989

Generally, snowfall was light in FCL during most of this period, with no deep cloud coverage. The small snowfall amounts (0.5 cm) were probably the result of weak upslope flow. However, the upper clouds associated with the Utah wave began to fill-in over northeastern Utah and northwestern Colorado. With time, the mass of cold clouds grew larger and moved east-northeastward. By about 2200, the effects had just reached the FCL area. Visibility began to drop again, and snowfall intensity increased significantly very late in the period.

The evening NGM analyses (not shown) indicated that the large mass of cold clouds was, indeed, associated with the Utah shortwave. The 850-500 mb relative humidity increased again southwest of FCL. At this time, the deep, cold cloud mass associated with the strong shortwave was poised just west of FCL, stretching from south-central Wyoming to west-central Colorado. It was expanding and deepening, most notably in the northwestern portion of the state.

0000-0600 UTC 5 February 1989

During this 6 hr period the FCL snow intensity increased dramatically, apparently due to large-scale dynamical forcing. The cold cloud mass associated with the Utah shortwave persisted and continued to move east-northeastward across northern Colorado and southern Wyoming. Once again, DEN profiler data (not shown) indicated some deepening of the shear zone at the top of the cold pool beginning at 2300. Surface pressure at FOR was approximately steady as the snowfall rate increased. Visibility was fairly constant (1.6 km or less) until 0600 when observations at FCL indicated both a sudden increase in visibility and the beginnings of a sharp decrease in the snowfall rate (to about 1/3 of what it had been). However, the only apparent change in the upper cloud field at this time was slight warming at cloud top. The coldest tops were found over southeastern Wyoming and exhibited a comma-shaped appearance. CYS reported moderate to heavy snowfall from 0200 to 0600, while DEN received light to moderate snowfall from 2300 to 0800. Measurable snow continued at both locations until approximately 1200.

According to the DEN sounding at 0000 UTC, easterlies in the lowest levels were no longer present. The 0000 UTC NGM analysis indicated that the SLP gradient strength was rapidly decreasing over northeastern Colorado, although PVA aloft was still fairly strong.

0600 UTC – 2100 UTC 5 February 1989

The upper cold cloud mass moved out of the area, visibility increased to 25 km or greater and the upslope ended (surface winds backed from easterly to northerly by 0600, then light and variable). By midnight, cloud top temperatures were increasing rapidly over the area of interest. Correspondingly, this time period marked the last of the snowfall for the storm along the northern Front Range. There was only very light snowfall reported at FCL, CYS and DEN. The FCL temperature began a steady climb from −29 to −17°C (−20°F to +1°F), the first time the mercury had been above −18°C (0°F) in 83 hours. By 1930, cloud cover was negligible in most of the mountainous regions to the west of FCL. NGM SLP analyses indicated that the intense pressure gradient over the region was

no longer present. Upper levels were apparently subsident, and the wind direction at 700 mb had switched to northeasterly.

3.1.3 Microphysical Considerations

Observations of snow crystal types during the snowstorm provided additional information regarding the location of the moisture source for the snowfall. Primarily dendritic and stellar crystals, predominantly aggregated and frequently heavily-rimed, were observed during several periods of moderate to heavy snowfall on the days of 2-4 February (during the four periods described in the previous section: 0000-0700 UTC 3 February, 0700-1200 UTC 3 February, 0000-1200 UTC 4 February, and 0000-0600 UTC 5 February). Several meteorologists (e.g. P. Schultz and J. Smart, personal communication, among others) in the Boulder area also reported primarily dendritic aggregates during moderate snowfall on both 3 and 4 February. Significant graupel accumulation was observed in FCL during two episodes of the evening hours of 3 February and the early morning hours of 4 February.

These crystals could not have originated within the -20 to -30°C conditions observed within the low-level cold air throughout the storm (see Figure 3.3). As shown in Byers (1965), crystal habits at these temperatures are primarily plates and columns. The moisture source apparently resided in the moist westerly flow aloft, which exhibited -10 to -20°C temperatures, a regime favorable for dendritic crystal growth. Such evidence is strongly supportive of the precipitation scenario described previously (see Figure 3.1).

3.1.4 Observational Summary of the 1-5 February 1989 Arctic Outbreak

Documented with standard NWS soundings surface observations and satellite data, the interaction of an intense cold pool with topography lead to enhanced snowfall along the Front Range despite frigid low-level temperatures. The author's experience in this region over the last 7 winters indicates that less extreme but dynamically similar events such as 19-23 December 1990, 19-25 December 1983, and 13-15 February 1990 occur with greater frequency. Strong overrunning in these cases is of much shorter duration.

3.2 9-10 February 1988

The storm of 9-10 February 1988 exhibited smaller snowfall totals (Figure 1.4) but again there was an extension of heavy snow onto the plains in the northern Front Range region. This case included the advection of a cold air mass from the north but was less extreme than the 1-5 February 1989 case. On the synoptic scale, at 0000 UTC 10 February, a weak but amplifying shortwave, evident on the 500 hPa NMC analysis (Figure 3.19a) was approaching Colorado from the northwest. Within a few hours, weak frontal passage occurred and snow showers began to fall over the northern portion of the Front Range, similar to the storm documented by Lilly (1981). As the positive vorticity center aloft moved closer, however, snow fell heavily for several hours, especially in and northwest of FCL. At the height of the storm (1200 UTC 10 February; Figure 3.19b) weak positive vorticity advection was occurring over the region, similar to the March storm discussed previously. An 80 m height fall at 500 hPa was recorded overnight at DEN. After the storm subsided, negative vorticity advection characterized the 500 hPa flow (Figure 3.19c).

As shown in these analyses and the 700 hPa analyses in Figure 3.20a-b, upper-level flow remained *northwesterly* throughout the storm, and no deep upslope developed as in the 30-31 March snow event. At the surface (Figure 3.21a-d), a polar frontal passage accompanied the lowering heights aloft. The gradual intrusion of extremely cold ($-18°C$ and below) Canadian air lagged the frontal passage by several hours. A weak cyclone developed by 0000 UTC 10 February just east of DEN, with frigid air moving southward through Wyoming and Nebraska. This pattern is similar to the anticyclonic upslope events discussed by Dunn (1987), and Boatman and Reinking (1984). By 0000 UTC 11 February (Figure 3.21d), the polar front had reached Texas. Strong postfrontal southeasterly upslope conditions persisted through the day over the Front Range.

A look at the meso-network streamline (Figure 3.22a-d), temperature and dew point analyses (Figure 3.23a-d) revealed some terrain blocking of upslope flow but no well-defined convergence line. A weak cold front had passed through the meso-network at about 0300 UTC. At 0600 UTC 10 February, when light snow had just begun to fall at FCL, a relatively

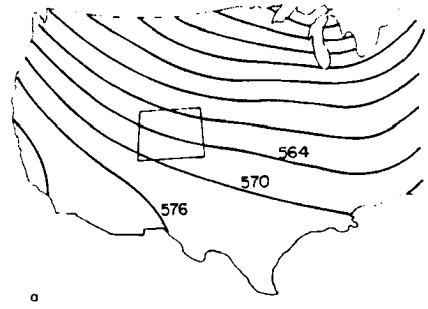

Figure 3.19: (a) NMC 500 hPa analysis for 0000 UTC 10 February 1988. Heights are in dm.

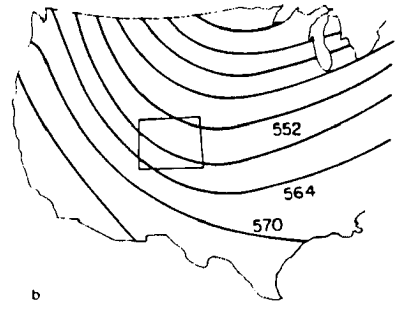

Figure 3.19: (b) NMC 500 hPa analysis for 1200 UTC 10 February 1988. Heights are in dm.

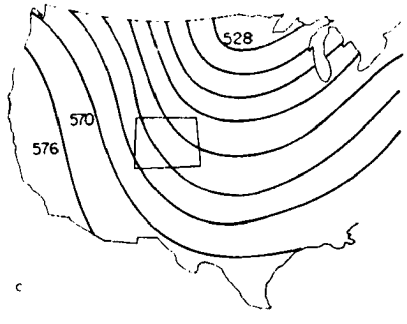

Figure 3.19: (c) NMC 500 hPa analysis for 0000 UTC 11 February 1988. Heights are in dm.

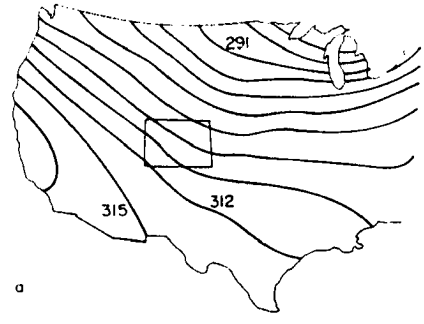

Figure 3.20: (a) NMC 700 hPa analysis for 1200 UTC 10 February 1988.

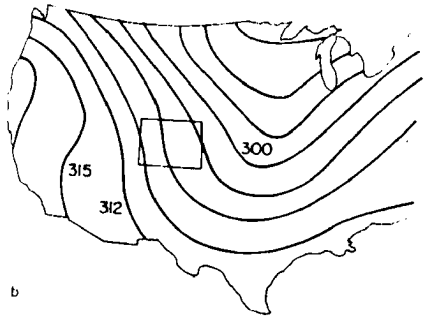

Figure 3.20: (b) NMC 700 hPa analysis for 0000 UTC 11 February 1988.

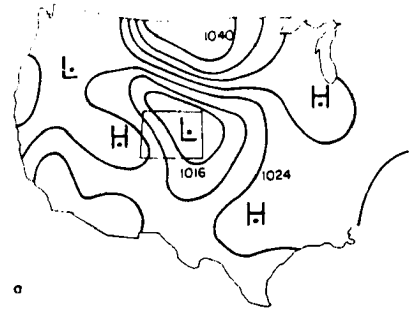

Figure 3.21: (a) NMC mean-sea level pressure analysis (hPa) at 0000 UTC on 10 February 1988.

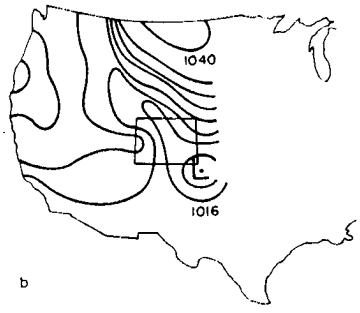

Figure 3.21: (b) NMC mean-sea level pressure analysis (hPa) at 0600 UTC on 10 February 1988.

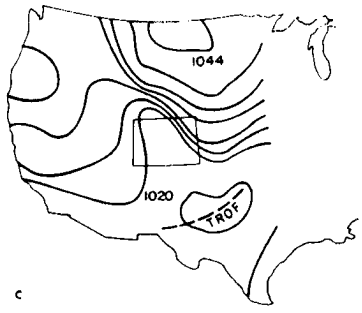

Figure 3.21: (c) NMC mean-sea level pressure analysis (hPa) at 1500 UTC on 10 February 1988.

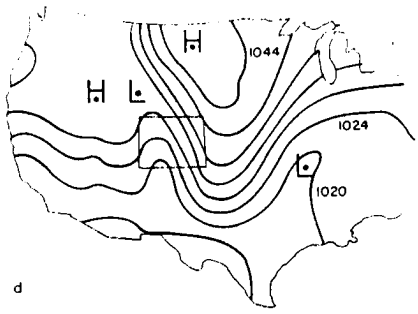

Figure 3.21: (d) NMC mean-sea level pressure analysis (hPa) at 0000 UTC on 11 February 1988.

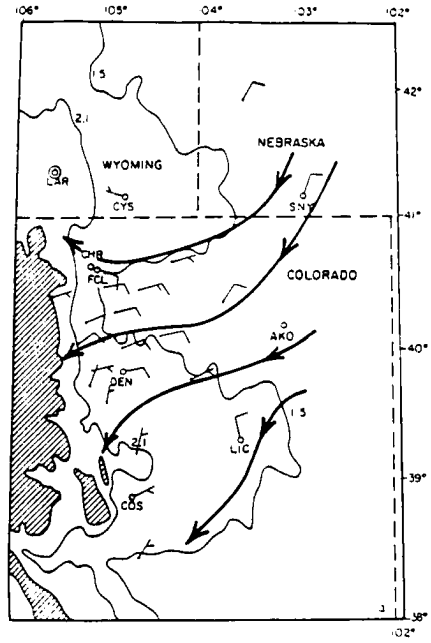

Figure 3.22: (a) Surface streamline analysis (by hand) over the PROFS meso-network at 0600 UTC on 10 February 1988. One full wind barb equals 5 m s^{-1}. Convergence line (see text) shown as heavy dotted line. Elevations, station identifiers, etc. are as in Figure 1.2.

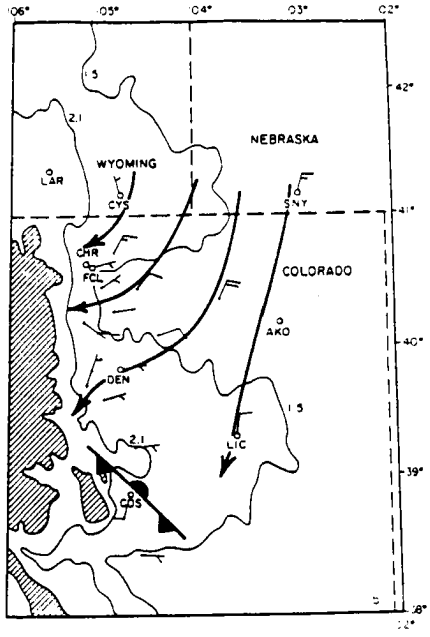

Figure 3.22: (b) Same as (a) except at 0900 UTC on 10 February 1988.

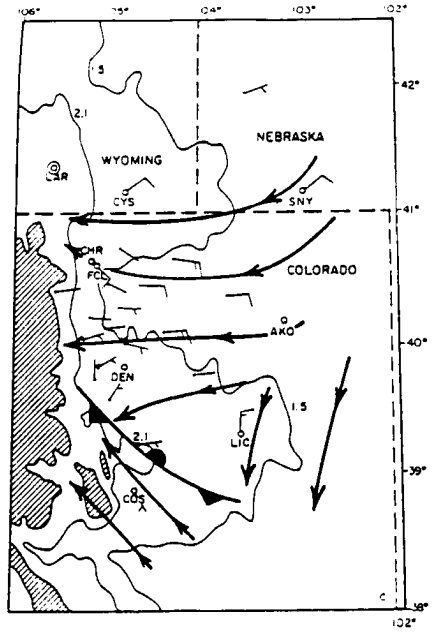

Figure 3.22: (c) Same as (a) except at 1200 UTC on 10 February 1988.

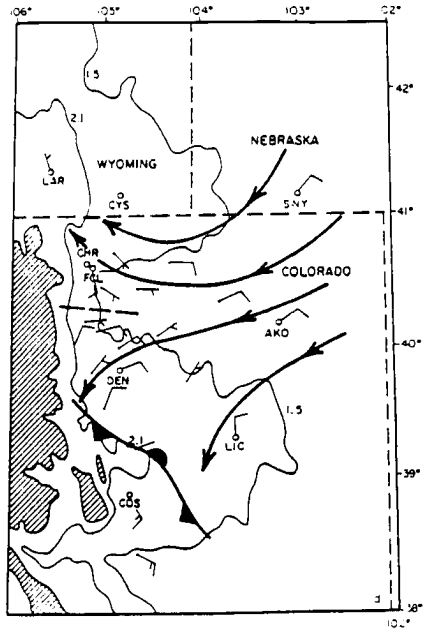

Figure 3.22: (d) Same as (a) except at 1500 UTC on 10 February 1988. Heavy dashed line indicates location of maximum divergence (see text).

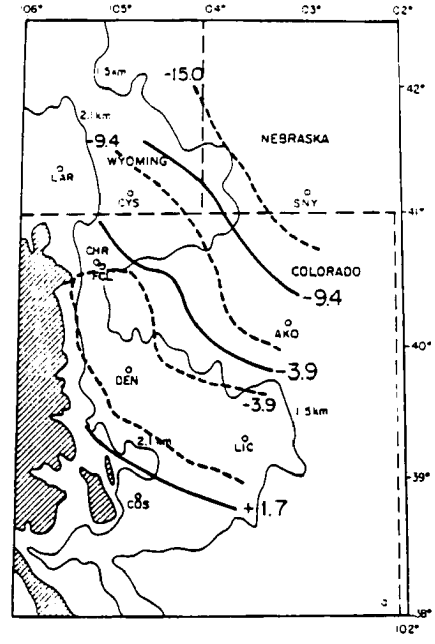

Figure 3.23: (a) Surface meso-analysis of temperature (°C; solid lines) and dew point (°C; dotted lines) over the PROFS meso-network (see text) at 0600 UTC on 10 February 1988. Extreme northern and southern portions of the figure are not analyzed due to lack of data. Elevations, station identifiers, etc., are as in Figure 1.2.

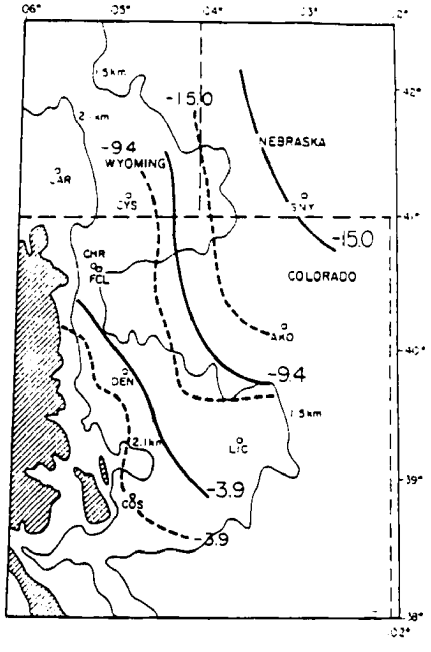

Figure 3.23: (b) Same as (a) except at 0900 UTC on 10 February 1988.

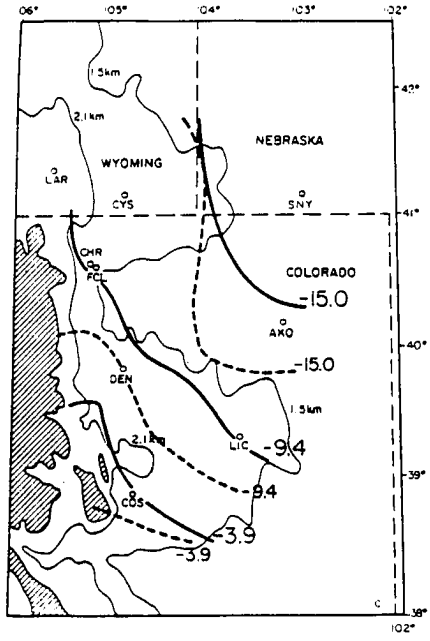

Figure 3.23: (c) Same as (a) except at 1200 UTC on 10 February 1988.

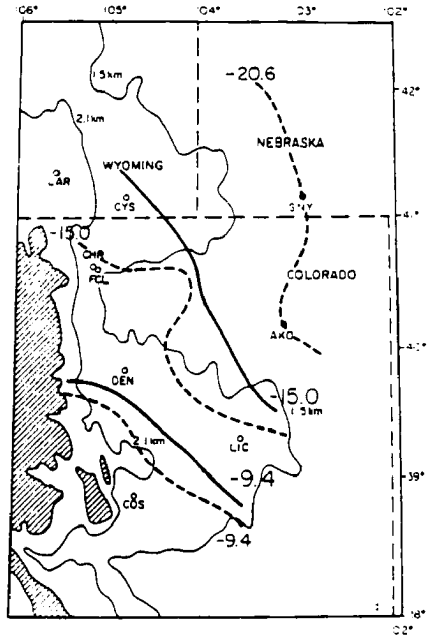

Figure 3.23: (d) Same as (a) except at 1500 UTC on 10 February 1988.

warm, moist air mass prevailed along the immediate Front Range. Strong advection of colder, drier air (in an absolute sense) from the northeast was occurring. Light easterly winds dominated the area from DEN to FCL, however, and nearly saturated conditions characterized this weak upslope. A weak wind shift from northeasterly to southeasterly was observed at the CHR ground station at approximately 0645 UTC, as snow intensity was increasing to heavy (Table 3.2). At 0900 UTC (Figures 3.22b and 3.23b), snowfall was heavy in the northern meso-network region. Later, during a brief period of easterly wind, snowfall intensity decreased to moderate until another switch to southeasterly flow. However, in contrast to the dammed cold air mass against the foothills in the 30-31 March 1988 case, temperatures nearest the foothills were actually warmer than those of the upstream easterly flow. By 1500 UTC, moderate east-northeasterly upslope winds were divergent, apparently due to topographic blocking, to the north and south along an east-west line approximately 30 km south of FCL. In addition, at 1200 and 1500 UTC, the polar front was located southwest of DEN and extended southeastward. Moderate snowfall was falling in COS at 1500 UTC near this cold front.

The CLASS soundings for this storm, shown in Figures 3.24, 3.25, and 3.26, also revealed a layered structure, but with some significant differences from the March 1988 storm. The first sounding, released during light snowfall at CHR, indicated two layers, one of northeasterlies and one of westerlies, separated by an inversion centered at approximately 730 hPa. By 0812 UTC, when snowfall at CHR was heavy, the height of the inversion increased to about 680 hPa. After the passage of the arctic front, three distinct layers were apparent (0957 UTC), also during heavy snowfall. The layers were separated at approximately 780 and 690 hPa, where significant shear and lapse rate changes occurred. The base of the lower inversion, as determined from BAO (Boulder Atmospheric Observatory near Erie, Colorado) and CHR data, varied from 250 to 700 m above the ground during the storm. The easterly upslope layer was much shallower for the present case than the March storm, and winds within the arctic air were southeasterly. At 1314 UTC (Figure 3.24b), snowfall had decreased to moderate intensity, and layer separation

Table 3.2: Snowfall intensity and wind observations at Christman Field for the 10 February 1988 storm.

Time, UTC	snowfall intensity†	wind direction	wind speed (m s^{-1})
0600	L	ENE	2.5
0630	M	ENE	2.5
0700	H	SE	1.5
0730	H	S	1.5
0800	H	SE	2.5
0830	M	E	2.5
0900	M	SE	5.0
0930	H	SE	3.5
1000	H	SSE	4.5
1030	H	SE	4.5
1100	M	SE	5.5
1145	H	-	-
1200	H	SE	4.0
1230	M	SE	5.0
1300	M	SE	5.0
1330	M	SE	5.0
1400	M	SSE	4.5
1430	M	S	3.5
1500	M	S	2.5
1530	L	SSE	5.0

†Snowfall intensities are based on horizontal visibility V.
H = heavy: V less than 0.6 km
M = moderate: V greater than 0.6 km but less than 1.2 km
L = light: V greater than 1.2 km

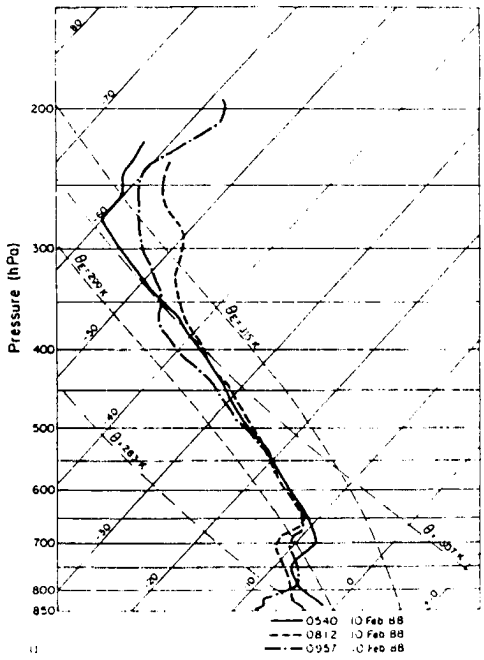

Figure 3.24: (a) CLASS temperature profiles for balloon releases at CHR for the 9-10 February 1988 storm. Horizontal solid lines are pressure (mb or hPa). Temperature (°C) values are the solid diagonal lines. Two labeled adiabats (dashed lines) are shown, as well as two moist adiabats (dashed-dotted lines).

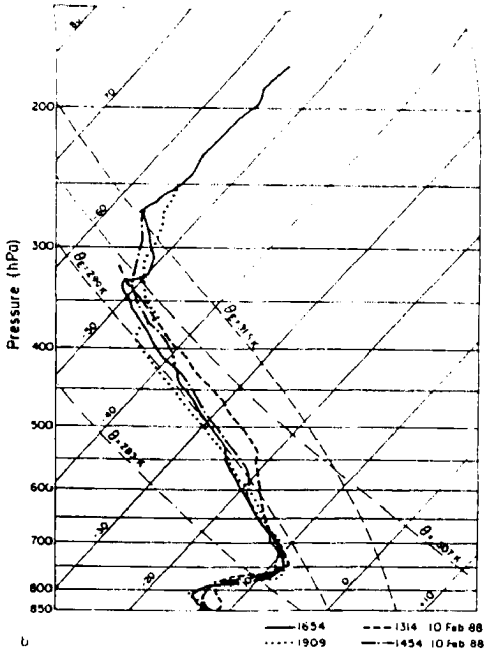

Figure 3.24: (b) Same as (a) except for the final three CLASS soundings of this storm.

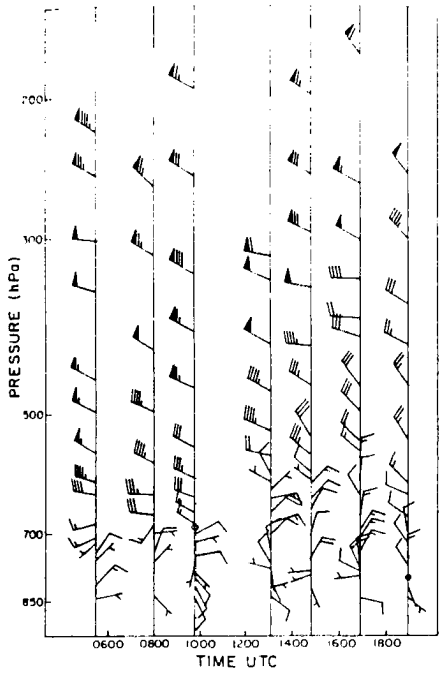

Figure 3.25: CLASS wind profiles for the 9-10 February storm. One full wind barb equals 5 m s^{-1}; one flag equals 25 m s^{-1}.

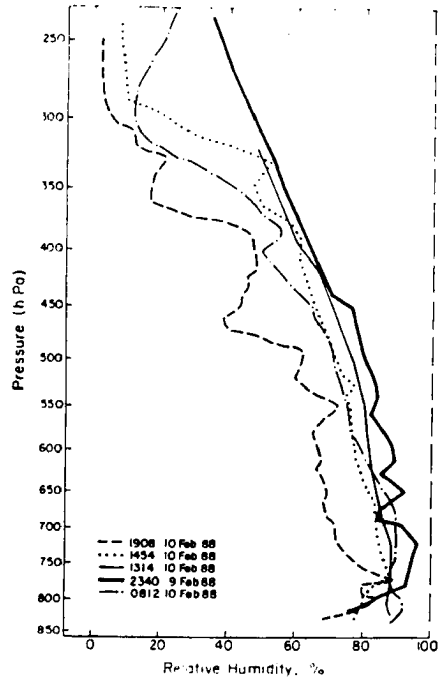

Figure 3.26: CLASS relative humidity profiles for the 9-10 February storm.

occurred at approximately 780 and 700 hPa. At 1454 UTC, cloud base was located within the strong inversion at the top of the arctic air mass. The lowest layer had cooled significantly by this time. The 1200 UTC 10 February DEN sounding showed no significant differences from the CHR profiles at 0957 and 1314 UTC aside from the absence of surface southeasterly flow. The inversions appear much less sharp on the reported DEN data, apparently due to the greatly reduced vertical resolution.

Lilly (1981) hypothesizes for the 9-10 February 1981 case that the amount of entrainment at the upper boundary of the cold mass air is critical to both the persistence of the cold upslope and the amount of low-level blocking present. Lee et al. (1989) found a similar relationship between entrainment and the persistence of the cold air mass in mesoscale model simulations. In the present case, the time period of a relatively high inversion (around 1314 UTC), implying reduced entrainment, was followed by upstream deceleration (Figure 3.23c-d), agreeing with the comments of Lilly (1981). The low-level arctic air mass in this storm did not exhibit a well-defined frontal boundary. The colder air filtered into the Front Range region beginning about 0600 UTC. The depth of the cold air increased to about 700 m over CHR at 1314 UTC (Figure 3.24) and actually decreased to about 400 m at 1654 UTC with nearly constant depth for the next few hours. As shown in Table 3.2, heaviest snowfall occurred as the depth of the cold air increased, similar to several periods of the 1-5 February 1989 event. Snow intensity decreased as the cold air lost depth.

Snow crystal types at CHR during the significant snowfall during the 9-10 February case were predominantly aggregated, heavily rimed spatial dendrites. A few of the aggregates were made up of planar dendrites. Irregular crystals comprised many of the aggregates, unidentifiable primarily due to the heavy riming; at times, the crystals had nearly enough riming to be considered graupel. Maximum aggregate diameters were typically 10 to 15 mm during the first few hours of heavy snowfall (approximately 0700-1100 UTC), and about 2 to 5 mm afterwards. The large rimed dendrites early in the storm probably grew to precipitation sizes well above the 700 hPa inversion shown in Figure

3.24a for 0812 and 0957 UTC. The temperature range conducive to dendritic growth at these times is confined to regions above 700 hPA. Some heavy snowfall occurred prior to 0957 UTC. After passage of the arctic front, it is likely that further dendritic growth occurred in the cold pool in the present case (Figure 3.24b), as crystals generated aloft descended. Aircraft reports (UND Citation, D. Burrows, personal communication) for the storm indicated persistent liquid water at and *below* the inversion at the upper boundary of the arctic air mass (Figure 3.24b). Liquid water amounts of a few tenths of g m^{-3} were measured for more than two hours. The predominance of heavily rimed crystals at the ground confirms the importance of these liquid water layers for precipitation growth.

Chapter 4

RAMS SIMULATIONS

Mesoscale model simulations, including prediction of cloud microphysics and precipitation, provided efficient complementary analyses to address the scientific objectives of this study.

The purpose of these numerical experiments was twofold:

1. To further analyze the terrain-induced snow production processes discussed previously in Chapters 2 and 3.

2. To assess the ability of RAMS (Regional Atmospheric Modeling System developed at Colorado State University; Walko and Tremback, 1991) to simulate a winter storm in the Front Range of the Rocky Mountains.

The approach adopted in this investigation was to run several idealized two-dimensional experiments, and then to run a three-dimensional simulation with microphysics activated. Since extensive data were available for the storms already discussed, certain portions of those data served as model initializations for each simulation.

The primitive equation RAMS produced these model simulations, using a telescoping, two-way nested grid. It utilizes the non-hydrostatic set of primitive equations. RAMS is a menu-driven modeling tool developed as a merger of several previous models (refer to Schmidt and Cotton, 1990; Nicholls *et al.*, 1990; Bossert, 1990 and Cram, 1990). The full microphysics version of the model has recently been successfully applied to winter storms in Colorado and California (Peterson *et al.*, 1991; Wesley *et al.*, 1990; Wesley *et al.*, 1988; Wesley and Pielke, 1988; Meyers, 1989; Meyers and Cotton, 1991; Cotton *et al.*, 1986).

4.1 Model Description

The surface layer energy calculation is achieved by the method presented in the study of Tremback and Kessler (1985) (a modification of the Mahrer and Pielke, 1977 algorithm). Radiative calculations include the effects of both longwave and shortwave energy, using the method of Chen and Cotton (1983). Turbulence calculations are achieved via the deformation-K closure scheme described in Tremback (1990). A Kuo-type cumulus parameterization employed on both grids complements the explicit cloud and precipitation predictions. For further details of RAMS not directly critical to the present study, refer to Walko and Tremback (1991).

The model microphysics module, presented originally in Cotton *et al.* (1982) and refined in Cotton *et al.* (1986) and Flatau *et al.* (1989), contains predictive equations for the mixing ratios of rain, graupel, pristine ice crystals and aggregates, and a diagnostic equation for cloud water. Concentrations of ice crystals are also predicted. Other physical processes modeled include vapor deposition, primary and secondary nucleation, and riming. The use of Fletcher curves in the model prediction of nucleation was recently upgraded, utilizing laboratory studies of the combined effects of deposition, condensation freezing, and contact nucleation (Meyers and Cotton, 1991). The new method predicts more realistic ice concentrations at cold temperatures (e.g., -10 to -30°C).

Previous simulations of blocking (Wesley and Pielke, 1988) have demonstrated the need for improved model initialization in order to predict small-scale storm structure, particularly for microphysical quantities such as cloud liquid water, ice crystal nucleation, aggregation and precipitation. The horizontally-homogeneous initialization approach, while useful for idealized two-dimensional experiments, simply cannot incorporate important larger-scale dynamical influences on the storm structure. In fact, upslope flow in the high plains is essentially forced by the larger, synoptic scale pressure fields. The interactive nesting capability, in combination with an NMC grid/radiosonde initialization, has been incorporated for the three-dimensional simulations in this study in order to capture processes occurring over this spectrum of scales. The NMC grids contain the fields of height,

wind, temperature, and relative humidity for mandatory pressure levels at 12-hour intervals. Observations of these properties at both mandatory and significant levels comprise the archived radiosonde data set. Finally, the surface data include wind, pressure, relative humidity, and temperature for the network of first-order stations throughout the grid domain. These data are analyzed hydrostatically on isentropic surfaces and then interpolated to the model grids (for a more detailed description of the analysis procedure see Tremback, 1990 and Cram, 1990).

Upon comparison with observational data sets, the nested mesoscale model should be an effective indicator of several key factors relating to the nature of low-level easterly flow: i.e., pre-existing low- and mid-level stability, surface wind direction and speed, evaporation, and secondary circulations induced by differential latent heating. The model can produce a three-dimensional field of vertical motion and condensate; these predictions form a convenient tool to analyze these features. Preliminary simulations have indicated that the orientation of the upstream surface flow is critical in establishing the regions of ascent as well as the orientation of the blocking-induced convergence line and thus may determine the location of heaviest snow for some situations. Furthermore, past studies (e.g., Lilly, 1981 and Cotton and Anthes, 1989) have pointed out an inverse relationship between entrainment at the inversion capping the cold pool and the extent of upstream blocking. With a sufficiently small vertical grid spacing, processes occurring at an inversion which caps blocked flow (e.g., Figure 3.3) can be evaluated with the mesoscale model. Indeed, this appears to be a region where liquid water production occurs. Riming and enhancement of ice crystal nucleation (Reinking and Boatman, 1986 and Rauber *et al.*, 1986) also may be significant in this layer.

4.2 Grid setup

The horizontal grid spacings for the coarse grid in the three-dimensional simulations, using a latitude-longitude mesh, are 1.0° and 1.3° in the y- and x-directions, respectively. At 40° latitude (the center of the domain), this spacing corresponds to 111.1 and 110.8 km, respectively. Vertical grid spacing is stretched from approximately 100 m near the

surface (50 m in the two-dimensional runs), to 500 m aloft, for both grids. The coarse (outermost) grid covers 88 to 140° in longitude and 25 to 55° in latitude (see Figure 4.1), and contains 44,400 grid points ($40 \times 30 \times 37$). The inner grid is centered over the domain of interest in northeastern Colorado (i.e. centered at latitude 40° and longitude 107°). Grid 2 employs one-fifth the grid spacing of the grid 1 and contains 109,668 grid points ($52 \times 57 \times 37$). Thus the horizontal grid spacing of grid 2 is 22.2 km in both the $x-$ and $y-$directions.

4.3 Two-dimensional Idealized Simulations

The modeling portion of this investigation was begun with simplified two-dimensional experiments. In order to further investigate the dynamics of the 1-5 February 1989 storm, and since any observational data set is somewhat limited in a three-dimensional sense, several two-dimensional experiments were performed using RAMS. The numerical model allowed some preliminary tests of the dynamical hypotheses discussed in Chapter 3. Interestingly, the NMC-based NGM with a horizontal grid spacing of about 85 km at latitude 45°N experienced serious problems with this storm throughout the U.S. high plains and mountains. NGM predictions of the evolution of the arctic air mass were consistently in error through 48 hours of simulation for several runs; these errors placed the cold air mass much too far north and under-predicted its depth along the eastern slopes of the Rockies (see Junker *et al.*, 1989).

Table 4.1 presents the basic options employed in this mesoscale model for the February 1989 storm simulations. The model was initialized horizontally homogeneously, using the temperature and wind profiles measured at DEN during the initial stages of the storm (see Figure 3.3a). Using this initialization, the cold air is confined to elevations below about 2.8 km MSL east of the barrier. The location of the east-west domain is approximately the latitude of DEN. The model thermodynamics only included water vapor as a passive tracer, with no moist processes.

Figure 4.2 shows the temperature field in the $x - z$ cross section after three hours of simulation. Note the strong inversion present at the top of the arctic air mass at

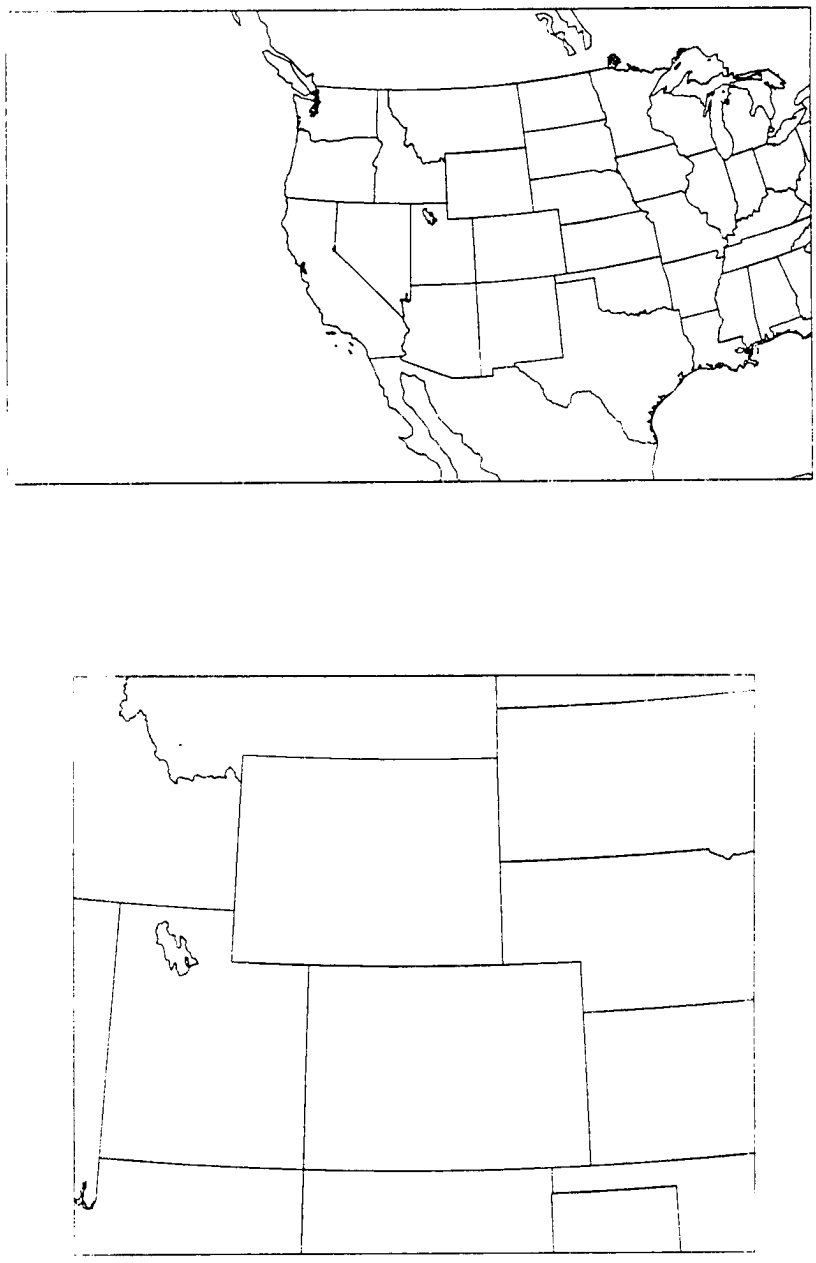

Figure 4.1: Model domain for both grids.

Table 4.1: Model options used in the Regional Atmospheric Modeling System (RAMS) for the February 1989 numerical experiments.

Model category	Option
initialization	horizontal homogeneous, DEN sounding 0000 UTC 3 Feb.
dimensions	2-dimensional east-west
top boundary condition	Rayleigh friction
height of model top	16 km
lateral boundary conditions	radiative, with mesoscale compensation region
thermodynamics	dry
radiation	longwave and shortwave parameterizations
horizontal grid, spacing, size	1 grid, 5 km, 100 grid points
vertical grid, spacing	1 grid, 50 m near surface stretched to 500 m above 10 km MSL
topography	silhouette-averaged from 30 sec data
time step	30 sec

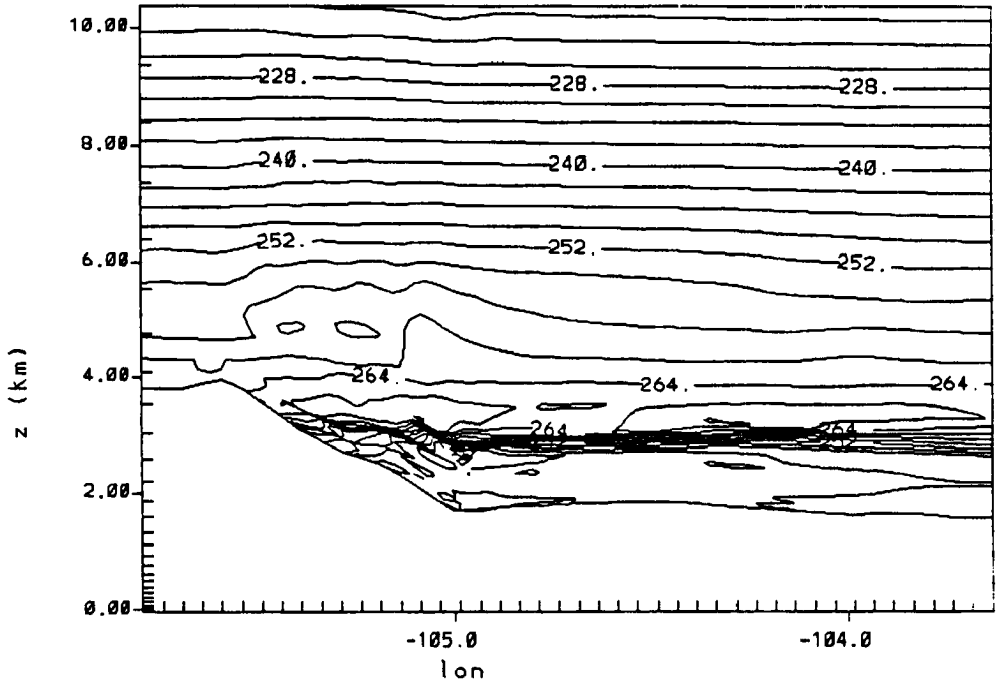

Figure 4.2: Model-predicted temperature field (K) over the Front Range region at three hours of simulation. Latitude of east-west domain is that of DEN. Region of close packing of isotherms is the inversion at the top of the arctic air mass. Temperatures within the cold pool are 240 to 250K. Contour interval is 3K.

approximately 2.8 km MSL. Of particular interest is the elevation of the temperature surfaces over the sloping terrain east of the mountain barrier at elevations of 3.1 to 3.3 km MSL. As previously discussed, a persistent bright band in the upslope cloud tops was observed along the foothills region for many hours during the storm. This band exhibited cloud-top temperatures approximately 3 to 5°C colder than the upslope cloud tops to the east. The similarity in the model features is striking.

The associated vertical motion field predicted by the model is shown in Figure 4.3. Immediately evident are the deep, terrain-induced gravity waves produced as the strong westerly flow crosses the mountain barrier. However, downward motion over the sloping foothills to the east, created by the flow over the barrier, is confined to regions above the inversion, and is much smaller in magnitude than that usually associated with strong cross-barrier flow, as reported in Lee *et al.*, 1989. Only weak vertical motion characterizes the region below the inversion. This is also consistent with the blocking scenario described previously.

In a separate sensitivity experiment, the cold pool was removed from the initialization. The original sounding (Figure 3.3a) was modified to exhibit a moist adiabatic lapse rate and moderate southwesterly flow between the surface and 700 mb. Figure 4.4 shows the resulting w field at three hours of simulation. The area of strongest downward motion just east of the barrier crest is larger in horizontal spatial extent and more intense (maximum -3 m s^{-1}, compared to -1.5 m s^{-1} in Figure 4.3). Downslope flow has propagated well down the east slope, into the foothills. Over the easternmost foothills, an area of moderate downward motion at 3.5 km MSL is evident; this is not present in Figure 4.4.

Further comparison of Figures 4.3 and 4.4 reveals a large difference in the w structure over the area of interest in this study (i.e. the extreme eastern portion of the steep terrain). The simulation with the cold pool (Figure 4.3) exhibits deep gravity wave structure above the bulge on the western edge of the cold pool, while the sensitivity run (Figure 4.4) produces only weak vertical motion in this region. In fact, an ascending portion of the gravity wave in Figure 4.4 is located directly over the western edge of the arctic air mass,

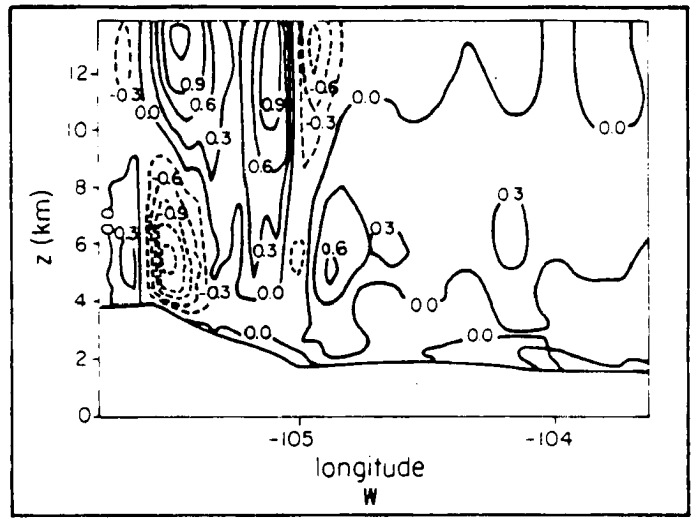

Figure 4.3: Model-predicted w field (m s^{-1}) over the Front Range region at three hours of simulation at 0300 UTC on 3 February 1989. Dotted lines are contours of negative w. Strong downslope is confined to heights above the arctic air mass. Maximum updraft speed for this portion of the domain is about 1.2 m s^{-1}, while maximum downdraft is 1.6 m s^{-1}. Contour interval is 0.3 m s^{-1}.

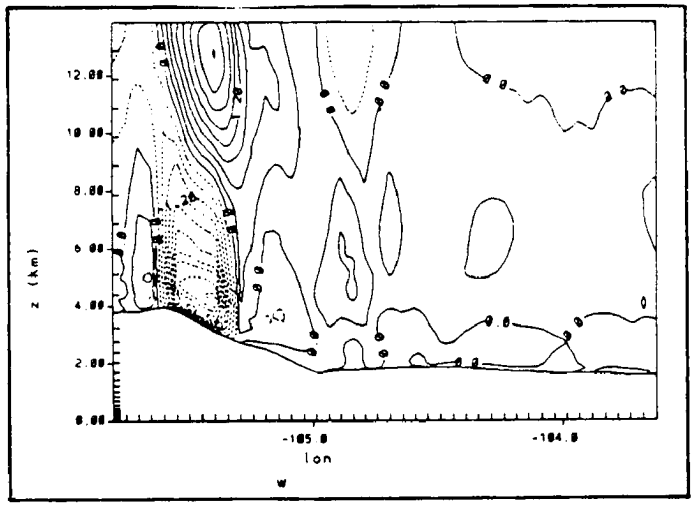

Figure 4.4: Same as Figure 4.3 except for the first sensitivity simulation. Model initialization does not include the cold pool. Maximum updraft speed for the cross section shown is about 2.4 m s^{-1}, while maximum downdraft is 3.0 m s^{-1}. Note the absence of gravity wave structure aloft well east of the barrier.

with upward motion exceeding 1 m s^{-1}. The location of the strongest ascent agrees qualitatively with the location of the snowfall enhancement.

A second and final sensitivity experiment was initialized identically to the simulation without the cold pool, with the exception of the lowest layers of the model. A cold pool was included in only the lower 150 m of the domain. Figure 4.5 shows the w field after two hours of simulation. Strong downslope flow has propagated rapidly down the slope to nearly the eastern plains, much further than in the previous two simulations. Apparently, the shallow cold pool effectively negates frictional retardation of downslope flow in this case, leading to an eastward extension of the strong descent region.

These two-dimensional simulations provide further confirmation that when a cold pool extends deep into the atmosphere along the eastern foothills of the Rocky Mountains during strong cold air outbreaks, the vertical extension provides a retardation of downslope flow associated with strong westerly winds aloft, and apparently generates a deep region of ascent over the western portion of the cold pool. As discussed in Chapter 3, heavy snowfall was observed in this region during a cold outbreak in February, 1989. This analysis is described in more detail in Wesley *et al.* (1990).

4.4 Three-dimensional Simulations

The numerical modeling portion of this study was then extended to three-dimensional simulations with microphysics activated, using a non-homogeneous initialization. Several additional important model features are noteworthy for this set of numerical experiments. First, at the top of the model a special absorbing layer, the modified Rayleigh friction layer, is utilized in order to handle large-scale variations in thermodynamic fields in this region, while minimizing downward reflection. This feature is described in detail in Cram (1990). Furthermore, model fields at the lateral boundaries for the coarse grid are nudged in a region five grid points wide along all four sides of the domain toward the objectively-analyzed assimilation fields produced prior to the simulation every 12 hours. The Davies nudging method is used, with strongest forcing at the coarse-grid boundary (Tremback, 1990). Model coarse-grid and fine-grid time steps are 90 and 18 sec, respectively.

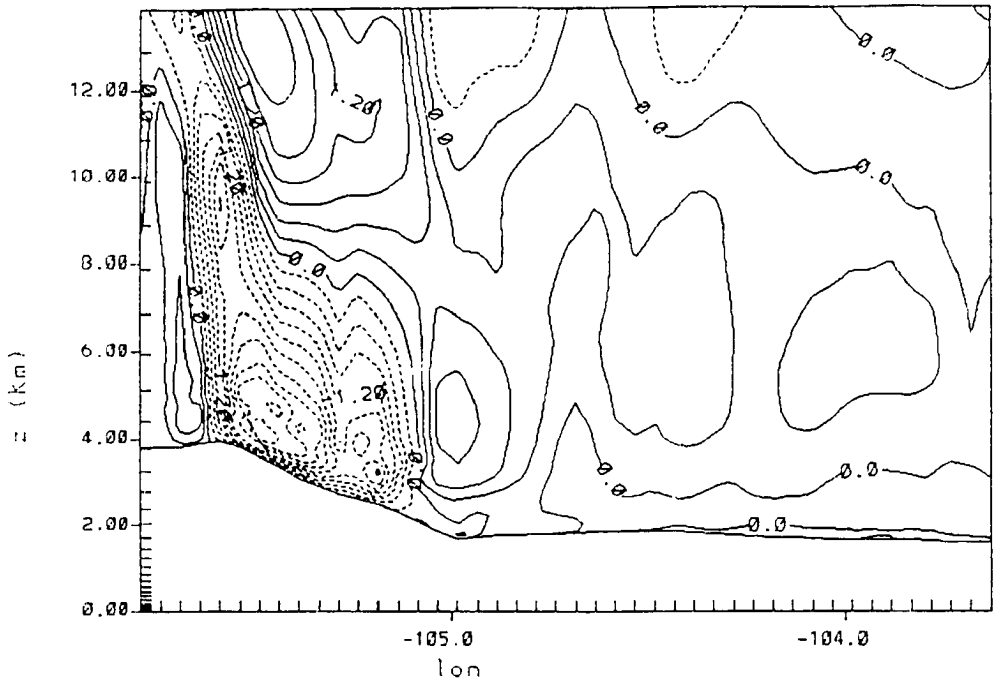

Figure 4.5: As in Figure 4.4 except for the sensitivity simulation initialized with a shallow cold pool. Shown is w field after 2 hours.

The model topography for both grids in the three-dimensional simulations is shown in Figure 4.6. Topography must be smoothed to some degree for numerical stability but the main topographical features, such as the Palmer Divide, Cheyenne Ridge, Platte River valley and major mountain peaks to the west, comprising the 3.8 km barrier, are retained. This smoothing is accomplished via the silhouette-average technique discussed in Bossert (1990). The nested terrain data set appears to be sufficient to investigate the topographical effects in these storms for the Front Range of the Rockies, and represents a major improvement over previous modeling studies in this region.

The 30-31 March 1988 event was chosen as model initialization for these simulations. The initial fields, as discussed previously, are the product of the objectively-analyzed NMC grids, surface observations and radiosonde data in the NCAR archive at this time.

The model initial winds (at 1200 GMT 30 March 1988) at the lowest two model levels are shown in Figures 4.7 and 4.8. At this time, a surface cold front, which resembled an inverted trough, stretched from central South Dakota, across western Nebraska and northwestern Colorado to the surface low pressure system just west of the four corners (refer to Figure 2.1). The associated model low-level winds in the vicinity of this unorganized low were northerly over western Utah and Nevada, and south-southwesterly over central and southeastern Colorado. Note that upslope flow has not yet developed over eastern Colorado or southeastern Wyoming. Strong convergence characterizes the front in extreme southeast Wyoming and western Nebraska. Other significant features dominating the surface wind pattern in both the model and the NMC analysis are a strong anticyclone off the west coast of northern California and Oregon, and a low-level southerly jet over eastern New Mexico and western Texas, into western Kansas ahead of the developing trough. Model winds compare favorably with the NMC mean sea level pressure (MSLP) analysis at this time over the coarse grid domain. One exception of note is the apparent northward misplacement of the surface front over eastern Colorado. As a result, DEN exhibits southwesterly low-level winds in the model. At the 2.65 km model level (Figure 4.9) which roughly corresponds to 700 mb, the trough to the west of Colorado appears to

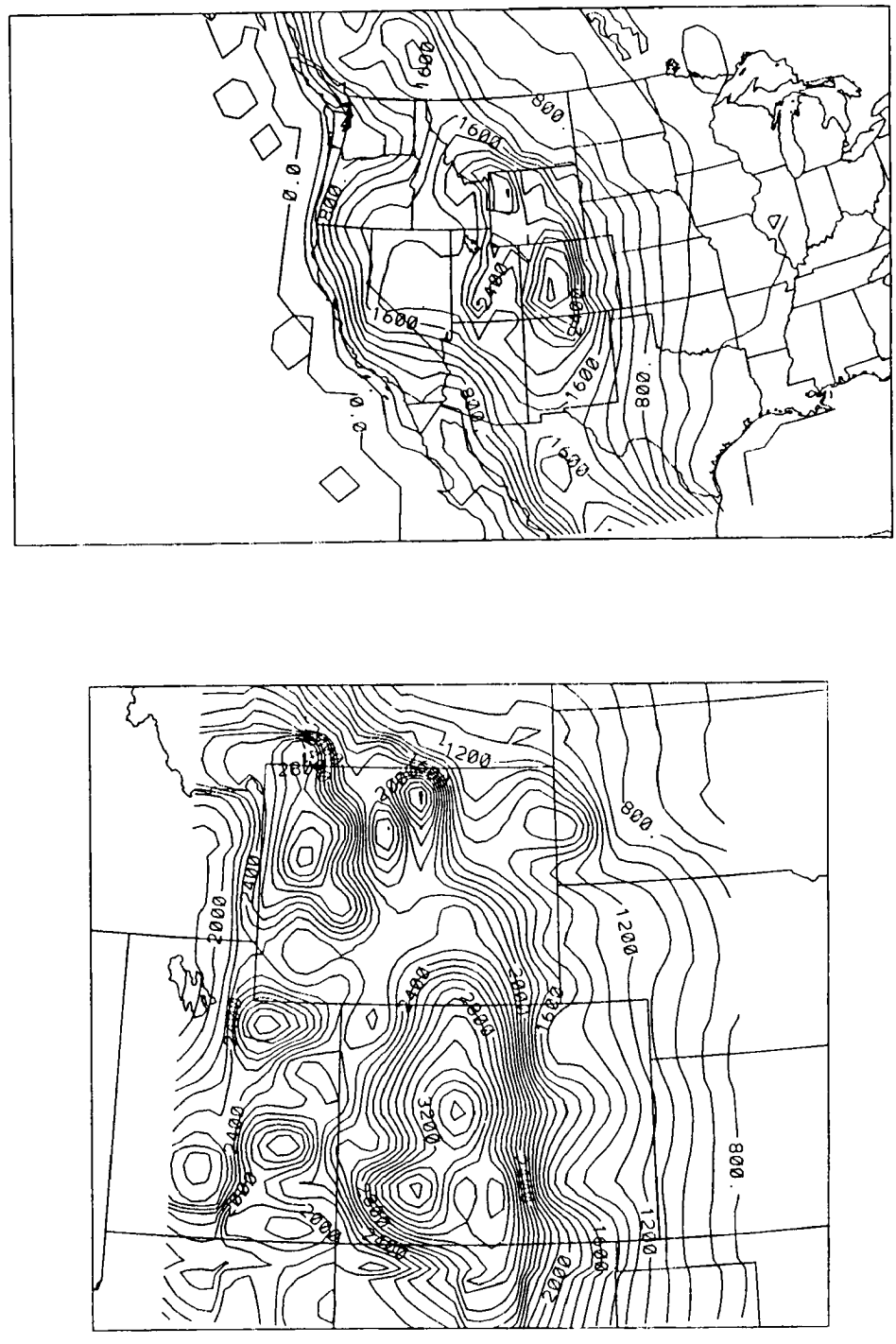

Figure 4.6: Model topography (elevations in m) for grids 1 and 2 (with grid spacings of approximately 110 and 22 km, respectively). Latitude/longitude values are shown on the grid corners.

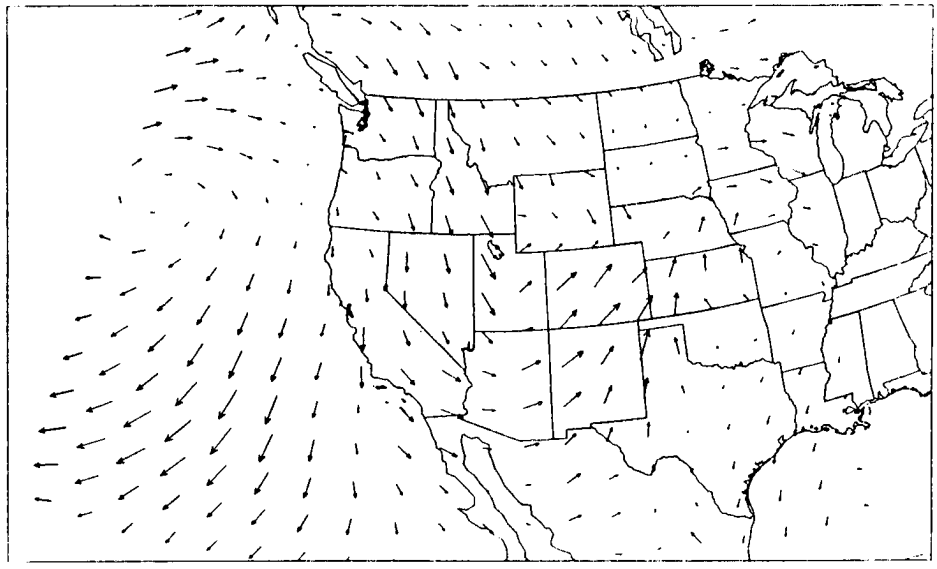

Figure 4.7: Initial model winds at $\sigma = 2$, 1200 GMT 30 March 1988. Maximum wind within domain shown is 16.3 m s^{-1}.

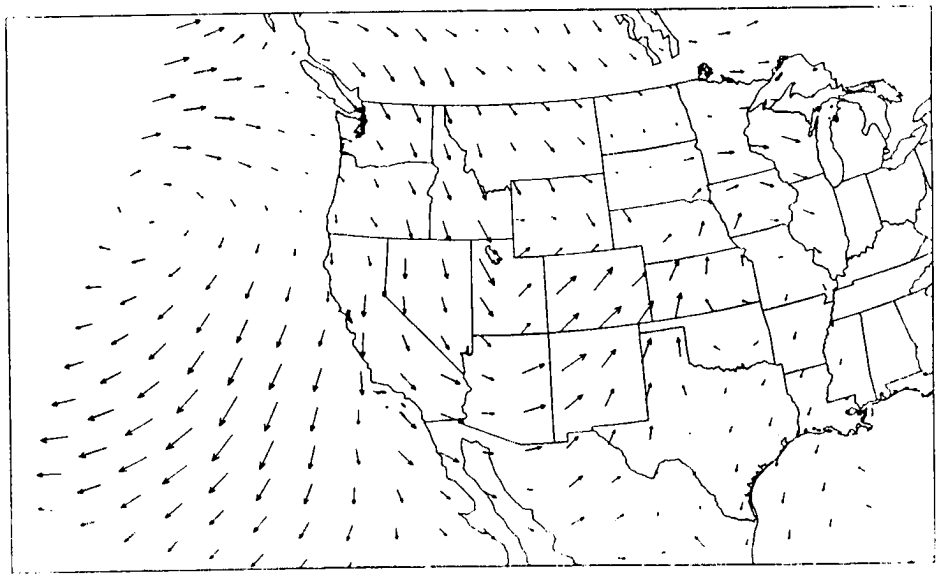

Figure 4.8: Initial model winds at $\sigma = 3$, 1200 GMT 30 March 1988. Maximum wind within domain shown is 16.2 m s^{-1}.

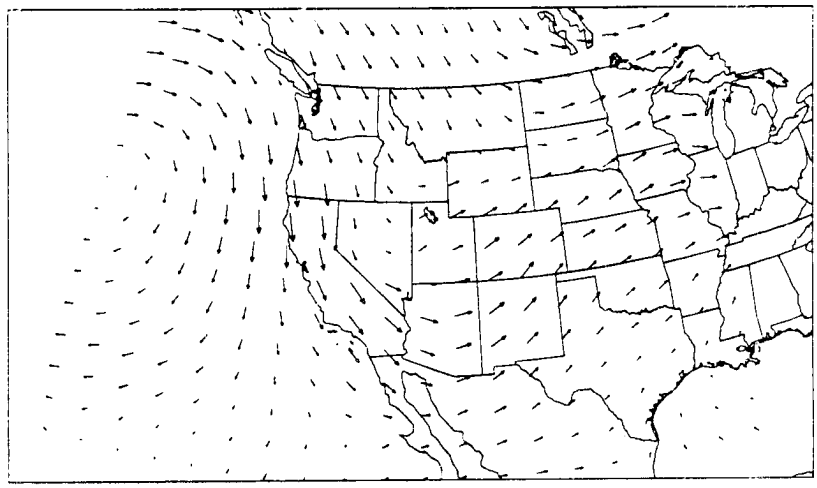

Figure 4.9: Model initial wind vectors at $\sigma = 13$, or 2.65 km over flat terrain. Maximum wind within domain shown is 28.7 m s^{-1}.

lie about 100 km west of its NMC-analyzed location. Southwesterly flow over northern and central Colorado appears to be somewhat stronger than that analyzed by NMC. A 50-60 knot northerly jet over southern California is analyzed well by the model, as is a shortwave ridge over Missouri and Iowa. Agreement is very good for winds at the 500 mb (model 5.65 km) level, with a strong jet maximum on the west side of the trough, a weak shortwave ride over eastern Wyoming, and the cutoff anticyclone off the west coast. At 300 mb (9.15 km), a slight discrepancy between the model analysis and that of NMC exists in the speed of southwesterly flow across Colorado and Nebraska, with the model fields indicating 40 to 60 knots and NMC analyzing 60 to 80 knots. Otherwise, the significant northerly jet maximum west of the trough, the subtropical jet stream and the off-coast ridge all appear to be well-analyzed by RAMS.

Figure 4.10 is an $x - z$ cross section of temperature along the latitude of Boulder, Colorado. Interestingly, a shallow warm pocket of air exists over northern Kansas and southern Nebraska. This feature is apparently the result of warm advection from the south in this region in association with the low-level jet. Note the well-defined tropopause at heights ranging from 9.5 to 12 km.

At 1600 GMT (after four hours of dry simulation with only the coarse grid), the convergence in the surface winds (i.e. the cold front) has moved southward into east-central Colorado (see Figure 4.11 and Figure 4.12) in agreement with surface observations at this time. As a result low-level northerly component covers the northern portions of the state. By this time, a weak upslope component has also developed over the Front Range. The previously mentioned warm pocket has weakened significantly (Figure 4.13) although surface temperatures along the Front Range remain well above freezing (Figure 4.14).

The second grid was added to the simulation at 1600 GMT, and full microphysics inserted two hours later. This approach was selected to reduce the computational expense for the simulation, and to allow superficial noise to dissipate before detailed microphysics were included. At 1800 GMT, as shown in the $x - z$ cross section of u for the fine grid in Figure 4.15, a layer of easterly flow has developed over the Front Range and eastern

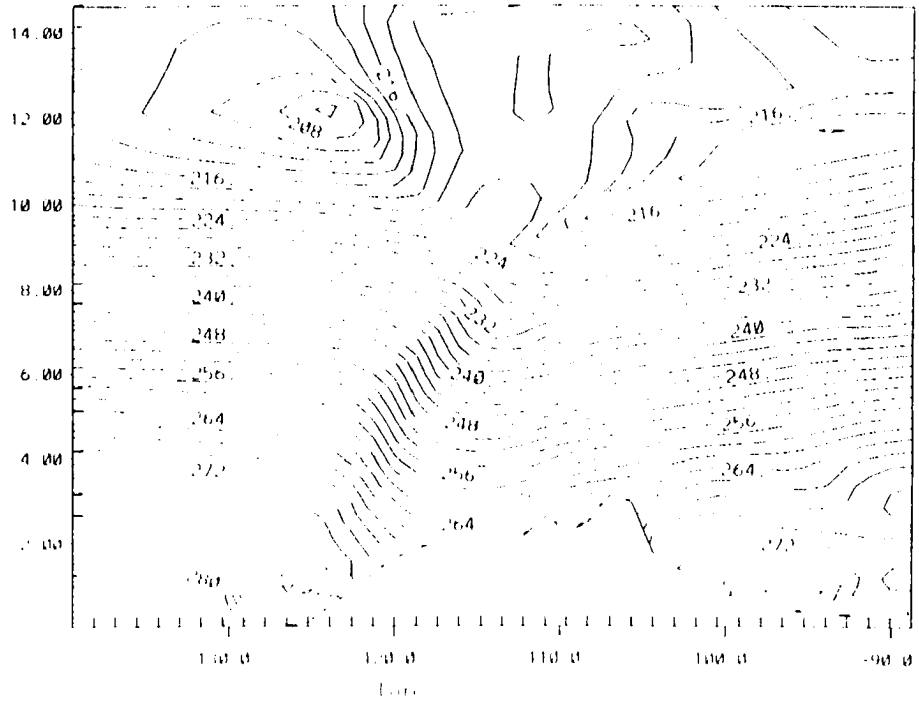

Figure 4.10: Initial model temperature (K), 1200 GMT 30 March 1988.

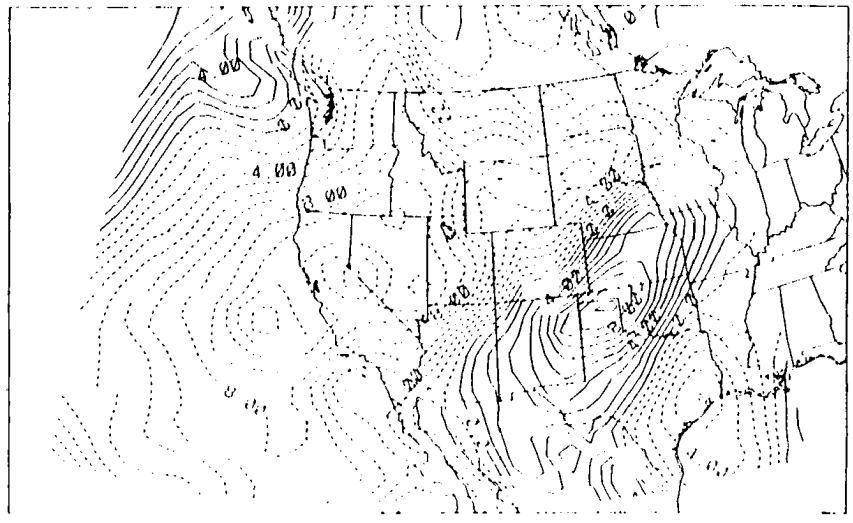

Figure 4.11: Model v-component (m s^{-1}), 1600 GMT 30 March 1988.

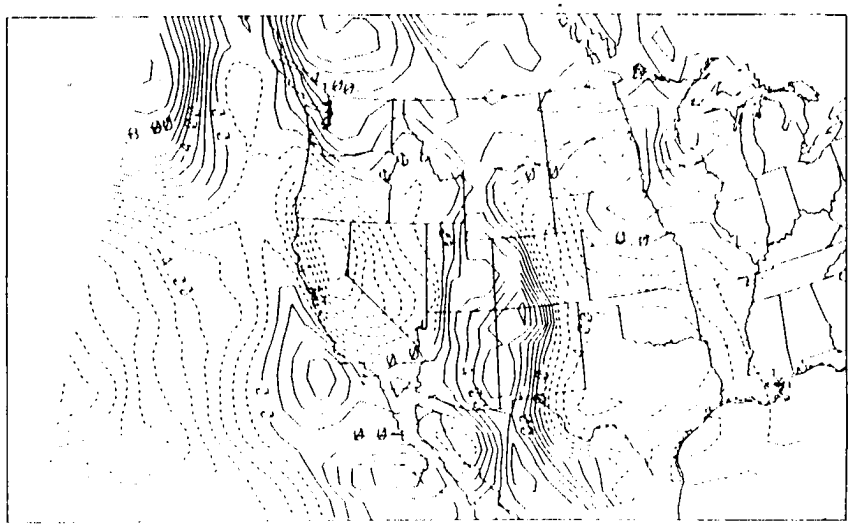

Figure 4.12: Model u-component (m s^{-1}), 1600 GMT 30 March 1988.

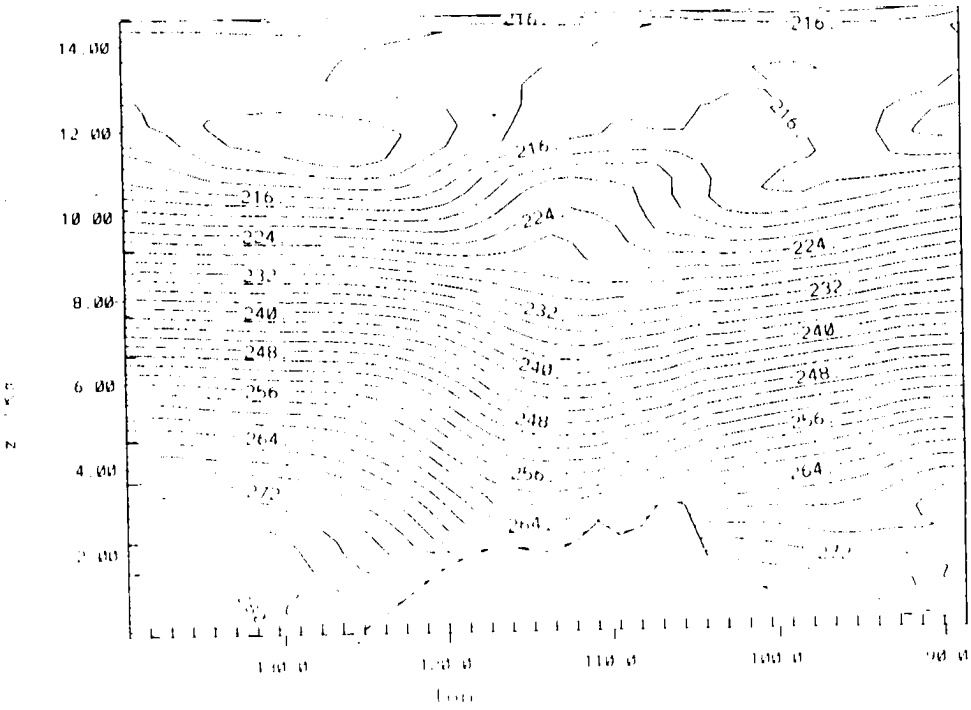

Figure 4.13: Model $x - z$ cross section of temperature, T (K), at 1600 GMT 30 March 1988.

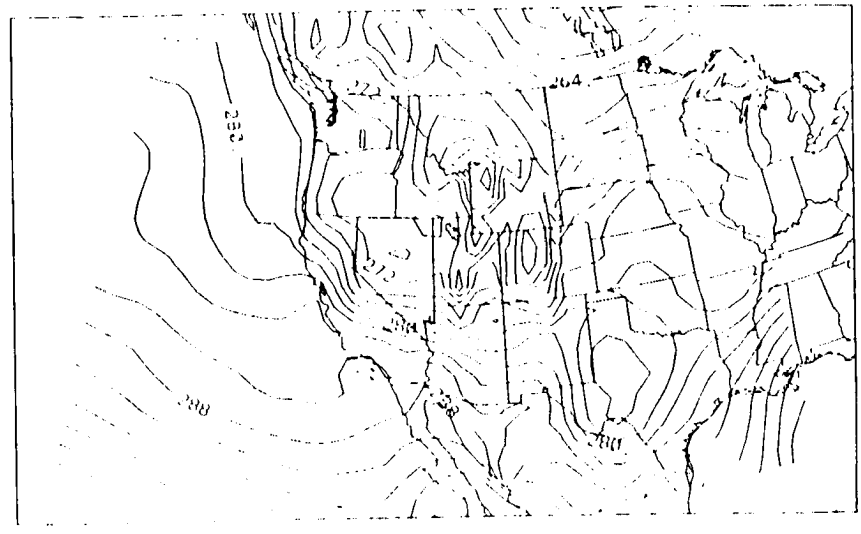

Figure 4.14: Model $x - y$ cross section of temperature, T, at 1600 GMT 30 March 1988.

plains of Colorado. This layer is about 1.5 km deep. The zero contour in this cross section exhibits somewhat less slope than the terrain. One hour later, the $x - y$ section of u at σ=2 (Figure 4.16) indicates significant upslope flow over northeastern and north-central Colorado, with an easterly component up to 9 m/s. Westerly flow at this point is confined only to elevated terrain in northern New Mexico. The corresponding temperature field (Figure 4.17) shows a warm pocket of air persisting in the Platte River Valley in northeastern Colorado, with surface temperatures as high as +3°C. At this point in the simulation, microphysics have been operating for only one hour. However, clouds and precipitation are already developing rapidly over the elevated terrain in Colorado. Figure 4.18 is an $x - z$ section of pristine ice crystal mixing ratio at 1900 GMT. As shown, ice fog and cloud are located over both high mountain regions, as well as in the North Park area. Some light precipitation is falling from the western portion of this cloudiness. Upslope flow east of the barrier is beginning to enhance the eastward extent of this cloudiness.

Several hours later, at 0000 GMT 31 March, the coarse-grid plots indicate the development of a synoptic-scale cutoff low pressure system over Utah, in agreement with the observations previously discussed. Figure 4.19 shows the total wind vectors at a model height of 2.65 km (note that this is plotted on a σ -surface, so in regions of highly varying terrain the actual MSL height of this surface is somewhat higher). Strong southerly flow is present east of this developing closed circulation. However, the center of the model-predicted cutoff at this level is about 100 km north-northwest of its actual location at this time, according to radiosonde observations. Easterly winds north of this low are somewhat weaker than geostrophic winds based on the NMC analysis. For example, the DEN radiosonde measured 15 knots of east-northeasterly wind at 700 mb; the model predicts 20 knots from the south-southwest. Off the Pacific Coast, the location and strength of the ridge, extending into southern British Columbia, compare well with the analysis. Winds at this level are also correctly predicted to be weak over most of Wyoming.

Comparison of the 850 mb analysis and the model-predicted low-level wind shows better agreement, with a developing trough extending from southern New Mexico into

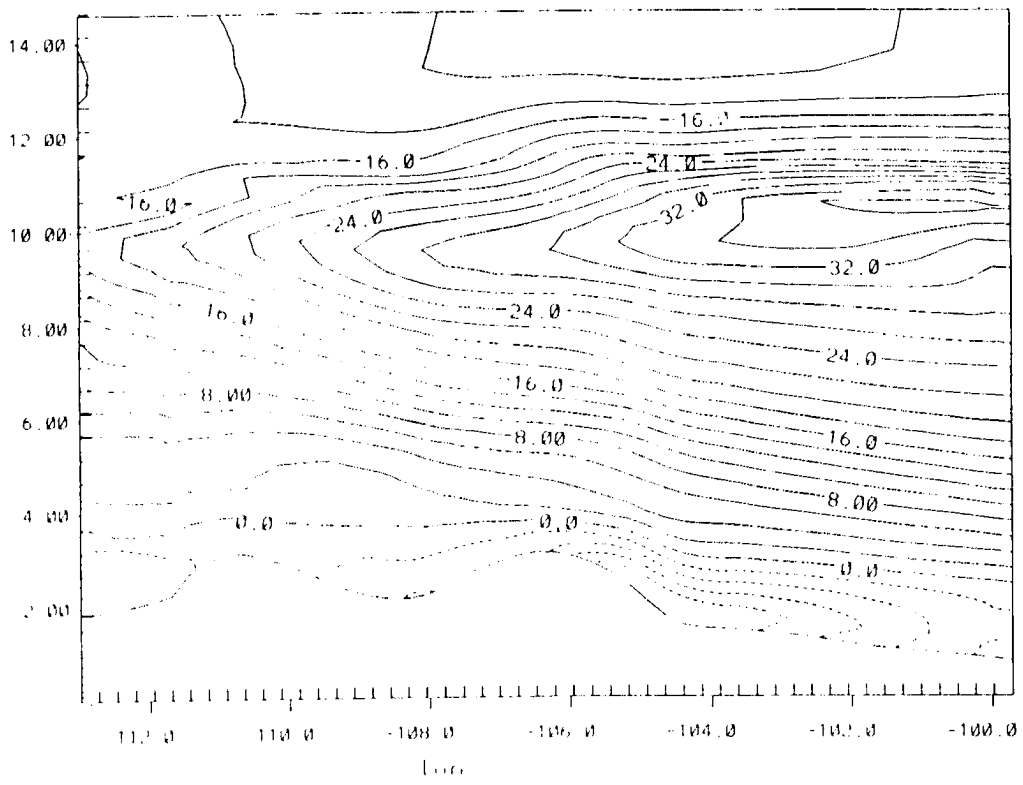

Figure 4.15: Model $x - z$ cross section of u-component (m s^{-1}), 1800 GMT 30 March 1988.

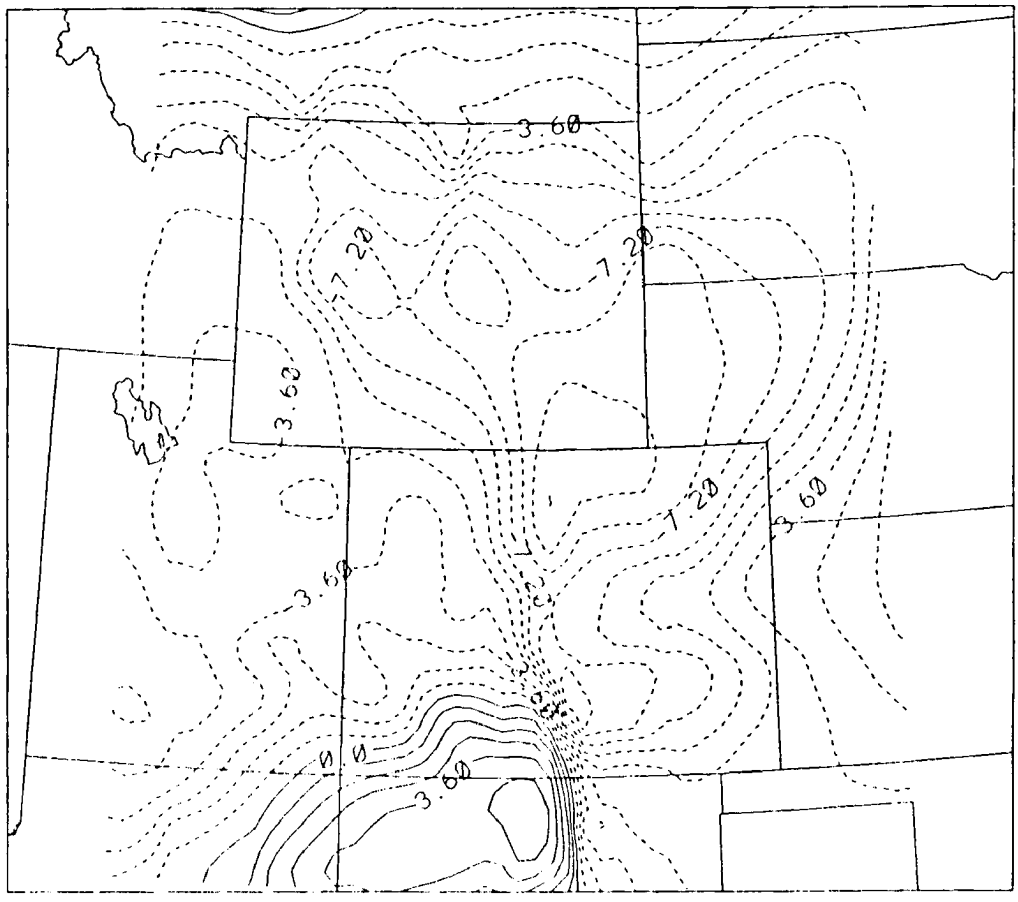

Figure 4.16: Model $x - y$ cross section of u-component (m s^{-1}), 1900 GMT 30 March 1988.

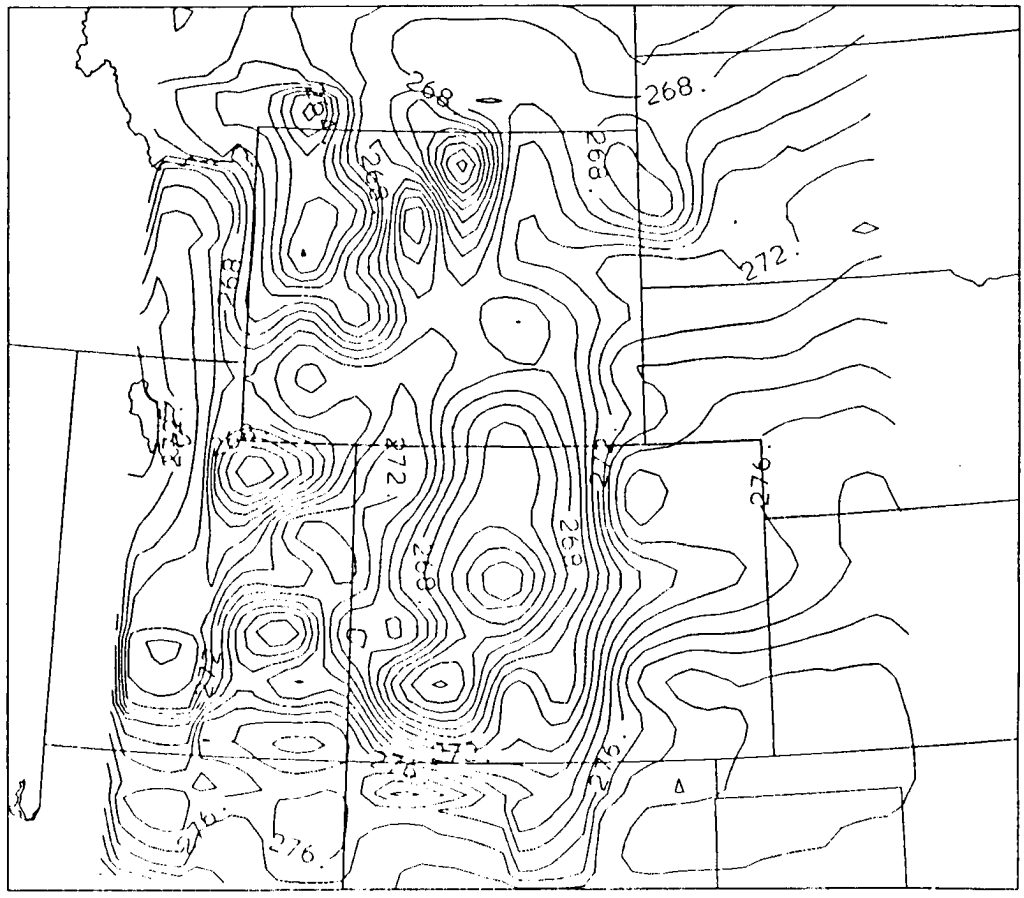

Figure 4.17: Model temperature, T (K), 1900 GMT 30 March 1988.

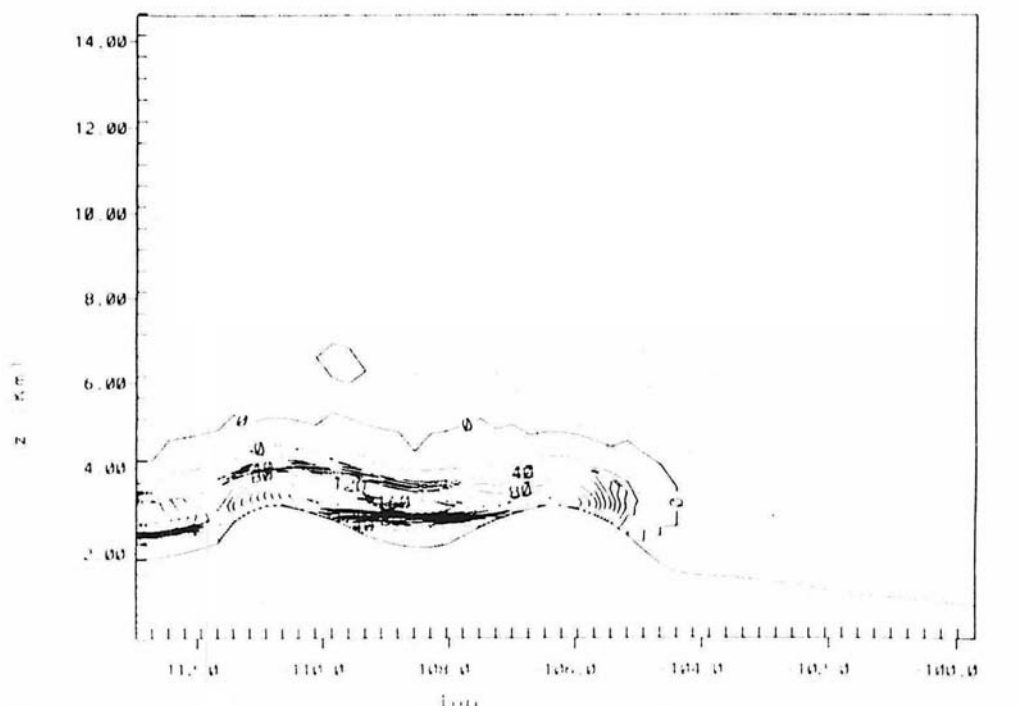

Figure 4.18: Model pristine ice crystal mixing ratio (g g^{-1}), 1900 GMT 30 March 1988.

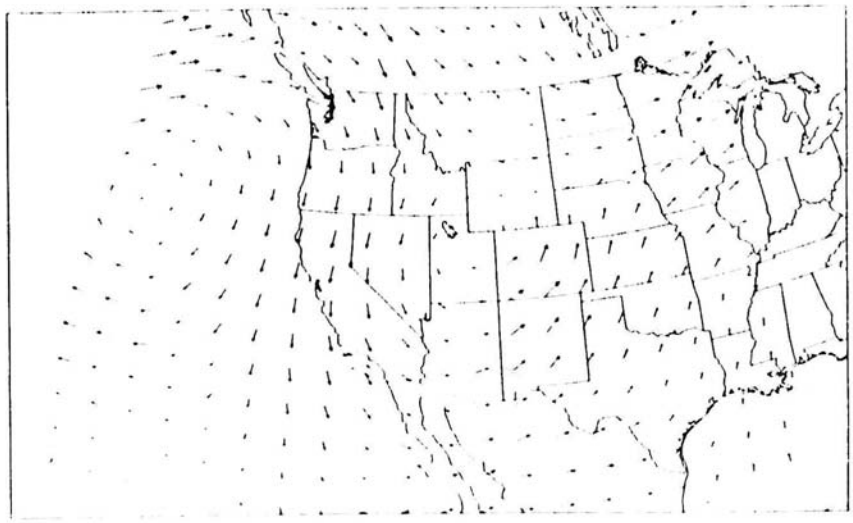

Figure 4.19: Resultant model wind vectors, 0000 GMT 31 March 1988. Maximum wind within domain shown is 25.8 m s^{-1}.

Colorado, strengthening easterly winds over southern Wyoming and northern Colorado, and strong southeasterly flow ahead of the trough. Brisk low-level northerly flow is correctly predicted west of the trough; another trough in southern Alberta appears very similar in both the NMC analysis and in RAMS. At 500 mb, however, the developing trough just west of Colorado is weaker in the model prediction than in the analysis. The developing closed circulation over southern Utah in the analysis appears as only a sharpening trough in RAMS, although the split flow in the westerlies, as well as the trough location, is generally well-represented.

The anticyclone off the west coast appears to be handled well by the model. Finally, major flow features at 300 mb compare well between model and analysis, with a northerly jet maximum over Oregon and western Nevada, and strong southwesterly flow ahead of the trough. Again, the trough is somewhat less sharp in the model.

Low-level upslope flow continues to strengthen during the 1800-0000 GMT time period over the Front Range in both the model and observations. As a result, 2.5 mm of total model-predicted precipitation has fallen by 0000 GMT 31 March over the mountains west of Fort Collins (see Figure 4.20). Note the correspondence of the sharp eastern edge of the precipitation with the location of foothills. Other areas of significant snowfall include southeastern and northwestern Wyoming. Moderate snowfall did occur between 1800 and 0000 GMT 31 March over the northern mountains of Colorado, southeastern Wyoming, and northwestern Wyoming, with some local amounts greater than the model predicted values.

A closer look at the predicted microphysical fields in an $x - z$ cross section through the Fort Collins area is shown in Figures 4.21, 4.22 and 4.23. Ice crystal concentrations up to 27 per liter are simulated, with maxima just below 8 km MSL over the Front Range and North Park. Secondary maxima are found near the ground from North Park into the eastern slope of the Zirkel range. Aggregate mixing ratios are rapidly increasing over the Front Range, to a height of about 4 km MSL, with maximum mixing ratios found at the ground. Apparently, initiation and growth of these aggregates is continuing all the

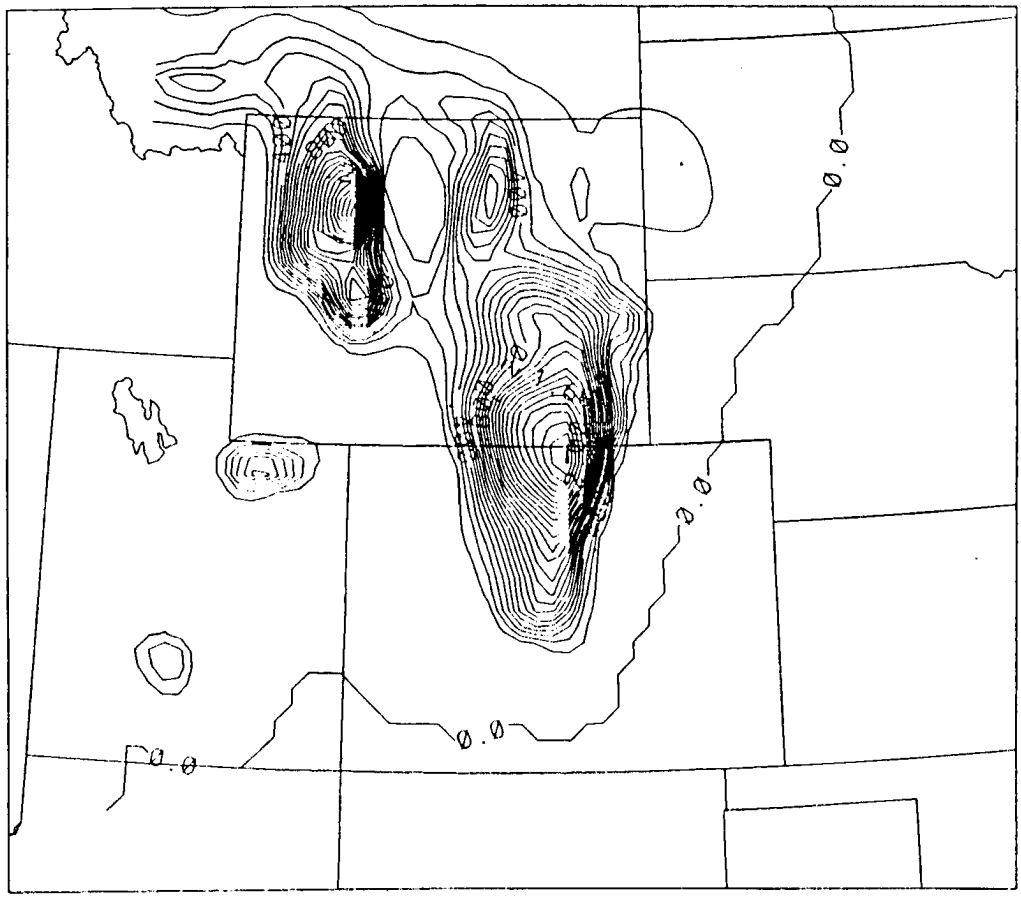

Figure 4.20: Total precipitation (mm) over 6 hours ending at 0000 GMT 31 March 1988.

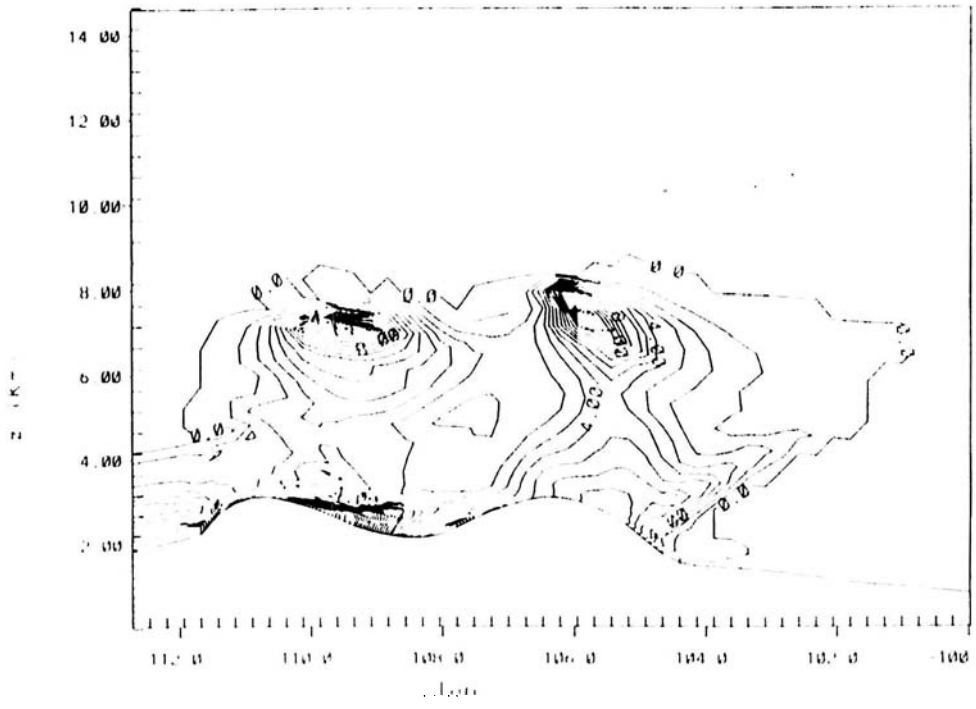

Figure 4.21: Model pristine ice crystal concentration (L^{-1}), 0000 GMT 31 March 1988.

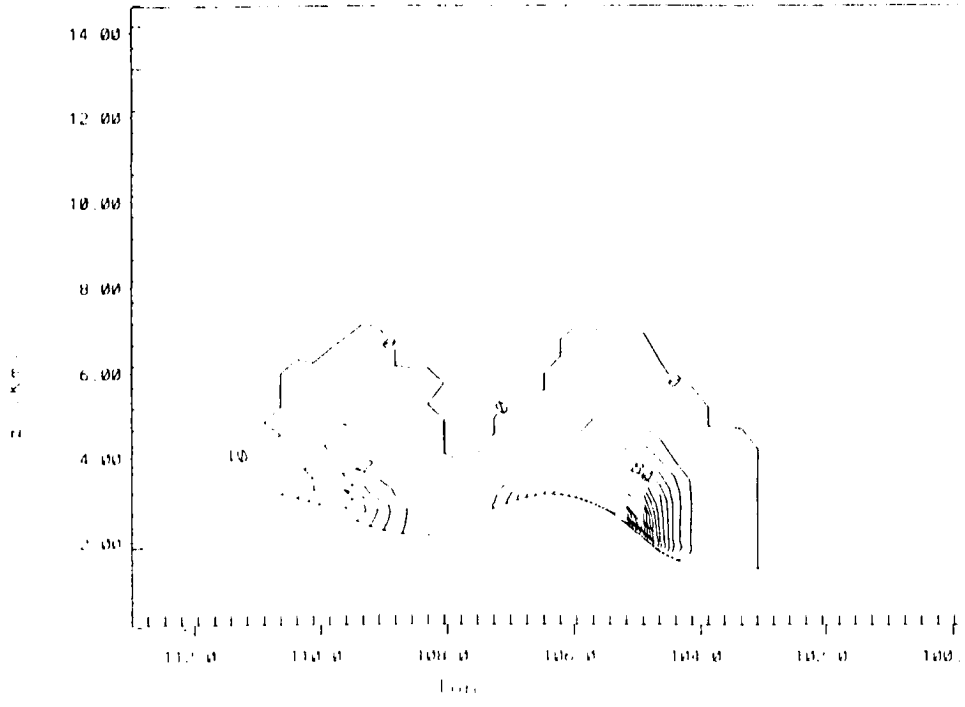

Figure 4.22: Model ice crystal aggregate mixing ratio (g g^{-1}), 0000 GMT 31 March 1988.

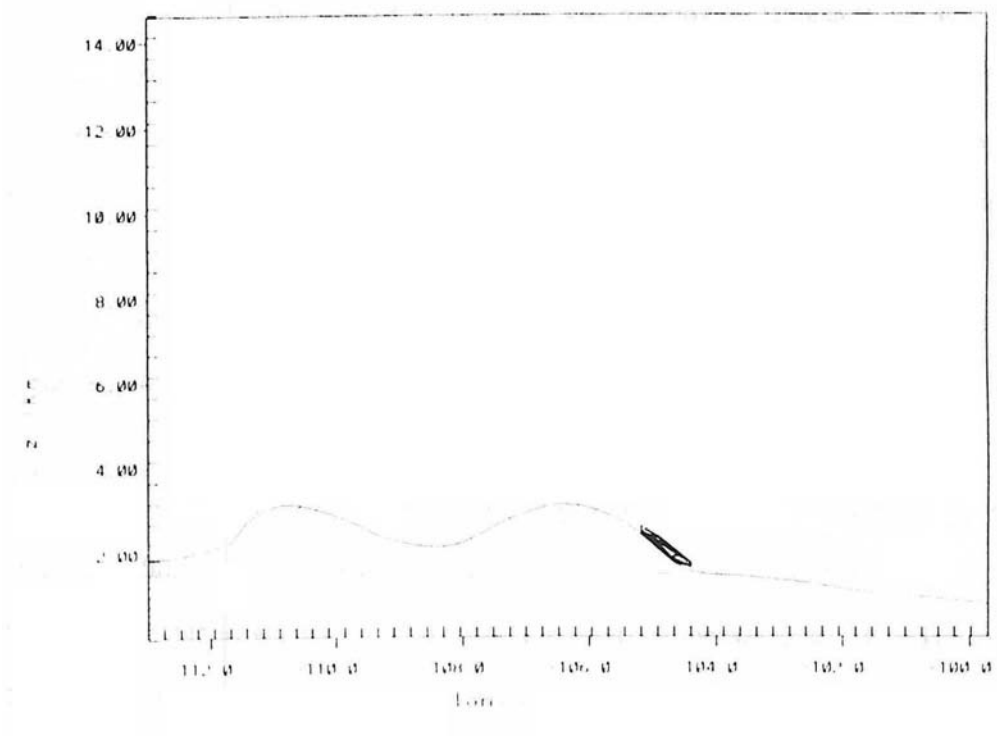

Figure 4.23: Model graupel mixing ratio (g g^{-1}), 0000 GMT 31 March 1988. Maximum mixing ratio is .0076 g kg^{-1} within domain shown.

way to the surface in the foothills area. Finally, some graupel development is noted near the surface over the Fort Collins area, where surface temperatures are near freezing. Just east of Fort Collins, a small fraction of the precipitation is melting prior to reaching the surface. The total aggregate precipitation up to 0000 GMT 31 March, shown in Figure 4.24, amounts to about one-fourth the total of all precipitation types over the foothills.

This simulation was continued until 1200 GMT 31 March, a total of 24 hours. At 0600 GMT 31 March, the coarse grid winds aloft indicate that the cyclonic circulation over Utah has not progressed eastward (see Figure 4.25), and moist southwesterly flow aloft continues over Colorado. Low-level easterly flow continues to strengthen over northeastern Colorado and southeastern Wyoming (see Figure 4.26) reaching speeds of 18 m s^{-1} over the eastern foothills along the Colorado/Wyoming border. Some of the higher terrain on the western slope of Colorado is in westerly flow at the surface. The layer of easterly winds near Forth Collins is strongest within a few hundred meters of the surface over the plains (Figure 4.27). In the foothills, the wind speeds are strongest. The corresponding cross-section for v (Figure 4.28) indicates that the southerly component is strongest (12 m s^{-1}) over the foothills at about 4 km MSL. At 50 m, the convergence in v-component is maximized along the Colorado/Wyoming border (Figure 4.29).

The strong low-level easterly winds generate a deep layer of ascent over the foothills west of the I-25 corridor. An $x - z$ section of w is shown in Figure 4.30. A maximum updraft of 0.4 m s^{-1} is centered at about 5 km MSL (i.e. just *above* the layer of easterly flow) over a point midway up the barrier. The zone of strong ascent is elongated vertically, and reaches nearly 10 km MSL; the zone is widest just above the barrier and extends to just west of the crest. Some enhanced upward motion is occurring well eastward, over the plains. Also, the tight east-west gradient in the lowest levels east of the foothills extends east of the foothills by several tens of kilometers.

The spatial extent of the strong upward motion is responsible for the active microphysical processes occurring in this region; the fields of total precipitation during the 18 hours of simulation (12 hours with microphysics activated) are shown in Figures 4.31, 4.32,

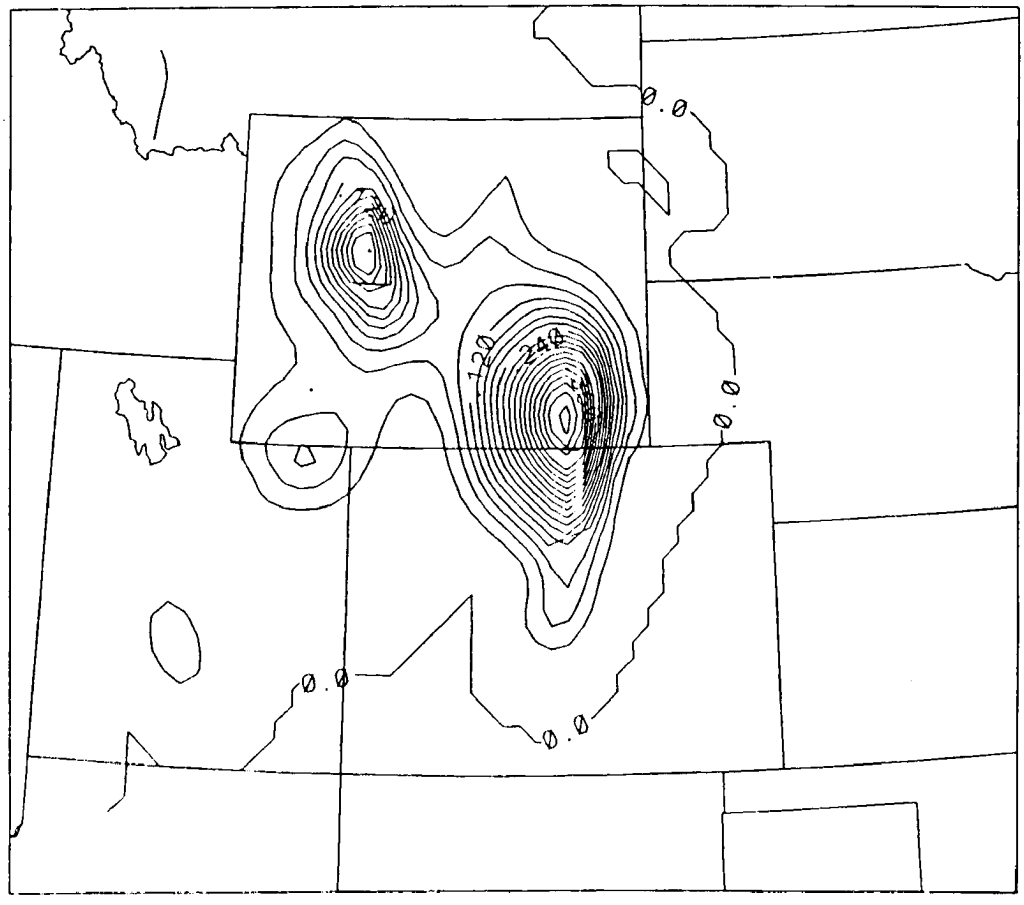

Figure 4.24: Total aggregate precipitation (mm) for 6 hours ending at 0000 GMT 31 March 1988.

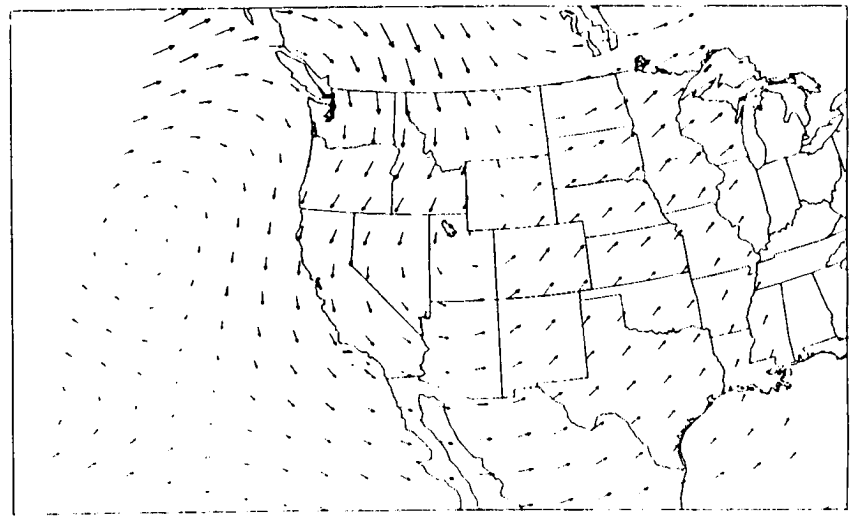

Figure 4.25: Resultant model wind vectors, 0600 GMT 31 March 1988. Maximum wind within domain shown is 41.0 m s^{-1}.

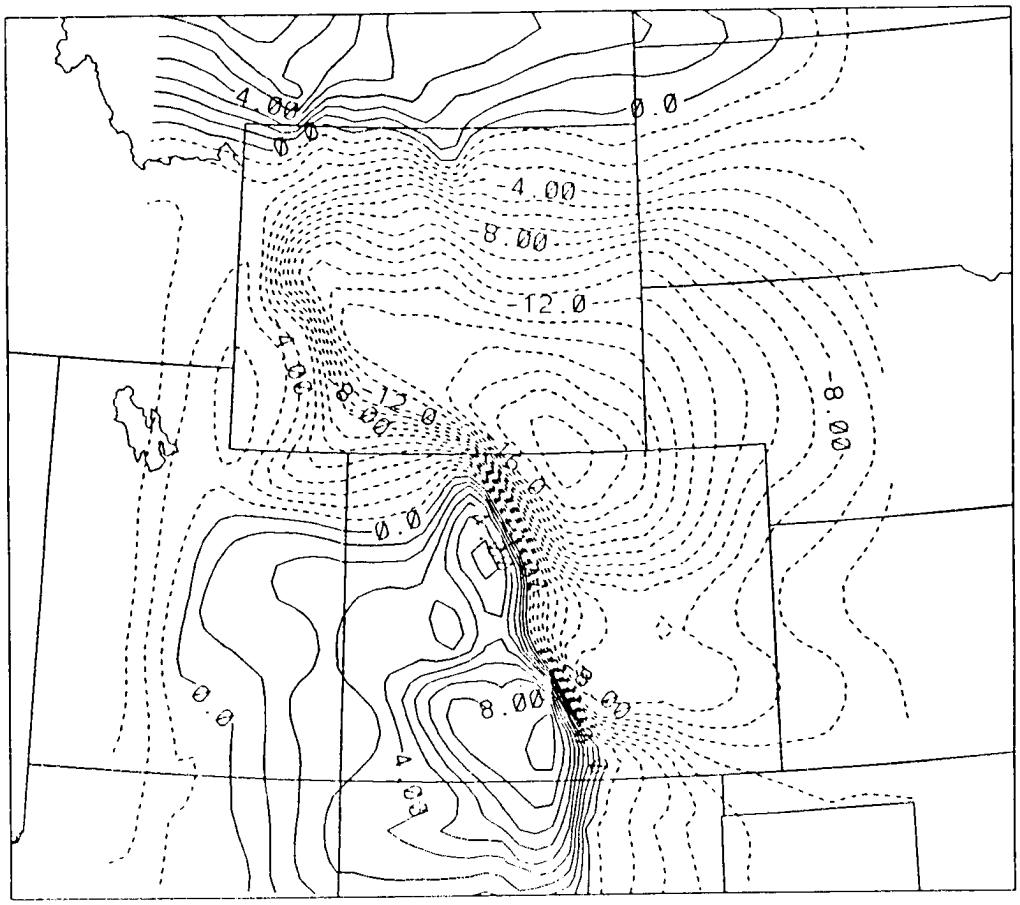

Figure 4.26: Model $x - y$ cross section of u-component (m s^{-1}), 0600 GMT 31 March 1988.

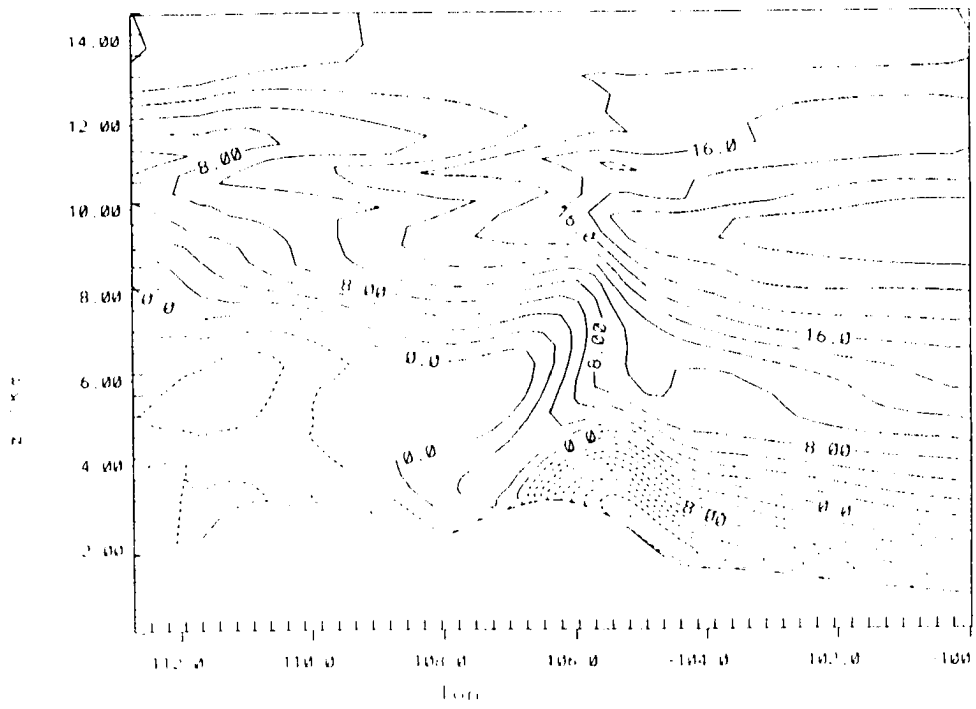

Figure 4.27: Model $x - z$ cross section of u-component (m s^{-1}), 0600 GMT 31 March 1988.

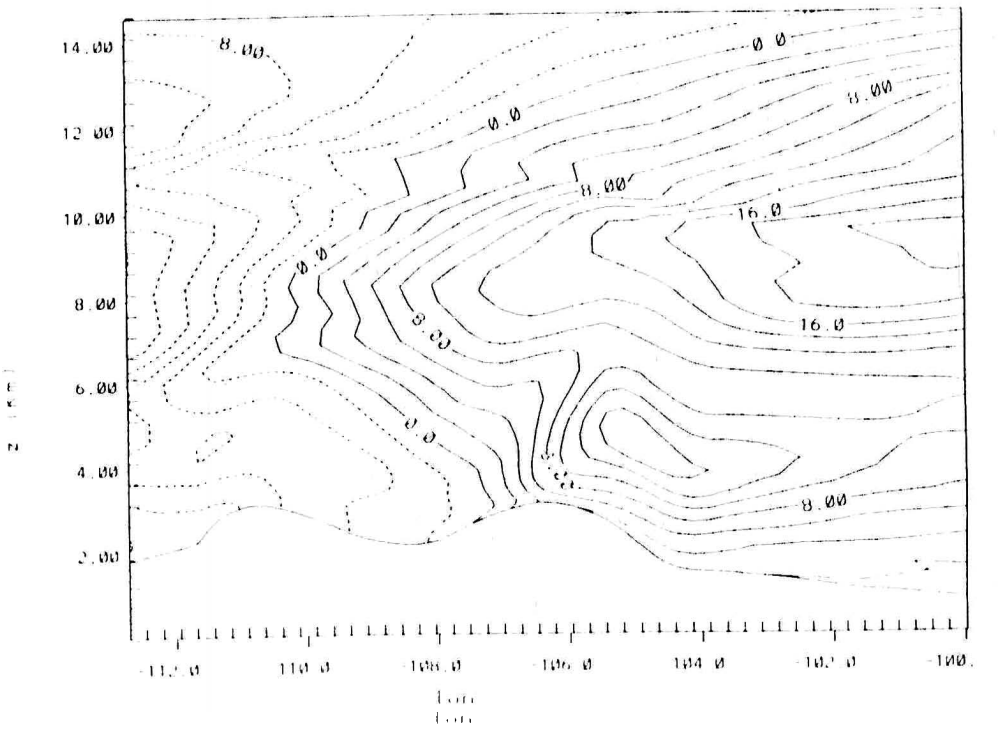

Figure 4.28: Model $x-z$ cross section of v-component (m s^{-1}), 0600 GMT 31 March 1988.

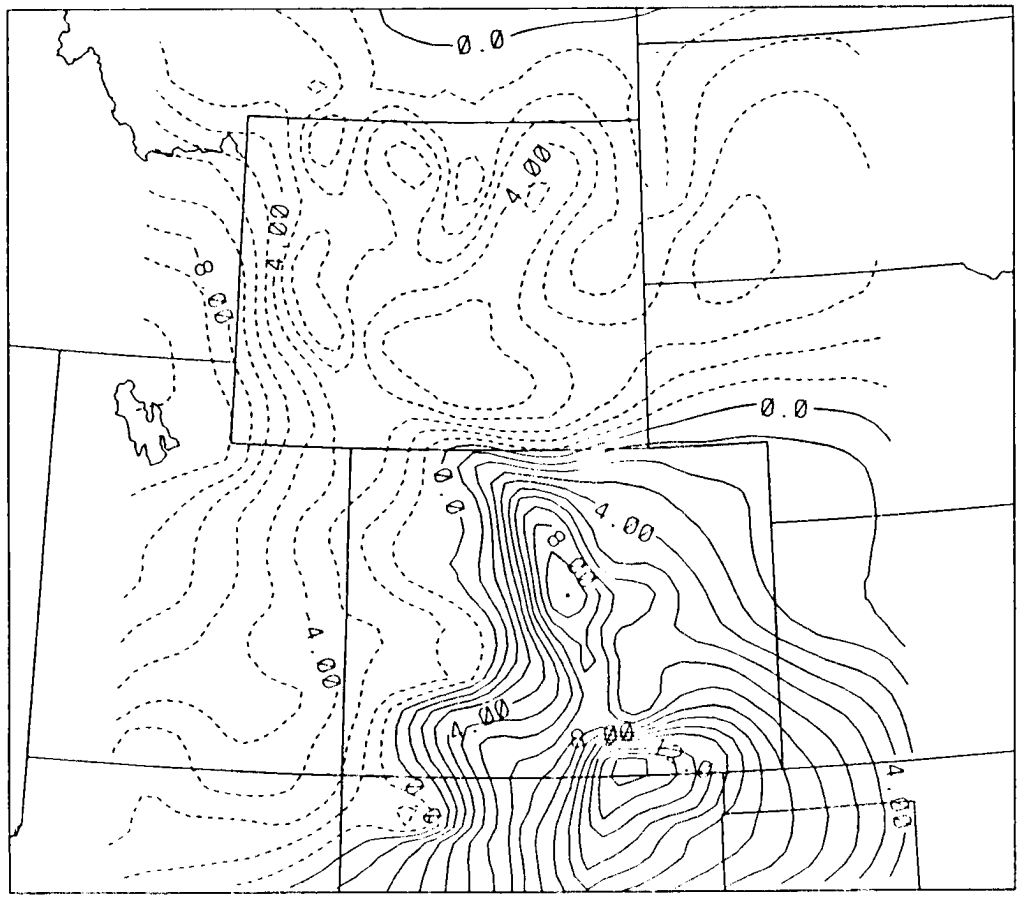

Figure 4.29: Model $x - y$ cross section of v-component (m s^{-1}), 0600 GMT 31 March 1988.

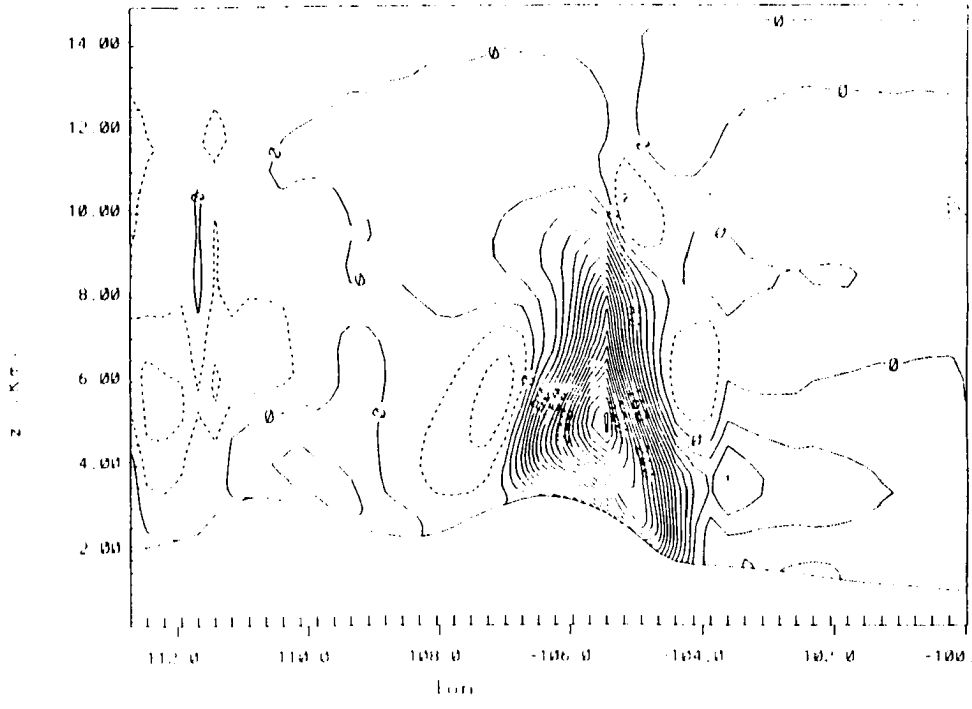

Figure 4.30: Model w-component (mm s^{-1}), 0600 GMT 31 March 1988.

4.33, and 4.34. Overall, to 0600 GMT 31 March, nearly 12 mm has fallen over the foothills west of Fort Collins, with less than 3 mm in the city. The steep terrain slope between this region and the barrier, in a north-south band from Fort Collins southward to near Colorado Springs, is characterized by an intense east-west gradient in total precipitation. A secondary maxima in precipitation is located in northwestern Wyoming. Aggregates of ice crystals account for nearly one-half of the precipitation over the elevated terrain. Dominance of aggregates was reported by spotters over the foothills and adjacent plains (see Table 2.2). However, east of the foothills rain and graupel are dominating the lesser precipitation amounts, each totaling 1 to 3 mm over an elongated north-south band whose width extends from the eastern edge of the foothills to about 50 km east of the foothills.

At the termination of the simulation, 1200 GMT 31 March 1988, the accumulated precipitation distribution (Figure 4.35) indicates a maximum of 34 mm near the Wyoming/Colorado border just northwest of Fort Collins. Most of this precipitation fell in this region in the form of aggregates in agreement with observations in the foothills. Note the persistence of the eastward extension of precipitation onto the plains in northeastern Colorado and southeastern Wyoming and the strong east-west gradient in precipitation over the foothills. This compares well with the observed snowfall gradient (see Figure 1.3) with the exception of significant underprediction between the I-25 corridor and the foothills. Examination of the u-component at this time (Figure 4.36) reveals that the maximum easterly component has propagated down the slope over the last several hours of simulation, and that west of the easternmost foothills, the upslope is actually decelerating, and thus creating strong convergence over the foothills. Also contributing to this convergence is the north-south component of wind. The result is deep tropospheric upward motion over the area, as shown in Figure 4.37, portions of which are contributing to the eastward extent of precipitation. The upward portion of the terrain-induced gravity wave over the lee side of the barrier is contributing to the upper section of this updraft.

A significant fraction of the precipitation east of the foothills continued to fall as graupel and rain in the model (Figure 4.38), as 50 m temperatures in this region remained

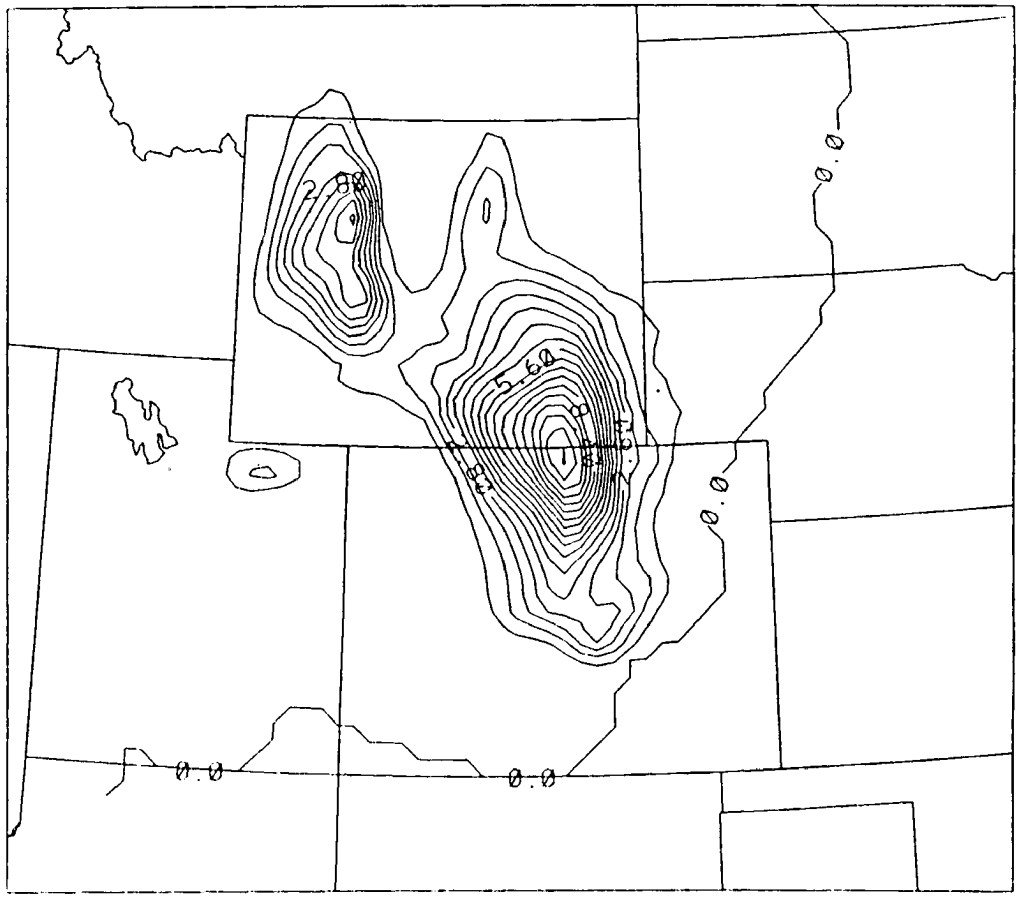

Figure 4.31: Total precipitation (mm) for 12 hours ending at 0600 GMT 31 March 1988.

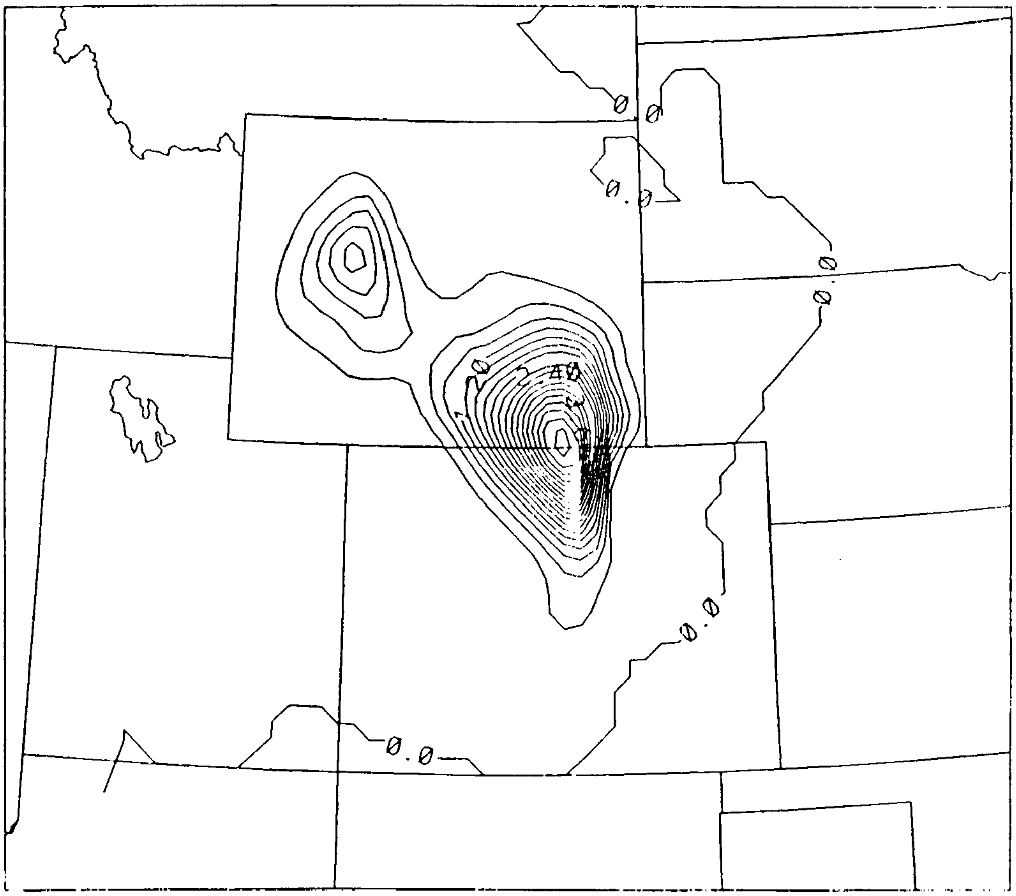

Figure 4.32: Total aggregate precipitation (mm) for 12 hours ending at 0600 GMT 31 March 1988.

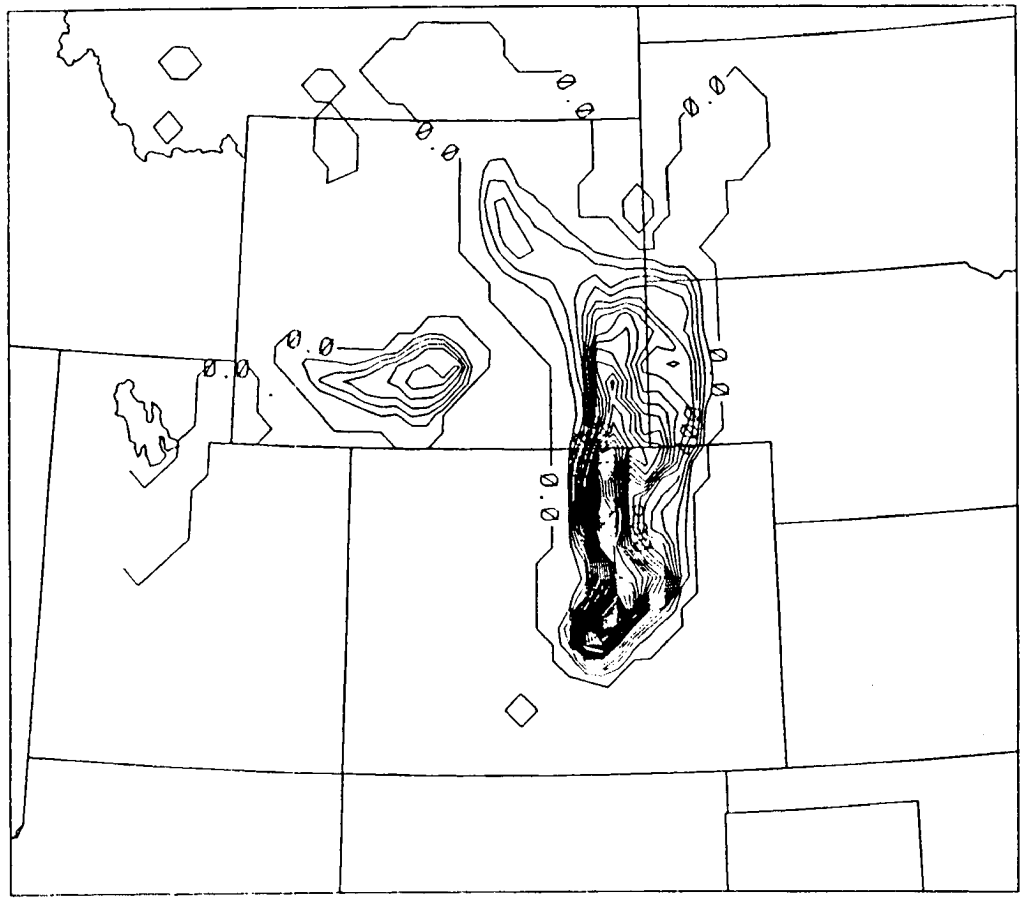

Figure 4.33: Total graupel precipitation (mm) for 12 hours ending at 0600 GMT 31 March 1988.

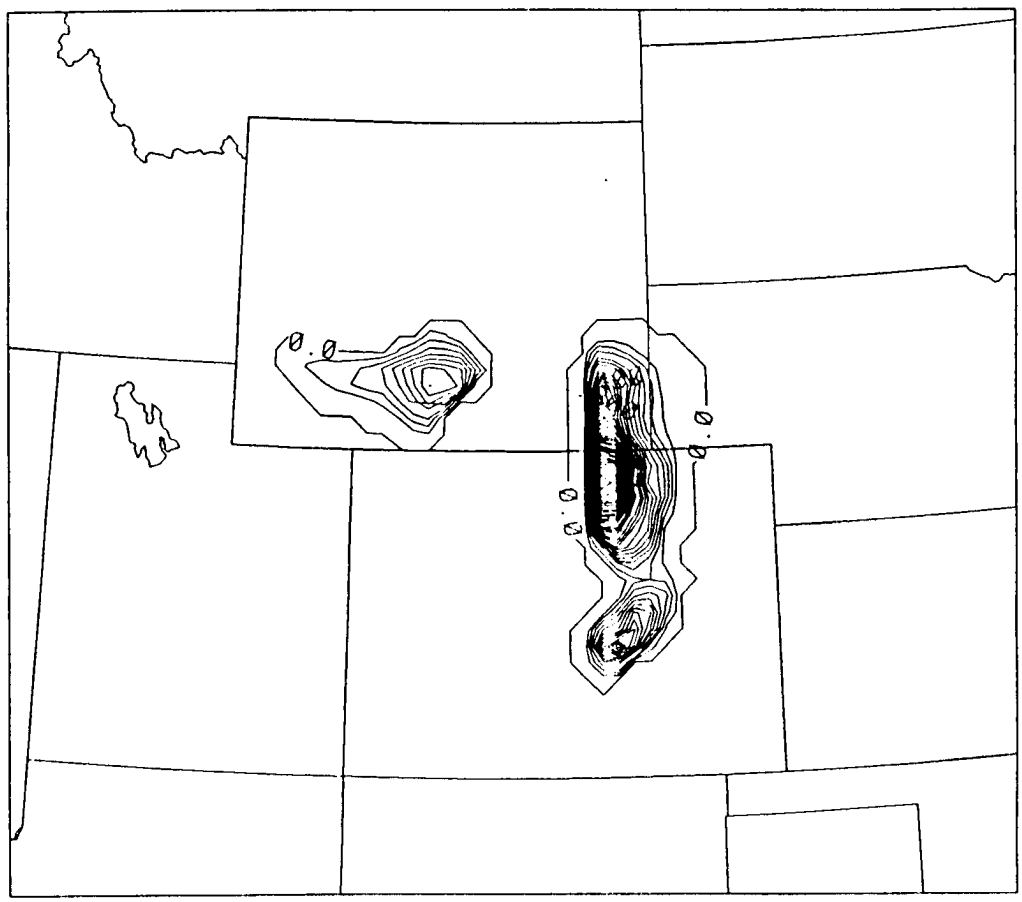

Figure 4.34: Total liquid precipitation (mm) for 12 hours ending at 0600 GMT 31 March 1988.

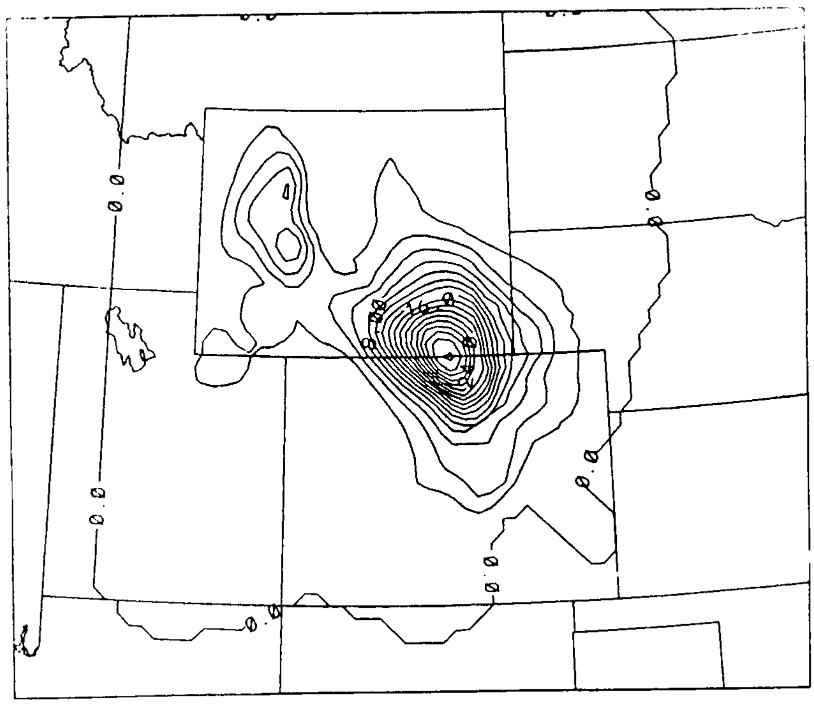

Figure 4.35: Total model-predicted accumulated liquid precipitation (mm) for 18 hours of simulation with microphysics activated ending at 1200 GMT 31 March 1988.

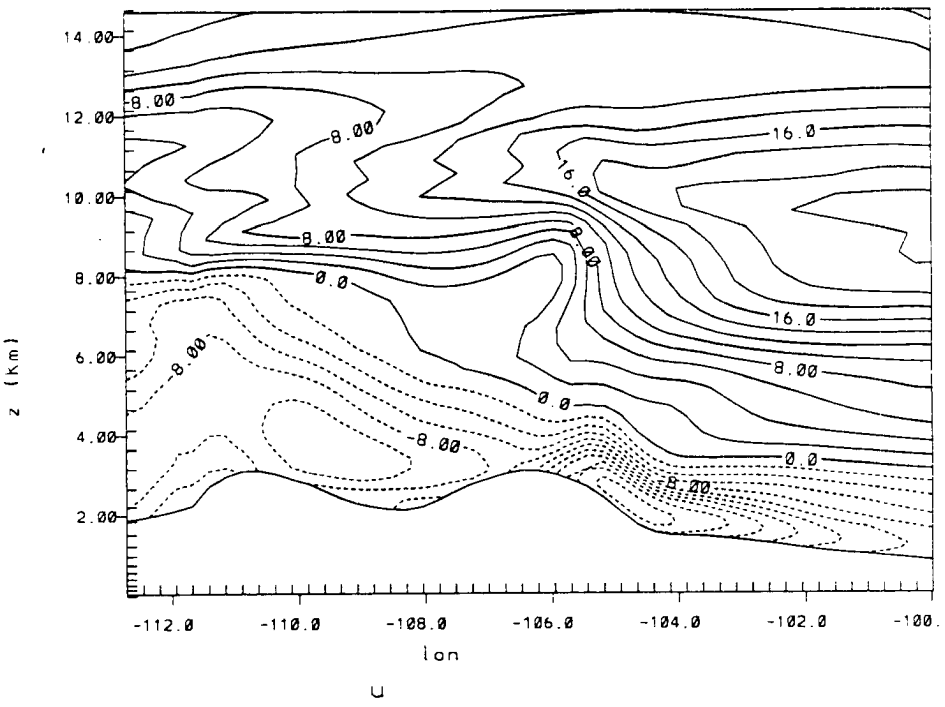

Figure 4.36: Model u-component (m s^{-1}) for $x-z$ cross section at 40.6° latitude, for 1200 GMT 31 March or 24 hours of simulation.

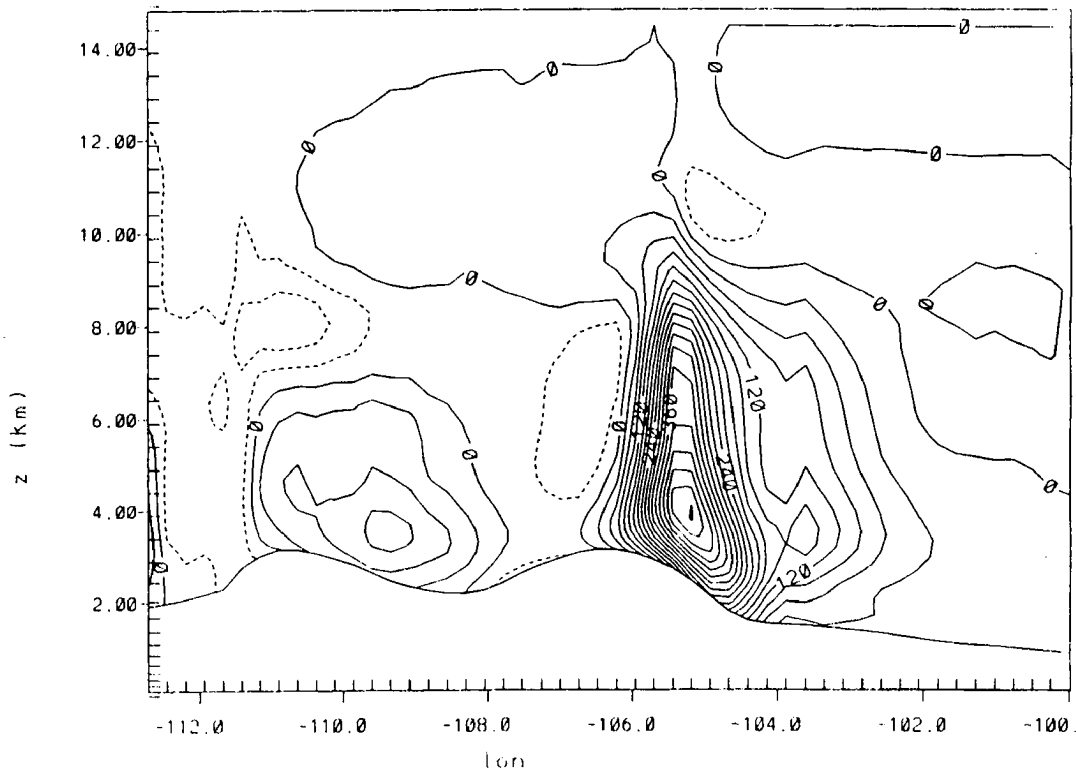

Figure 4.37: Model w-component (mm s^{-1}) for $x - z$ cross section at 40.6° latitude, for 1200 GMT 31 March or 24 hours of simulation.

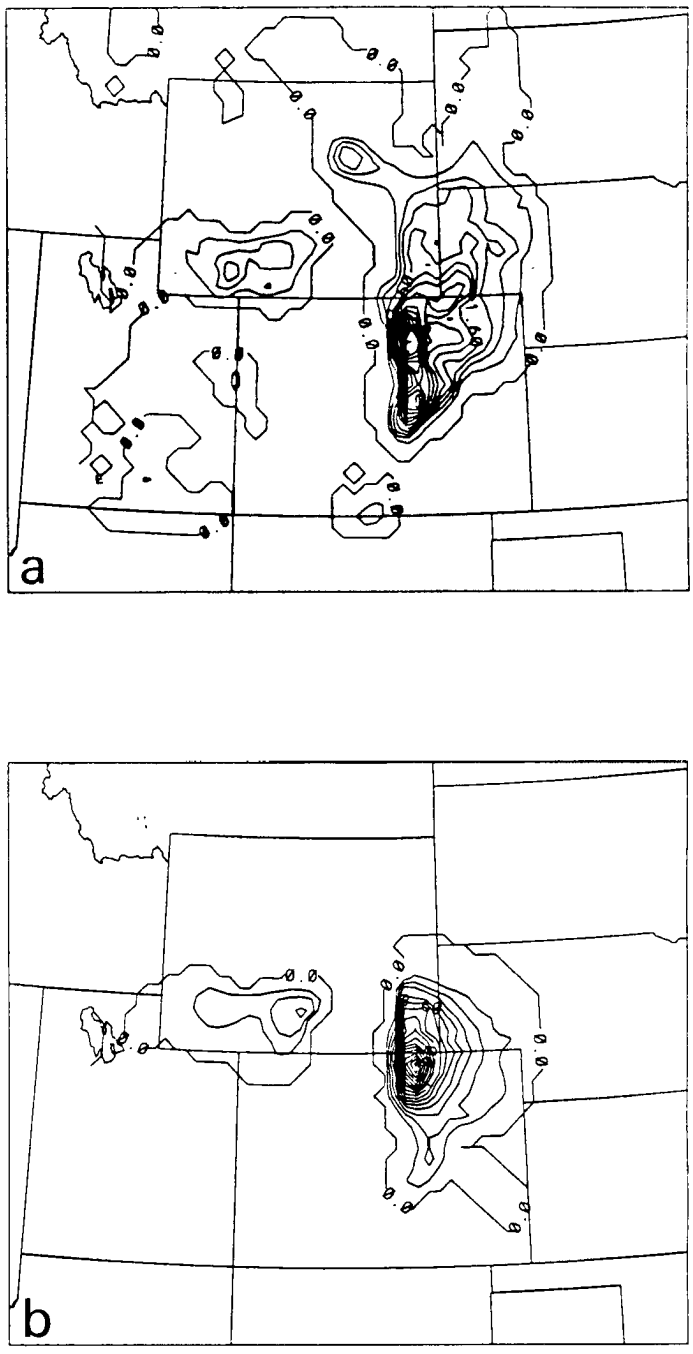

Figure 4.38: As in Figure 4.35 for (a) graupel, and (b) rain.

above freezing. Maximum accumulated quantities, located just east of the foothills by about 50 km, were 6.4 mm and 15.3 mm for graupel and rain, respectively.

In order to further evaluate this three-dimensional RAMS simulation, it is worthwhile to compare the 24-hour model fields with the NMC analysis at this time (i.e. 1200 GMT 31 March). The fine-grid winds at $\sigma = 2$ (Figure 4.39) compare well with the geostrophic wind as indicated on the 850 mb analysis, with brisk east-southeasterly flow in eastern Colorado. (Note: the agreement with geostrophy is as expected since the lowest model level is 50 m above the surface). This upslope flow backs to east-northeasterly in Nebraska and western South Dakota. The strong southeasterly winds in eastern New Mexico are predicted well by the model. The surface low position is predicted accurately, but appears somewhat disorganized in the model winds. The center of the anticyclone in western South Dakota is replicated very well in the model prediction. However, observed ageostrophic northerly flow south of the high did not extend into Colorado in the simulation.

The comparison at 700 mb (approximately 2.65 km model height) reveals well-simulated general features, but problems in the small-scale details. The location of the center of the cutoff low is predicted accurately, but is too weak and disorganized in the simulation. As a result, the southerly wind component along the Front Range is overestimated. Features in agreement include the strong ridge off the west coast and the shortwave north of Montana. The fields at 500 mb and 300 mb indicate continued underprediction of the strength of the circulation associated with the cutoff system near the Four Corners region. This error is evident in the 300 mb model-predicted southwesterly wind of 80 knots, while the observed DEN wind was 55 knots and southerly. However, at both levels the northerly jet maximum over and north of western Montana is predicted well, as is the slight southward progression of the off-coast ridge.

4.4.1 Overview of Verification of the 30-31 March 1988 simulations

The model precipitation fields for this storm compare well to observations over the foothills. The model has successfully developed strong (i.e. 5 to 15 m s^{-1}) easterly low-level flow over southeastern Wyoming and northeastern Colorado (see Figure 2.1) in

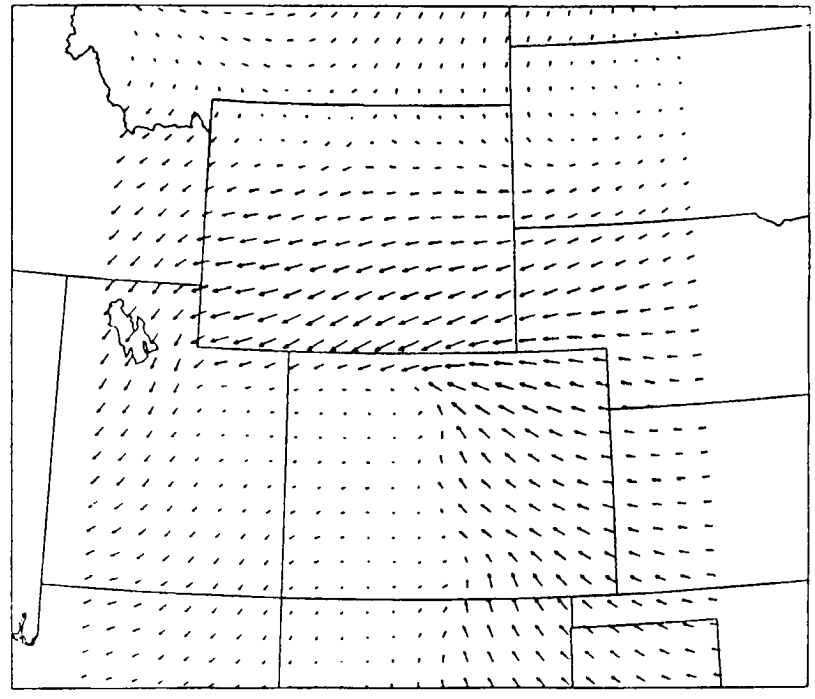

Figure 4.39: Model wind vectors at $\sigma = 2$ after 24 hours of simulation. Maximum wind within domain shown is 21.6 m s^{-1}.

advance of an intensifying storm system to the west. Flow aloft (i.e. above 5 km MSL) at 0600 GMT 31 March (Figure 4.25) is correctly predicting 20 to 30 m s^{-1} southwesterlies over the Front Range as shown in Figures 2.1 and 2.5. However, for regions east of the northern Colorado foothills, serious problems are evident in the model fields, both in low-level winds and precipitation type. The rainfall predicted in this region was not observed in this storm after 0000 GMT 31 March. Close monitoring of the low-level temperatures predicted by the model revealed a +1-3°C error compared to mesonet and NWS observations, which easily could have accounted for the problems with precipitation type. The wind fields predicted by the model, while in good agreement overall, show poor agreement in several localized areas of measurements. The simulation lacks the development of blocked flow in the low levels in the foothills/I-25 corridor (see Chapter 2 for a detailed discussion of the observations). By 0300 GMT 31 March the blocked flow was well-established along the Front Range. However, in the simulations the rapid increase of surface pressures over eastern Wyoming during the evening of 30 March and early morning of 31 March, in association with the building and southward progression of a Canadian anticyclone in the Dakotas, was substantially underpredicted. Subsequently, strong stable lapse rates and blocking did not dominate the low levels just east of the foothills.

Furthermore, the model did not predict the development of a layer of strong *east-northeasterly* flow near the 700 mb level along the Front Range during the period 0000 GMT – 1200 GMT 31 March. Instead, south-southeasterly winds were predicted at this level. As a result of these two related errors, both cold advection from the north in the lowest layers and overrunning by the 700 mb flow were not predicted by the model. These problems were associated with the underprediction of the strength of the 700 mb low center. The simulations do predict some weak adiabatic cooling over the foothills in easterly flow, but it is not enough to build the low-level cold pool and decelerate the upslope flow east of the foothills. As previously mentioned, low-level model temperatures

were too warm just east of the foothills. Deceleration in the model upslope flow was confined to the foothills region.

Another question is whether a simulation with grid spacing of 22 km horizontally (and the associated terrain smoothing) and 100 m vertically can resolve the blocking processes sufficiently to reproduce the observations of wind and precipitation in the blocked flow regime. It is not clear whether most of the small-scale details can be captured, but if the larger-scale features, such as the 700 mb flow and cold low-level advection, can be predicted, certainly some of the dynamics of the blocking are within reach of this type of simulation. The Dakotas anticyclone in this case is deep enough to span at least 10 vertical levels in the model and its horizontal extent is several hundred kilometers, so that even the coarse grid spacing is sufficient. If this larger-scale feature is not handled by the model, then the small-scale blocking in the area of interest cannot be simulated. The model has captured other features in the synoptic-scale patterns, such as the ridge off the west coast, a jet maximum in the northern Rockies and strong low-level upslope over northeastern Colorado and southeastern Wyoming. The problems with other features in the larger-scale fields are apparently related to the initialization of the model, as well as the nudging on the coarse grid at 12 hour intervals. Indeed, the northern portion of the anticyclone does lie within the nudged part of the coarse grid. Another possible contributor to the underprediction of the cutoff low aloft is the terrain smoothing required for a simulation with 22 km horizontal grid spacing.

Because of these model shortcomings for the 30-31 March 1988 case, the decision was made to terminate the simulation at 24 hours.

4.4.2 Assessment of the NGM Simulations for 30-31 March 1988

Further insight into the RAMS simulations for this case can be obtained indirectly via an analysis of the operational NGM simulations which are routinely available from the NMC. This model, as described in Hoke *et al.* (1989), employs a similar objective analysis of NMC gridded data, radiosonde, and surface observations as the RAMS initial fields, in this case for 1200 GMT 30 March 1988. Two grids comprise the NGM domain,

with the coarse mesh covering a much larger area than the RAMS grid 1 shown in Figure 4.1 (see Figure 5 in Hoke *et al.*, 1989). Grid 2 of the NGM with a horizontal spacing of approximately 85 km at a latitude of 45°N extends over the entire U.S., most of Canada and Mexico, the central and eastern Pacific Ocean, and the central and western Atlantic Ocean. Thus the NGM grid 2 encompasses a significantly larger area than grid 1 of RAMS in this case. Vertically, the model has 17 levels. Model microphysics are simplified in comparison with RAMS. For example, precipitation predictions include only the liquid phase.

This comparison used primarily the NMC analysis of MSLP, 850 mb, 700 mb, and 500 mb heights, and radiosonde observations at those heights. At 1200 GMT 30 March 1988, the MSLP analysis (not shown) for the NGM is slightly smoothed in comparison to the NMC analysis, as is usually the case. For example, the developing low pressure over the southern Utah border is 2 mb weaker (higher) on the NGM. Pressures along the Front Range and northward into Montana are 1-2 mb too high. At 850 mb (see Figure 4.40) the NGM analyzes a dual cutoff low to the southwest and northeast of Colorado, while the NMC analysis exhibits only a trough through this region. The 700 mb developing trough west of Colorado is slightly weaker in the NGM, while the strong ridge of the west coast is within 1 dm of agreement. At 500 mb, where observed winds are primarily in gradient balance on the NMC analysis, the two analyses are nearly identical. In fact, overall, the agreement between the two analyses at all four pressure levels is very good with the minor exceptions just described.

Twelve hours later, at 0000 GMT 31 March, there are some problems with the 12-hour NGM forecast when compared to the NMC analyses. Generally, the developing storm, centered just south and west of the state, is forecast too *strong* for MSLP as well as at the 700 and 500 mb levels. The surface low is too far north by about 150 km (i.e. near Trinidad, Colorado) and 3 mb too deep. The strengthening high pressure over eastern Montana is underforecast by 3 to 7 mb. However, some anticyclonic enhancement in the strong north-south gradient in MSLP along the Wyoming and Colorado Front Range is

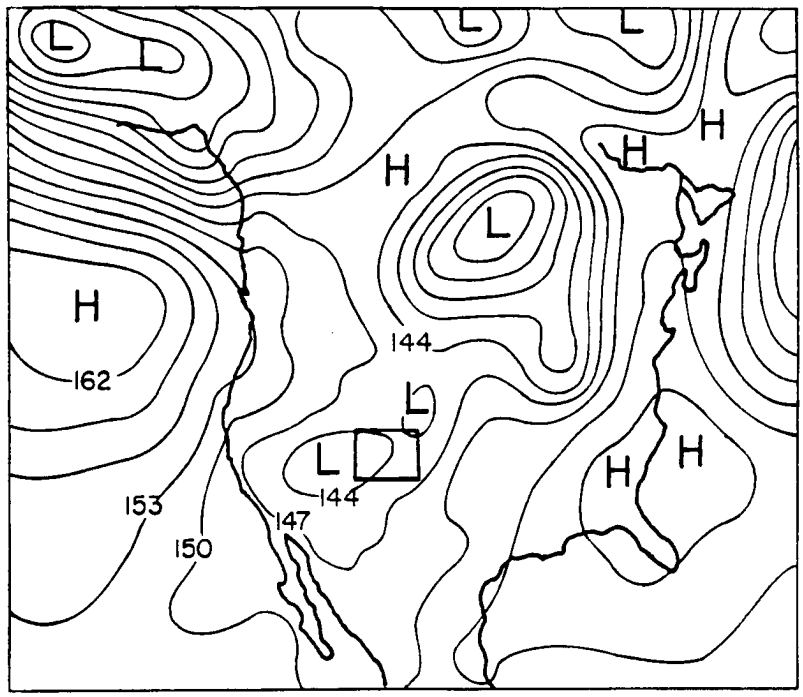

Figure 4.40: NGM initial height field (dm) for 850 mb surface at 1200 GMT 30 March 1988.

predicted correctly by the NGM. Generally, the orientation of MSLP gradients is handled well by the model. At 700 mb (Figure 4.41) the overprediction of the strength of the developing cutoff is significant (i.e. 5 dm at the center). The model forecast of a cutoff (6 dm contour intervals) at 500 mb at this time is incorrect, with a 5 dm error at the center. The ridge off the west coast is 3 dm too strong in the model predictions.

The NGM forecast of 12-hour accumulated liquid precipitation exhibits generally light (0.01"–0.15") amounts over a broad region from just west of AKO, to just north of CYS, through the Rock Springs, Wyoming and GJT areas. The maximum predicted precipitation is 0.19" just southwest of Craig, CO. The southeastern boundary of this region is near DEN. Overall, this is an accurate prediction, considering the horizontal grid spacing of this model. Front Range precipitation during this 12 hours was in the 0.05"–0.25" range, with higher amounts near the Continental Divide.

At 1200 GMT 31 March, the 24-hour NGM MSLP prediction underforecasts the strength of the high pressure system over eastern North Dakota slightly, and centers it too far to the north. The inverted trough extending from southeastern Colorado to central Wisconsin is predicted well, as is surface pressure at CYS. Some ridging in the MSLP prediction is evident over northeastern Colorado. The main low is centered about 150 km northwest of its actual location, but its strength is correctly predicted. Thicknesses between 1000 and 500 mb have decreased rapidly over northeastern Colorado, implying that low-level cold advection in this region is significant. The ridge over the Great Basin is seriously underforecast, however. At 700 mb, the NGM's prediction of the strength of the cutoff is good, though the center is 4 km overforecast and about 100 km north of its analyzed location. A weak shortwave ridge over central Nebraska is present on both the model prognosis and the NMC analysis. The off-coast anticyclone now is predicted well. Finally, the 500 mb comparison (Figure 4.42) indicates a relatively good model forecast, with only a 75 km and 2 dm error in cutoff location and strength, respectively. The model correctly predicts strong diffluence in the geostrophic flow over the Colorado Front Range.

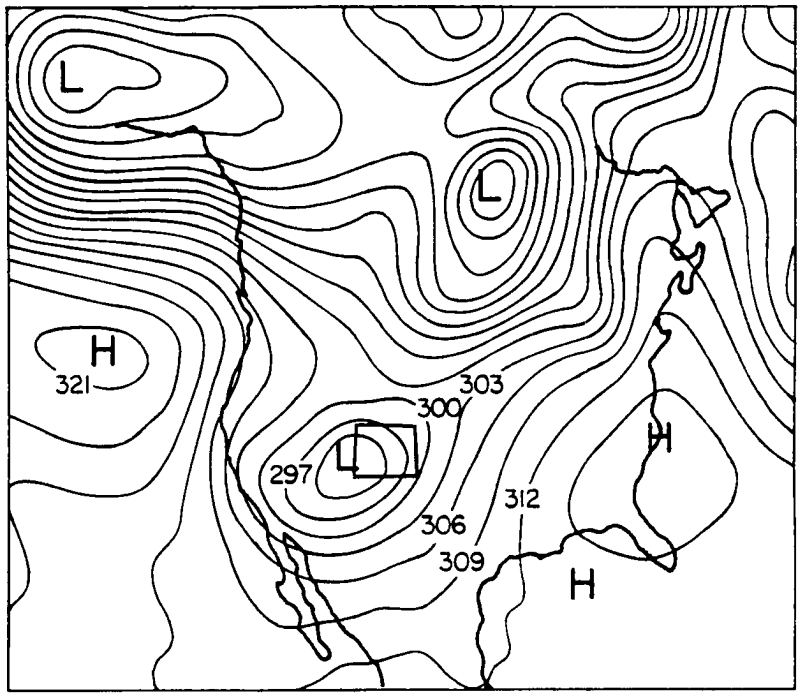

Figure 4.41: NGM 12-hour predicted 700 mb heights (dm).

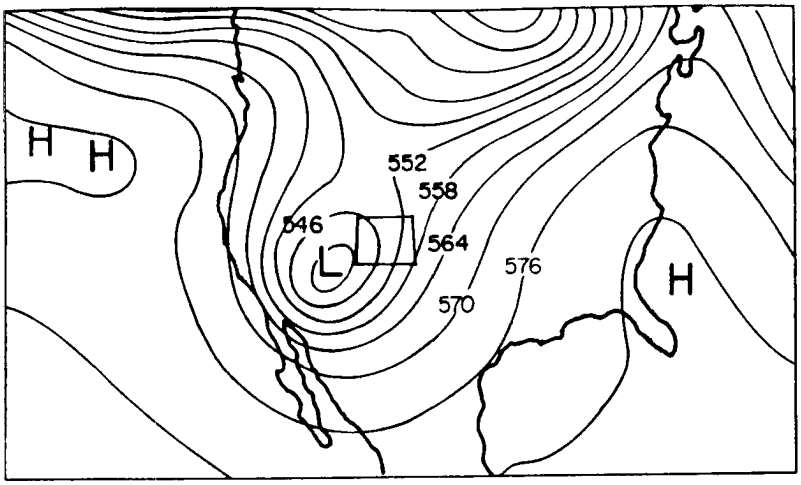

Figure 4.42: NGM 24-hour predicted 500 mb heights (dm).

A strong vorticity maximum just south of the cutoff is located about 200 km southeast of its analyzed location.

The NGM 12-hour accumulated precipitation prediction at 1200 GMT, 31 March (Figure 4.43) generally is good in terms of areal coverage but poor in magnitude. Smaller-scale details such as the observed damming-induced heavy precipitation over the eastern foothills and adjacent plains over northeastern Colorado (Figure 1.3) are not predicted. The model predicts a maximum of 0.79" near Sidney, Nebraska, which is an overprediction of nearly 0.50". Model precipitation amounts *decrease* westward, in direct contradiction to the observations. The northern I-25 corridor is within the approximate 0.50" predicted 12-hour total contour, with lesser amounts over the foothills. As shown in Figure 1.3, actual amounts were more than twice that from just west of the I-25 corridor into the northern Colorado foothills, using the observed ratio of snow accumulation to liquid equivalent, 10 to 15. Apparently, the model prediction does not capture the strong orographic forcing of snowfall and the associated damming-induced enhancement over the foothills and adjacent plains, despite the presence of low-level cold advection.

4.4.3 Comparison of Performance of NGM vs. RAMS

In the previous sections, strengths and weaknesses of the RAMS and NGM were discussed based on simulations of the evolution of a strong storm over the southern and central Rocky Mountains during the 24-hour period ending at 1200 GMT 31 March 1988. In light of future modeling efforts for winter storms such as this one, a comparison of the two models, with significantly different horizontal and vertical grid spacings, is valuable. Table 4.2 is an overall evaluation of the performance of the two models for several important factors in the development of this snowstorm along the Colorado Front Range.

It is immediately apparent that the improved horizontal grid spacing in grid 2 of RAMS (22 km vs. about 85 km in the NGM) and its associated more realistic topography (see Figure 4.6 of this study and Figure 3 in Hoke *et al.* 1989) have enabled a much improved representation of orographic effects on vertical motion and precipitation, and some improvement in capturing the effects of blocking. As a result, precipitation predictions

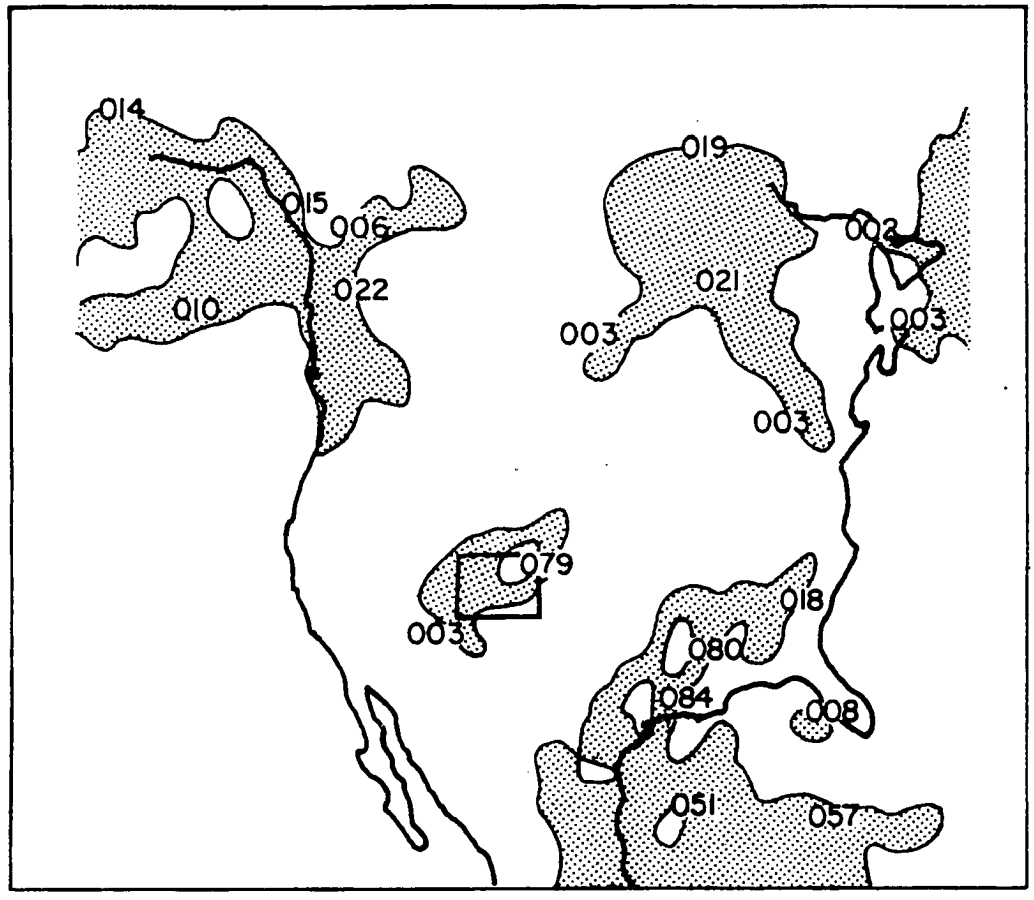

Figure 4.43: NGM prediction of accumulated precipitation (inches) for 12 hours ending at 1200 GMT 31 March 1988. Simulation began at 1200 GMT 30 March.

Table 4.2: Qualitative comparison between NGM and RAMS for several important aspects of their simulations for 30-31 March 1988.

Observed Feature	Overall Degree of Accuracy in Simulations	
	NGM	RAMS
Topography	moderate	high
Initial + 12 hr fields	high	moderate
Large-scale general features	high	moderate
Strength/location of cutoff	high	moderate
Development of upslope flow	high	high
Low-level cold advection	moderate	low
Orographic effect on precip.	low	high
Blocking-induced convergence	low	moderate
Precipitation type	N/A	moderate

by RAMS were much more accurate. A basic limitation of the degree of resolution in the topography of a three-dimensional simulation is the horizontal grid spacing. Topographic features exhibiting wavelengths of less than about four times the model grid spacing lead to numerical errors in the model calculations; thus the topography must be smoothed or averaged until these features disappear. The NGM, with approximately four times the spacing of this version of RAMS, must utilize a much smoother topography. In a storm such as 30-31 March 1988, where terrain influences were critical on all relevant scales, this difference leads to major discrepancies in model precipitation predictions (see Figures 4.43 and 4.35).

The model initiated and nudged 12-hour fields were apparently better analyzed by the NGM. This led to a more accurate prediction of the development of the cutoff low system, as well as the low-level cold advection to the east. Furthermore, the size of the fine-grid domain in the NGM, which was much larger than both grids in RAMS, may have contributed to this improved accuracy. The synoptic-scale features, many of which were far removed from the area of interest in this study, may require a large grid domain (even with a coarser grid resolution) for a more accurate simulation of a Front Range storm.

Chapter 5

DISCUSSION AND CONCLUSIONS

This study utilized detailed observational data to document and describe several aspects of the topographical effects on snowstorms in the Front Range of the Rocky Mountains. Specifically, the processes contributing to enhanced snowfall along the foothills and adjacent plains were emphasized, using primarily a special spotter network and tri-hourly radiosonde releases at Fort Collins. Several mesoscale model experiments complemented the analysis of observational data. Frequently, simple topographic lifting concepts are insufficient in adequately explaining several persistent snowfall patterns in this region; this discrepancy motivated the investigation. The results of the study indicate that so-called "upslope" flow in the high plains actually involves a complex system of dynamical and microphysical processes which occur over a wide spectrum of spatial scales.

Through analysis of data from special radiosondes, surface meso-network, volunteer spotters, geostationary satellite, profilers, Doppler radars, and standard NMC gridded files, a series of storms were analyzed in detail in order to isolate the various topographical influences. After completion of the case studies, more generalized applications of these terrain-induced phenomena were made based on these results as well as additional monitoring and forecasting Front Range winter storms over the past six winters. The author also performed a series of RAMS simulations, some including full microphysics, to further evaluate terrain-forced regions of ascent in the lower troposphere.

The first case, the 30-31 March 1988 event, exhibited deep, cyclonic features accompanied by blocked low-level structure; snowfall was heaviest over and next to the foothills. Cold-air damming persisted at about the same strength for more than 12 hours, and induced strong overrunning of easterly flow between 800 and 600 mb. Analysis of a series of

special CLASS soundings released at Fort Collins indicated a persistent 3-layer structure in the dynamic and thermodynamic profiles: a shallow low-level blocked region, moist and vigorous mid-level upslope, and strong southerly to southwesterly flow aloft, the latter owing its existence to the synoptic-scale features. The moist air mass aloft acted as a crystal generator region for the storm, and coupled with the mid-level upslope and blocking-induced ascent constituted an efficient seeder-feeder process over the Front Range region. Crystals generated aloft in this layer can be particularly important for snow events in which clouds in the blocked layer and the upslope flow are too warm to naturally glaciate, as is sometimes the case. Predominance of heavily-rimed, dendritic aggregates implied lifting associated with the layered vertical structure in the 30-31 March 1988 storm. Bands of enhanced Doppler reflectivity exhibited significant correlation with blocking-induced ascent as well as snowfall intensity. Superimposed on the dammed structure was strong orographically-induced ascent over the foothills.

Detailed observations of several arctic outbreaks provided evidence of another unique precipitation enhancement process induced by blocking along the east slope of the Rocky Mountains. During 1-5 February 1989, the combination of moisture advection aloft with an extremely cold low-level air mass produced heavy precipitation along the Front Range despite strong mid-level *westerly* winds. Again, critical snow accumulation and crystal habit reports from the spotter network provided the data needed to assess the microphysical evolution of the storm. From this case, and others where satellite and other data were available to identify the cold pool depth, the following sequence can occur in place of, or as a supplement to, more common precipitation scenarios (i.e., simple synoptic forcing or upslope):

- The magnitude of the low-level geostrophic easterly component increases with time as a synoptic-scale disturbance approaches.
- Within the cold pool, mass (and, therefore, surface pressure) increases along the foothills as the cold air is unable to ascend the steep topography.
- The cold pool, as a result, deepens locally on its western edge.

- Enhanced condensation (or reduced evaporation or sublimation) occurs above the cold pool, as the moist westerly flow aloft overruns the deepening cold dome. These precipitation particles fall through the western portion of the cold air to the ground.

The deeper cold air acts as a barrier to the westerly flow and prevents downslope. In addition, enhanced ascent probably occurs over the western edge of the cold

pool. Observations of crystal habits in this storm confirmed that the moisture source during significant snowfall was the relatively warm westerly flow aloft. Furthermore, low-level blocking apparently deflected synoptic southeasterly flow toward high pressure in portions of the Front Range area, contradictory to classical blocking theory for the Northern hemisphere. Similar blocking occurred in the 10-11 February 1988 storm.

The modeling approach in this study was to run a series of numerical experiments to further analyze the general applicability of terrain-induced processes documented from observations. Simplified two-dimensional mesoscale model simulations captured the development of overrunning and a bulge on the western edge of the cold pool in the 1-5 February 1989 case. Generally, strong downslope flow east of the mountains in the low levels was retarded by the arctic air mass if the latter was sufficiently deep. The magnitude of the downward portion of the gravity-wave structure to the lee of the barrier was reduced approximately by a factor of two when compared to a sensitivity simulation without the cold pool. The presence of the heightened inversion also lead to the formation of deep tropospheric ascent above this region.

A three-dimensional, nested cloud simulation for the 30-31 March 1988 storm captured the development of strong upslope flow and the associated production of large amounts of precipitation, mainly in the form of aggregates. Additional rain and graupel fallout occurred to the east of the foothills. Precipitation predictions agreed well with observations over the foothills, but errors were noted in areas further east. Due to the under-prediction of a low-level anticyclone to the north, cold advection and northeasterly low-level winds were underestimated by the model. As a result, the simulation did not develop a blocked dynamic structure along the I-25 corridor, although some blocking-induced convergence

occurred over the foothills. This deficiency underscored the importance of low-level cold advection in this storm, as well as the sensitivity of this simulation to the initial fields and boundary conditions. This problem may have been related to the fact that the model did not correctly simulate the intensity of the large-scale cutoff low pressure system aloft. Upon comparison of model performance of RAMS with the NGM for this storm, two important features are evident: orographic enhancement of precipitation was predicted much more accurately by RAMS, while synoptic-scale fields aloft were forecast better by the NGM. A potential solution for this problem with RAMS is to enlarge the domain of grid 2 in these simulations by at least a factor of two.

The importance of meso-gamma-scale observations of snow accumulation and crystal habits from the spotter network in this study cannot be overemphasized. The analysis of the origin of snow crystals, and thus, the regions of ascent under ice-saturated conditions, could not be accomplished without either a large set of aircraft data or the surface network and special sounding data available in the present investigation.

The dynamical interaction of the upslope flow with moisture aloft can be critical to understanding the snowfall distributions associated with arctic outbreaks along the east slopes of the Rocky Mountains. The findings of this investigation will benefit the scientific knowledge of winter storms occurring throughout the United States and the rest of the world, especially in complex terrain. Both cold-air damming and arctic air mass overrunning occur not only along the entire lee side of the Rocky Mountain barrier, but also near mountain ranges in other parts of the world. Overrunning of arctic air not associated with mountains also exhibits some similar features.

The fundamental research in this investigation dealt directly with a more general problem evident in atmospheric science at this time; specifically, this is the understanding of physical processes involved in mesoscale precipitating systems. Snowfall distributions in complex terrain persistently exhibit significant variations on spatial scales of a few to 50 km, and much more research is required to quantitatively assess the underlying causes of this variability. The present study furthers the fundamental understanding of snowstorm

microphysical and dynamical processes both in Colorado and any other region of complex terrain. WISP is currently applying the findings of this study to the analysis of two years of field data.

5.1 Suggestions for Future Research

In light of the presence of WISP, further observational analysis would provide answers to several key questions posed in this study:

- Does the formation of the barrier jet require cyclogenesis to the south in this region?
- Precisely what is the effect of latent cooling induced by melting or evaporation on blocking?
- How much additional uplift and/or blocking results from a low-level northerly surge?
- How often is the upstream stratification too unstable to lead to blocking?

The continued enhancement of the speed of supercomputers opens up a number of options in simulating these winter storms with RAMS. Certainly, experiments with larger grid and domain sizes, while simultaneously reducing horizontal grid spacings to values smaller than those discussed in Chapter 4, would be enlightening. The associated more realistic topography might lead to an improved simulation. Model initialization and four-dimensional data assimilation also require further experimentation. Furthermore, all of the above questions posed to the observationalists could be investigated with a model such as RAMS.

REFERENCES

Abbs, D.J. and R.A. Pielke, 1986: Thermally forced surface flow and convergence patterns over northeast Colorado. *Mon. Wea. Rev.* **114**, 2281-2296.

Abbs, D.J. and R.A. Pielke, 1987: Numerical simulations of orographic effects on NE Colorado snowstorms. *Meteor. and Atmos. Phys.*, **37**, 1-10.

Arritt, R.W., G.S. Young and R.A. Pielke, 1987: An examination of the Denver convergence zone using a mesoscale numerical model. *Proceedings, 4th Conference on Mountain Meteorology*, August 1987, Seattle, Washington.

Auer, A.H. Jr. and J.M. White, 1982: The combined role of kinematics, thermodynamics and cloud physics associated with heavy snowfall episodes. *J. Meteor. Soc. Japan*, **60**, 500-507.

Bell, G.D. and L.F. Bosart, 1988: Appalachian cold-air damming. *Mon. Wea. Rev.*, **116**, 137-162.

Bennetts, D.A. and B.J. Hoskins, 1979: Conditional symmetric instability – a possible explanation for frontal rainbands. *Quart. J. Roy. Meteor. Soc.*, **101**, 595-602.

Boatman, J.F. and R.F. Reinking, 1984: Synoptic and mesoscale circulations and precipitation mechanisms in shallow upslope storms over the western high plains. *Mon. Wea. Rev.*, **112**, 1725-1744.

Bosart, L.F., 1975: New England coastal frontogenesis. *Quart. J. Roy. Meteor. Soc.*, **101**, 957-978.

Bossert, J.E., 1990: Regional-scale flows in complex terrain: an observational and numerical investigation. Department of Atmospheric Science, Colorado State University, Paper. No. 472, 254 pp.

Byers, H.R., 1965: *Elements of Cloud Physics.*, University of Chicago Press, 109-140.

Carlson, T.N., 1980: Airflow through midlatitude cyclones and the comma cloud pattern. *Mon. Wea. Rev.*, **108**, 1498-1509.

Chen, C. and W.R. Cotton, 1983: A one-dimensional simulation of the stratocumulus-capped mixed layer. *Bound.-Layer Meteor.*, **25**, 289-321.

Cotton, W.R., M.A. Stephens, T. Nehrkorn, and G.J. Tripoli, 1982: The CSU cloud/mesoscale model – 1982. Part II: An ice phase parameterization. *J. Rech. Atmos.*, **16**, 295-320.

Cotton, W.R., G.J. Tripoli, R.M. Rauber, and E.A. Mulvihill, 1986: Numerical Simulation of the effects of varying ice crystal nucleation rates and aggregation processes on orographic snowfall. *J. Climate Appl. Meteor.*, **25**, 1658-1680.

Cotton, W.R. and R. Anthes, 1989: *Storm and Cloud Dynamics.* Academic Press, Inc., New York, 883 pp.

Cram, J.M., 1990: Numerical simulation and analysis of the propagation of a prefrontal squall line. Department of Atmospheric Science, Colorado State University, Paper. No. 471, 332 pp.

Crook, N.A., T.L. Clark, and M.W. Moncrieff, 1990: The Denver cyclone. Part I: Generation in low Froude number flow. *J. Atmos. Sci.*, **47**, 2725-2742.

Dunn, L., 1987: Cold-air damming by the Front Range of the Colorado Rockies and its relationship to locally heavy snows. *Wea. Forecasting*, **2**, 177-189.

Dunn, L., 1988: Vertical motion evaluation of a Colorado snowstorm from a synoptician's perspective. *Wea. Forecasting*, **3**, 261-272.

Emanuel, K.A., 1983: On assessing local conditional symmetric instability from atmospheric soundings. *Mon. Wea. Rev.*, **111**, 2016-2033.

Flatau, P.J., G.J. Tripoli, J. Verlinde and W.R. Cotton, 1989: The CSU-RAMS cloud microphysics module: general theory and code documentation. Department of Atmospheric Science, Colorado State University, Paper. No. 471, 332 pp.

Forbes, G.S., R.A. Anthes, and D.W. Thomson, 1987: Synoptic and mesoscale aspects of an Appalachian ice storm associated with cold-air damming. *Mon. Wea. Rev.*, **115**, 564-591.

Hjelmfelt, M.R. and R.R. Braham, Jr., 1983: Numerical simulation of the airflow over Lake Michigan for a major lake-effect snow event. *Mon. Wea. Rev.*, **111**, 205-219.

Hoke, J.E., N.A. Phillips, G.J. DiMego, J.J. Tuccillo, and J.G. Sela, 1989: The regional analysis and forecast system of the National Meteorological Center. *Wea. Forecasting*, **4**, 323-334.

Iskenderian, H., 1988: Three-dimensional airflow and precipitation structure in a nondeepening cyclone. *Wea. Forecasting*, **3**, 18-32.

Jiusto, J.E., 1967: Nucleation Factors in the Development of Clouds. Ph.D. Thesis, Pennsylvania State University, University Park, PA, 124 pp.

Junker, N.W., J.E. Hoke, and R.H. Grumm, 1989: Performance of NMC's regional models. *Wea. Forecasting*, **4**, 368-390.

Lee, T.J., R.A. Pielke, R.C. Kessler, and J. Weaver, 1989: Influence of cold pools downstream of mountain barriers on downslope winds and flushing. *Mon. Wea. Rev.*, **117**, 2041-2058.

Lilly, D.K., 1981: Doppler radar observations of upslope snowstorms. *Preprints, 2nd. Conf. on Mountain Meteorology*, AMS, Steamboat Springs, CO, Nov. 1981, 346-353.

Mahrer, Y. and R.A. Pielke, 1977: A numerical study of the airflow over irregular terrain. *Beitrage zur Physik der Atmosphere*, **50**, 98-113.

Marwitz, J. and D. Day, 1991: The effect of melting in a Denver snow dump. Preprints, *First International Symposium on Winter Storms*, 14-18 Jan. 1991, New Orleans, 241-244.

Meyers, M.P., 1989: An evaluation of the factors affecting wintertime quantitative precipitation forecasts in an explicit cloud model over mountainous terrain. M.S. Thesis, Colorado State University, Fort Collins, Colorado, 120 pp.

Meyers, M.P. and W.R. Cotton, 1991: Evaluation of the potential for wintertime quantitative precipitation forecasting over mountainous terrain with an explicit cloud model. Part I: Two-dimensional sensitivity experiments. *J. Appl. Meteor.*, (in press).

Michaels, P.J., 1991: Bringing in the sleeze. *Virginia Climate Advisory*, **14**, 3-14.

Nicholls, M., R.A. Pielke and W.R. Cotton, 1990: A two-dimensional numerical investigation of the interaction between sea-breezes and deep convection over the Florida peninsula. *Mon. Wea. Rev.*, **118**, 298-323.

Nielsen, J.W., 1989: The formation of New England coastal fronts. *Mon. Wea. Rev.*, **117**, 1380-1401.

O'handley, C. and L.F. Bosart, 1989: Subsynoptic-scale structure in a major synoptic-scale cyclone. *Mon. Wea. Rev.*, **117**, 607-630.

Parish, T., 1982: Barrier winds along the Sierra Nevada mountains. *J. Climate Appl. Meteor.*, **21**, 925-930.

Peterson, T.C., L.O. Grant, W.R. Cotton, and D.C. Rogers, 1991: The effects of decoupled low-level flow on winter orographic clouds and precipitation in the Yampa River Valley. *J. Appl. Meteor.*, **30**, 368-386.

Pielke, R.A. and J.M. Cram, 1987: On an alternate procedure for analyzing surface geostrophic winds and pressure over elevated terrain. *Wea. Forecasting*, **2**, 229-236.

Pielke, R.A., 1974: A three-dimensional numerical model of the sea breezes over South Florida. *Mon. Wea. Rev.*, **102**, 115-139.

Pierrehumbert, R.T. and B. Wyman, 1985: Upstream effects of mesoscale mountains. *J. Atmos. Sci.*, **42**, 977-1003.

Politovich, M.K., 1989: Aircraft icing caused by large super-cooled droplets. *J. Appl. Meteor.*, **28**, 856-868.

Pruppacher, J.D. and H.R. Klett, 1980: *Microphysics of Clouds and Precipitation*, D. Reidel, Boston, Massachusetts, 714 pp.

Rasmussen, R.M. and M.K. Politovich, 1990: WISP Scientific Overview. NCAR publication available from authors, PO Box 3000, Boulder, CO 80307.

Rasmussen, R.M., M.K. Politovich, J. Marwitz, J. McGinley, J. Smart, W. Sand, G. Stossmeister, B. Bernstein, R. Pielke, D. Wesley, S. Rutledge, K. Elmore, E. Westwater, B. Stankov, and D. Burrows, 1991a: Winter Icing and Storm Project (WISP). *Bull. Amer. Meteor. Soc.*, submitted.

Rasmussen, R.M., M. Murakami, G. Stossmeister, B. Bernstein, and B. Stankov, 1991b: Super-cooled liquid water in Colorado Front Range winter storms: case study of the 1990 Valentine's Day storm. Preprints, 4th International Conference on the Aviation Weather System, Paris, 24-26 June 1991.

Rauber, R.M., D. Feng, L.O. Grant and J.B. Snider, 1986: The characteristics and distribution of cloud water over the mountains of northern Colorado. Part I: Temporal variations. *J. Climate Appl. Meteor.*, **25**, 468-488.

Reinking, R.F. and J.F. Boatman, 1986: Upslope precipitation events. Chapter 19 in *Mesoscale Meteorology and Forecasting.* Ed. P.S. Ray, AMS, Boston, MA, 437-471.

Sanders, F. and L.F. Bosart, 1985: Mesoscale structure in the mega-lopolitan snowstorm of 11-12 February 1983. *J. Atmos. Sci.*, **42**, 1050-1061.

Schlatter, T. and J. Henz, 1983: Profiling the Christmas blizzard. *Weatherwise*, **36**, 60-66.

Schmidt, J. and W.R. Cotton, 1990: Interactions between upper and lower tropospheric gravity waves on squall line structure and maintenance. *J. Atmos. Sci.*, **47**, 1205-1222.

Schultz, P., M.C. McCoy, R.W. McGowan, and J.S. Wakefield, 1985: The first experiment in forecasting cool-season weather with the PROFS system. *NOAA Tech. Memo.*, ERL ESG-16, April 1985.

Smart, J.R. and J.A. McGinley, 1989: The use of radar reflectivity to determine snowfall over northeast Colorado. *Preprints, 12th Conference on Weather Analysis and Forecasting*, October 2-6, 1989.

Smith, R.B., 1979: The influence of mountains on the atmosphere. *Adv. Geoph.*, **21**, 87-230.

Szoke, E.J., 1991: The eye of the Denver Cyclone. *Mon. Wea. Rev.*, **119**, 1283-1292.

Tanaka, H.L. and M.F. Milkovich, 1990: A heat budget analysis of the polar troposphere in and around Alaska during the abnormal winter of 1988/89. *Mon. Wea. Rev.*, **118**, 1628-1639.

Toth, J.J., 1987: Interaction of shallow cold surges with topography on scales of 100-1000 kilometers. CIRA Publication, Colorado State University, Fort Collins, ISBN No. 0737-5352-8, 135 pp.

Tremback, C.J., 1990, Ph.D. Thesis: Numerical simulation of a mesoscale convective complex: Model development and numerical results. Colorado State University, Department of Atmospheric Science, 247 pp.

Tremback, C.J. and R. Kessler, 1985: A surface temperature and moisture parameterization for use in mesoscale numerical models. *Preprints, 7th Conference on Numerical Weather Prediction*, June 17-20, 1985, Montreal Quebec, Canada, AMS.

Walko, R.L. and C.J. Tremback, 1991: *The RAMS Version 2c, User's Guide.* ASTeR Inc, PO Box 466, Fort Collins, CO 80521.

Wesley, D.A. and R.A. Pielke, 1988: Simulations of blocked upslope flow along the Colorado Front Range. *Proceedings, 2nd International Cloud Modelling Workshop*, August 8-12, 1988, Toulouse, France, World Meteorological Organization, 317-322.

Wesley, D.A., M.J. Weissbluth, R.A. Pielke, and W.R. Cotton, 1988: Microphysical and dynamical interactions in Colorado Front Range upslope storms. *Proceedings, 10th International Cloud Physics Conference*, August 15-20, 1988, Bad Homburg, Germany, **1**, 359-361.

Wesley, D.A. and R.A. Pielke, 1990: Observations of blocking-induced convergence zones and effects on precipitation in complex terrain. *Atmospheric Research*, **25**, 235-276.

Wesley, D.A., J.F. Weaver, and R.A. Pielke, 1990: Heavy snowfall during an extreme arctic outbreak along the Colorado Front Range. *Natl. Wea. Dig.*, *15*, 2-19.

Wilczak, J.M. and T.W. Christian, 1990: Case study of an orographically induced mesoscale vortex. *Mon. Wea. Rev.*, **118**, 1082-1102.

Wolfsberg, D.G., K.A. Emanuel, and R.E. Passarelli, 1986: Band formation in a New England winter storm. *Mon. Wea. Rev.*, **114**, 1552-1569.